

Generation and characterization of cardiac valve endothelial-like cells from human pluripotent stem cells

Lingxi Cheng

Institute of Hydrobiology

Yu Song

Huazhong University of Science and Technology

Yanyong Zhang

Institute of Hydrobiology

Yingchao Geng

University of Chinese Academy of Sciences

Weilin Xu

Wuhan Textile University

Zheng Wang

Union Hospital, Huazhong University of Science and Technology <https://orcid.org/0000-0002-9330-0728>

Lin Wang

Huazhong University of Science and Technology

kai huang

Huazhong University of Science and Technology

Nianguo Dong

Wuhan Union Hospital

Yuhua Sun (✉ sunyh@ihb.ac.cn)

Institute of Hydrobiology <https://orcid.org/0000-0001-7902-9022>

Article

Keywords: hPSCs, valve endothelial cells, valve organoids, DCVs

Posted Date: October 19th, 2020

DOI: <https://doi.org/10.21203/rs.3.rs-91459/v1>

License:   This work is licensed under a Creative Commons Attribution 4.0 International License.

[Read Full License](#)

Version of Record: A version of this preprint was published at Communications Biology on September 6th, 2021. See the published version at <https://doi.org/10.1038/s42003-021-02571-7>.

Generation and characterization of cardiac valve endothelial-like cells from human pluripotent stem cells

LX Cheng^{1,8}, Y Song⁴, YY Zhang^{1,8}, YC Geng^{1,8}, WL Xu⁷, Z Wang^{4,6}, L Wang^{4,5}, K Huang³, NG Dong^{2*} & YH Sun^{1,8*}

^{1*}University of Chinese Academy of Sciences, Beijing 100049, China

^{2*}Department of Cardiovascular Surgery, Union Hospital, Tongji Medical College, Huazhong University of Science and Technology, Wuhan 430022, China

³Department of Cardiovascular Internal Medicine, Union Hospital, Tongji Medical College, Huazhong University of Science and Technology, Wuhan 430022, China

⁴Research Center for Tissue Engineering and Regenerative Medicine, Union Hospital, Tongji Medical College, Huazhong University of Science and Technology, Wuhan 430022, China

⁵Department of Clinical Laboratory, Union Hospital, Tongji Medical College, Huazhong University of Science and Technology, Wuhan 430022, China

⁶Department of Gastrointestinal Surgery, Union Hospital, Tongji Medical College, Huazhong University of Science and Technology, Wuhan 430022, China

⁷Wuhan Textile University, Wuhan, China

^{8*}Institute of Hydrobiology, Chinese Academy of Sciences, Wuhan 430070

Corresponding author: sunyh@ihb.ac.cn

Summary

The cardiac valvular endothelial cells (VECs) are an ideal cell source that could be used for making the valve organoids. However, few studies have been focused on the derivation of this important cell type. Here we describe a two-step chemically defined xeno-free method for generating VEC-like cells from human pluripotent stem cells (hPSCs). hPSCs were specified to KDR⁺/ISL1⁺ multipotent cardiac progenitors (CPCs), followed by differentiation into valve endothelial-like cells (VELs). Mechanistically, administration of TGFb1 and BMP4 may specify VEC fate by activating the NOTCH/WNT signaling pathways and previously unidentified targets such as ATF3 and KLF family of transcription factors. When seeded onto the surface of the de-cellularized porcine aortic valve (DCV) matrix scaffolds, hPSC-derived VELs exhibit superior proliferative and clonogenic potential than the primary VECs. Our results suggest that hPSC-derived VELs could serve as a potential platform for the mechanistic study of valvulogenesis, and as starting materials for the construction of the valve organoids.

Keywords: hPSCs, valve endothelial cells, valve organoids, DCVs

Highlights:

1. Valve endothelial-like cells (VELs) could be efficiently derived from hPSCs by a two-step method
2. The combined treatment with TGFb1 and BMP4 induces VEC fate by activating NOTCH signaling and enhancing the expression of *ATF3* and *KLFs*
3. HPSC-derived VELs resemble the isolated primary VECs morphologically, molecularly and functionally
4. HPSC-derived VELs exhibit proliferative and functional potential similar to the primary VECs when seeded onto the DCVs

Introduction

Valve disease is one of the most common cardiac defects (Combs and Yutzey, 2009). As there are currently no good medical treatments for the dysfunctional valves, surgical replacement with mechanical and bioprosthetic valves is the major option. However, the current mechanical and bioprosthetic valves have their limitations due to the requirement of lifelong anti-coagulation, poor durability, and lack of self-growth and self-renewal capacity (Hu et al., 2013; Zhou et al., 2013). The iPSC-based valve organoids or next generation tissue engineered heart valves may offer a potential remedy to the challenge, which however requires the generation of or obtaining a large number of genuine valvular cells (Glaser et al., 2011; Nejad et al., 2016).

There are two major types of valvular cells: the valvular endothelial cells (VECs) lining the outer surface of the valve cusps and the valvular interstitial cells (VICs) embedded in a stratified extra-cellular matrix. HPSCs (including human embryonic stem cells and iPSCs) are known to have the potential for unlimited expansion and differentiation into any cell types in a petri dish. For instance, cardiovascular endothelial cells can be efficiently generated from hPSCs (Wilson et al, 2014). Few studies, however, have been focused on the derivation of valve endothelial-like cells, likely due to incomplete understanding of VEC biology.

From the viewpoint of developmental biology, a reliable approach to generate the valvular-like cells would be to recapitulate the embryonic valvulogenesis under chemical defined medium based on the understanding of the signaling intricacies involved in the process. A growing body of studies support the notion that the

endocardial cells are derived from *Isl1*⁺/*Kdr*⁺ multipotent progenitors via cardiogenic mesoderm cells expressing *T*⁺/*Mesp1*⁺ (Andersen et al., 2018; Nakano et al., 2016; Hoffman et al., 2011). And genetic studies using mice and zebrafish models have suggested that the majority of valvular cells are of endocardial cell origin (Hinton and Yutzey, 2011). At E9.5 of mouse embryos or week 5 of human fetus, a subset of endocardial cells at defined regions of the atrio-ventricular (AV) canal and the outflow tract (OFT) (referred as the endocardial cushion cells/ECCs) are induced to lose the contact with neighboring cells, and undergo an EndoMT (endocardial to mesenchymal transition) to form the valve mesenchymal cells or adopt the VEC fate (Wu et al., 2011). However, the exact mechanisms by which the ECCs are induced within the endocardium and VEC identity is established remain unclear.

Previous studies have shown that components of multiple signaling pathways (such as BMP, FGF, WNT, NOTCH and TGF- β) are expressed in a spatial-temporal manner during endocardial cushion formation and EndoMT (Cui et al., 2019; Garside et al., 2013; Wu et al., 2011; Yang et al., 2017), suggesting that signaling pathways may play key roles in ECC induction and valvular cell formation. Besides, transcriptional regulation has been shown to play a key role in valvulogenesis (Hinton and Yutzey, 2011). Of note, NFATc1 (nuclear factor in activated T cell, cytoplasmic 1) is critically important for the maintenance of VEC identity (Wu et al., 2011, 2012, 2013). Consistently, NFATc1^{low} cells will undergo EndoMT to form VICs while NFATc1^{high} cells remain the endothelial phenotype.

In this work, we reported that using a chemically defined xeno-free method,

valve endothelial-like cells (VELs) can be efficiently derived from hPSCs (human ESCs and iPSCs) in 9 days. HPSC-derived VELs exhibit morphological, molecular and functional similarities to that of primary VECs isolated from normal human aortic valves. When day 7-9 hPSC-derived VEC-like cells were seeded onto the surface of the de-cellularized porcine aortic valve (DCV) matrix scaffolds, they exhibited proliferation and survival potential similar to the primary VECs. Our results suggest that hPSC-derived valvular cells could serve as a potential platform for the study of valve development and disease, and as starting materials for the construction of the valve organoids.

Results

Efficient generation of ISL1⁺ cardiac progenitor cells from hPSCs

It is widely accepted that the mammalian embryonic heart is primarily originated from cardiac progenitor cells (CPCs) expressing marker genes such as *ISL1*, *NKX2.5* and *KDR* (Hinton and Yutzey, 2011; Lui et al., 2013; Misfeldt et al., 2009; Morreti et al., 2006). We and several other groups have previously generated the CPCs from hPSCs (Berger et al., 2016; Colunga et al., 2019; Lyer et al., 2015; Nakano et al., 2016; Patsch et al., 2016; Sahara et al., 2014; Sriram et al., 2015; Tan et al., 2013; White et al., 2013). The common theme of the various differentiation protocols is the activation of WNT and BMP signaling pathways, which mimics the signaling requirement during early specification of heart mesoderm (Ansersen et al., 2018; Nakano et al.,

2016; Puceat, 2013).

It has been shown that there is a greater propensity for isolated ISL1⁺ cardiac progenitors to give rise to endothelium when NKX2.5 is low or absent (Morreti et al., 2006; Nakano et al., 2016). We therefore aimed to generate ISL1⁺KDR⁺NKX2.5^{low} CPCs from hPSCs by modifying our previously published protocol (Berger et al., 2016). HPSCs were initially treated with BMP4 and WNT agonists (WNT3a or the small molecule CHIR99021) for 3 days, and the expression of *T*, a primitive streak and early mesodermal marker, was monitored daily (Figure 1a; Supplementary Figure 1a-b). CHIR99021 is a highly specific glycogen synthase kinase-3 (GSK3) inhibitor that can activate canonical Wnt signaling (Sun et al., 2020). Compared to the treatment with BMP4 or WNT3a only, combined treatment with BMP4 and WNT3a resulted in a quick induction of *T*, reaching its maximum expression levels at day 1 (Supplementary Figure 1a). Next, day 1 *T*⁺ cells were treated with bFGF and BMP4 for 6 days, and qRT-PCR analysis was performed to examine the expression of CPC markers such as *ISL1* and *NKX2.5*. The qRT-PCR results showed that *ISL1* and *KDR* were highly induced, peaking at day 2 post-treatment, while *NKX2.5* and *TBX5* were barely up-regulated (Supplementary Figure 1b,c). Immunofluorescence (IF) staining of day 3 CPCs showed that a vast majority (> 90%) of cells were ISL1 positive while cells displayed negligible expression of NKX2.5 (Figure 1c-d; Supplementary Figure 1d). Western blot analysis confirmed that ISL1 and KDR were abundantly expressed in day 3 hPSC-derived CPCs (Figure 1e). Finally, the flow cytometry analysis further revealed that approximately 80% of day 3 CPCs were KDR positive and over 93% of

cells were ISL1 positive, indicating that hPSC cardiogenic mesodermal differentiation was of high efficiency (Figure 1f).

Based on the above results, we concluded that ISL1⁺KDR⁺ CPCs could be efficiently generated from hPSCs in 3 days (Figure 1g).

One-step differentiation of CPCs into VEC-like cells

It is widely accepted that endocardial cells are derived from *Isl1*⁺/*Kdr*⁺ multipotent CPCs (Andersen et al., 2018; Nakano et al., 2016; Milgrom-Hoffman et al., 2011). It is also firmly established that heart valves originate from a subpopulation of endocardial cells called endocardial cushion cells (ECCs) or valve endocardial cells located at defined regions of the AVC and the OFT. Recent studies have shown that the ECCs or valve endocardial cells express marker genes such as *NPR3*, *CDH11*, *EDN1*, *MEF2C*, *SOX17*, *THSD1*, *EMCN*, *TGFβ2*, *NOTCH4*, *DLL3/4* and *JAG1* (designated as ECC genes thereafter) (Cui et al., 2019; Holliday et al., 2011; Hulin et al., 2019; Neri et al., 2019; Wu et al., 2011).

Studies using mice and zebrafish models have provided important clues that signaling pathways, such as the BMP, FGF, TGFβ and NOTCH pathways, may play key roles in the induction of valve endocardial or ECC fate (Harris and Black, 2010; Hinton and Yutzey, 2013; McCulley et al., 2008; Nakano et al., 2016; Papoutsi et al., 2018; Puceat, 2013). We therefore investigated the effects of modulating the BMP, FGF, TGF-β and NOTCH signaling on day 3 hPSC-derived CPCs, in the presence of VEGFA (Figure 2a). VEGF has been shown to be important for endothelial cell

differentiation from hPSCs (Neri et al., 2019; Sahara et al., 2014). Initially, hPSC-derived CPCs were treated with activators or inhibitors of various signaling pathways for 3 days, and the expression of ECC genes was examined. When FGF/ERK signaling was modulated by treatment with different doses of bFGF and FGF/MEK inhibitors PD0325901/PD98059 (Supplementary Figure 2a), the expression of ECC genes was barely altered. It has been shown that there is an increased expression of both *TGF β* and *BMPs* in the endocardial cushion cells (Kruithof et al., 2012; McCulley et al., 2008), and that the combined treatment with BMP4 and TGF β /ActivinA promotes hPSC differentiation into cardiovascular endothelial cell types (Di Bernardini et al., 2014; White et al., 2013). Based on this observation, we speculated that a crosstalk between BMP and TGF- β signaling pathways might be involved in the initiation/induction of ECC fate (Hinton and Yutzey, 2013; Nolan et al., 2013). We found that this was likely the case. Although administration of BMP4 or TGF β 1 moderately altered the expression of ECC genes, combined treatment with BMP4 and TGF β 1 led to a marked up-regulation of the same genes (Figure 2b; Supplementary Figure 2b-c). The Notch signaling pathway is well-known to be implicated in endocardial cushion formation (Papoutsi et al., 2018; Sahara et al., 2014; Wang et al., 2013). Surprisingly, modulating Notch signaling (by the addition of different doses of the Notch ligand DLL4 or the Notch signaling inhibitor DAPT) had a minimal effect on the expression of ECC genes except *NFATc1* (Supplementary Figure 2d), and addition of DLL4 in the combined presence of BMP4 and TGF β 1 did not further augment ECC gene expression (Supplementary Figure 2e).

The above data suggested that combined treatment with BMP4 and TGFb1 may promote CPCs to an ECC fate. To further investigate this, day 3 hPSC-derived CPCs were treated with VEGFA/BMP4/TGFb1 for a time course of 9 days, and the dynamic expression of ECC genes was carefully monitored. The treated cells adopted the typical cobber-stone EC morphology from day 2 post-treatment and remained the morphology up to 12 days (Supplementary Figure 2f). As shown in Figure 2c, the ECC genes such as *NPR3*, *KDR*, *ENG*, *EMCN*, *MEF2C*, *JAG1*, *DLL4* and *NOTCH1/4* were quickly induced, most of which exhibited highest expression levels at day 2-3 post-treatment. Therefore, CPCs at day 3 post-treatment (or day 6 hPSC-derived cells) were chosen for further analysis as described below. IF staining results showed that day 6 hPSC-derived cells readily expressed general EC markers CD31 and VE-cad, as well as ECC markers such as NOTCH4, DLL4 and JAG1 (Figure 2d). Quantitative analysis of IF staining revealed that approximately 90% of the cells were VE-cad/NOTCH4, CD31/JAG1 and VE-cad/DLL4 double positive (Figure 2e). Flow cytometry analysis of day 6 hPSC-derived cells revealed that approximately 95% and 84% of the cells were JAG1/VE-cad and GATA4/VE-cad double positive, respectively (Figure 2f; Supplementary Figure 2g). Thus, day 6 hPSC-derived cells displayed a gene expression profile similar to that of the pre-EMT ECCs (Hulin et al., 2019; Neri et al., 2019).

With the prolonged treatment with VEGFA/BMP4/TGFb1, the expression of ECC genes gradually decreased. Interestingly, known VEC-specific marker genes such as *NFATc1*, *NTRK2*, *SMAD6* and *HAND2* were gradually induced, peaking at day

4-6 post-treatment (Figure 2c) (Cui et al., 2019; Neri et al., 2019; Wu et al., 2013). This observation suggested that prolonged treatment with the signaling molecules may lead to the induction of VEC fate. IF staining results showed that day 8 hPSC-derived cells (CPCs at day 5 post-treatment) abundantly expressed VEC markers NFATc1, PROX1, HEY2 and TBX2 (Figure 2g; Supplementary Figure 2h). WB analysis confirmed that NFATc1, NOTCH1/3, HEY1/2 and TBX2 were strongly induced in day 8 hPSC-derived cells (Figure 2h). Finally, flow cytometry analysis revealed that approximately 82% of the cells were NFATc1/VE-cad double positive, and that approximately 67% of cells were TBX2/VE-cad positive (Figure 2i).

Based on above results, we concluded that under the combined treatment with VEGFA/BMP4/TGFb1, ECC-like and VEC-like cells could be efficiently derived from hPSC-derived CPCs, in a time dependent fashion.

Comparative transcriptome assay of hPSC-derived VELs and the primary VECs

Next, we asked that to what extent hPSC-derived VEC-like cells resembled the genuine VECs, in particular the embryonic-type VECs. It is widely accepted that hPSC-derived derivatives in vitro resemble embryonic type cells more than adult. First, to understand the gene expression signature of embryonic VECs, we consulted the single-cell RNA-sequencing (scRNA-seq) data of cardiac tissues of human embryos ranging from 5 to 25 weeks of gestation (Cui et al., 2019). As previously reported, the VEC subcluster can be identified based on the expression of *NFATc1* and *NTRK2*, and the endocardium subcluster can be identified based on the expression of

NPR3 and *CDH11* (Figure 3a; Supplementary Figure 3a-b). Next, a pseudotime trajectory was built to reveal the developmental progression of embryonic VECs. As expected, cells were ordered in a pseudotime consistent with the actual developmental stages, showing that embryonic VECs were primarily originated from endocardium of early stage (Figure 3b; Supplementary Figure 3c). Temporal gene expression dynamics were analyzed during the progressive formation of embryonic VECs. Based on the pseudotime trajectory, we identified two major gene groups showing distinct expression patterns, with 1,104 genes for group 1 (G1) and 896 genes for group 2 (G2) (Figure 3c). *Dll4* and *WNT2* are shown as representatives for G1 and G2 genes, respectively (Figure 3d). GO (gene ontology) analysis of G1 genes showed that they were enriched for terms such as cardiovascular development, anatomical structure and multicellular organism development, and regulation of developmental progress. GO analysis of G2 genes revealed an enrichment for terms such as response to organic substance and chemical stimulus, response to cytokine and shear stress, and cytokine-mediated pathways (Supplementary Figure 3d). KEGG pathway analysis revealed that the G1 genes were enriched for regulation of cardiac development and NOTCH signaling pathway while the G2 genes were enriched for MAPK, PI3K/AKT and RAS signaling pathways (Supplementary Figure 3e).

The G1 genes were expressed in endocardial cells of week 5-15 human embryos (early stage), but not in VECs of week 21-25 human embryos (late stage) (Figure 3c; Supplementary Figure 3f). The G1 was enriched for embryonic heart developmental genes such as *FOXC1*, *CDH5*, *KDR*, *F8*, *vWF*, *FLRT2*, *SOX17*, *MEF2C*, *FNI*,

NKX2.5, *GATA3*, *PDGFRB*, *WT1*, *ETV5* and *TBX5*. Remarkably, ECC genes such as *NPR3*, *KDR*, *vWF*, *ENG*, *GATA4*, *SOX17*, *EMCN*, *MEF2C*, *JAG1*, *DLL3/4*, *NOTCH4* and *TGF β 2* belonged to G1. The G2 genes were barely expressed in early stage, but highly expressed in VECs of week 21-25 human embryos (late stage), including *NFATc1*, *NTRK2*, *CDH13*, *HEY2*, *FOS*, *NR4A2*, *CD44*, *CDKN1A*, *CCND1*, *NFKB1*, *CCDC141*, *HEY2*, *HAND2*, *WNT2/4*, *PROX1*, *DKK2/3*, *BMP4*, *IDI1/2*, *SMAD6*, *GATA2*, *THBD*, *MSX1*, *SELE*, *ATF3*, *KLF2/4/9/11* and *CAV1*. Of which, *NFATc1*, *NTRK2*, *PROX1*, *SMAD6*, *MSX1*, *SELE* and *IGFBP7* are known to be VEC-specific or enriched marker genes (Cui et al., 2019; Hulin et al., 2019; Neri et al., 2019). The observation strongly indicated that G1 genes were enriched for ECC markers and G2 genes were enriched for VEC markers. To understand the dynamic signaling requirement and transcription program for the induction of VEC fate, we characterized the progressive expression of G1 and G2 genes over the trajectories. The heat map showed that VEC formation coincided with the up-regulation of a panel of TFs, including *NFATc1*, *HEY2*, *GATA2*, *ATF3*, *KLFs* and *HAND2* (Figure 3e, bottom). These TFs were not or lowly expressed at early stage, but dramatically up-regulated at the late stage. In fact, *NFATc1*, *HEY2*, *HAND2* and *GATA2* have been shown to be important for VEC maintenance/function (Mahamud et al., 2019; Neri et al., 2019; VanDusen et al., 2014; Wu et al., 2012). The expression of *KLFs* (such as *KLF2* and *KLF4*), *Egr1*, *Cxcl2* and genes reflecting NF κ B and JNK activation (Jun, Junb, Jund, Fos, Fosb, Atf3), was in line with the physiological conditions of VECs (shaped by laminar shear flow and fluid shear stress). Based on the dynamic

expression of signaling components and their target genes (Figure 3e, top), a temporal requirement of signaling pathway activities was observed, with NOTCH signaling being active at early stage, and WNT and BMP signaling being active at late stage. Furthermore, the co-expression of a subset of TFs with WNT- (*WNT2/4*, *DKK2/3*) and BMP-related (*BMP4*, *ID1/2* and *SMAD6*) genes strongly suggested that embryonic VEC induction may require both WNT/BMP signaling activation and expression of defined TFs such as *NFATc1/HAND2/HEY2/ATF3/KLFs*. It is known that either the NOTCH/WNT/BMP axis or sustained *NFATc1/HEY2/HAND2* expression are required for normal heart valve development (van der Berg et al., 2015; VanDusen et al., 2014; Wang et al., 2013; Wang et al., 2020; Wu et al., 2013).

The identification and characterization of ECC-enriched gene network (G1 genes) and VEC-enriched gene network (G2 genes) from cardiac cells of human embryos allowed us to better compare our hPSC-derived VELs with human embryonic VECs. During hPSC differentiation into VEC-like cells, ECC-enriched genes such as *NPR3*, *KDR*, *TEK*, *MEF2C*, *JAG1*, *DLL3/4*, *NOTCH4* and *TGFβ2* were induced, peaking at day 2-3 post-treatment, while VEC-enriched genes such as *NFATc1*, *HAND2*, *GATA2*, *WNT2*, *DLL4*, *NOTCH1/4* and *TGFβ1* were up-regulated at later time points, reaching their highest expression levels at day 4-6 post-treatment (Figure 2C). Thus, day 6 hPSC-derived cells exhibited a gene expression profile analogous to that of the ECCs, and day 7-9 hPSC-derived cells displayed a gene expression signature similar to the embryonic VECs. To comprehensively compare hPSC-derived VELs with human embryonic VECs, we performed the heat map analysis using G1 and G2 genes. Again,

the results showed that day 6 hPSC-derived cells highly expressed G1 genes and day 9 hPSC-derived VELs highly expressed G2 genes (Figure 3f). Based on these observations, we concluded that the developmental hierarchy of in vitro hPSC VEC differentiation faithfully recapitulates embryonic valve development events.

Transcriptome analysis of postnatal heart valve cells of different stages has demonstrated that valve endothelial cells are relatively consistent in gene expression throughout early development (Hulin et al., 2019). We therefore asked whether a subset of VEC-enriched genes (G2) are persistently expressed in VECs of adult hearts. To this end, single-cell RNA sequencing analysis was performed for valvular cells of two healthy aortic valves from around 40-year old. After removing apoptotic cells, approximately 3,600 cells used for subsequent transcriptome analysis, and on average 3,300 genes were detected in each single cell. Unsupervised hierarchical clustering analysis was performed and a total of fourteen clusters were identified. Based on the highly expressed intra-correlated genes, we were able to determine the cell identity of each cluster. This revealed three heterogeneous subclusters of resident valve interstitial cells (VICs), three types of immune-derived cells, two types of valve endothelial cells (VECs), and six novel valve derived stromal cells (VDSC) (Figure 3g-h). Based on the expression of side-specific valvular EC genes such as *VCAMI* and *MGST1* (which are more highly expressed in aortic side than in ventricular side) (Simmons et al., 2005), it was likely that the two VEC subclusters may represent the aortic and ventricular side of VECs, respectively (Figure 3i-j). Remarkably, we found that compared to other subclusters, the VEC subclusters indeed highly expressed a

subset of G2 genes such as *HEY2*, *GATA2*, *HAND2*, *ATF3*, *KLFs*, *CDH13*, *SELE*, *FOS*, *NR4A2*, *S100A4*, *CD44*, *CDKN1A*, *CCND1*, *NFKB1*, *BMP4*, *ID1/2*, *WNT2/4*, *DKK2/3*, *CAVI*, *ATF3*, *THBD* and *KLF2* (Supplementary Figure 3g). Our qRT-PCR analysis of the selected G2 genes showed that they are expressed at much higher levels in VECs than in HAEC and HUVEC (Figure 3k).

Next, bulk RNA-sequencing analysis was performed for hPSC-derived VELs and the primary VECs isolated from normal aortic valves of different ages (7-, 9-, 10-, 20-, 30, 40, 50-year old). Human ESC H9 cell line (H9), Human foreskin fibroblast cells (HFF), human valvular interstitial cells (hVICs), human umbilical vein endothelial cells (HUVEC) and aortic endothelial cells (HAEC) were used as controls (Figure 4a). The RNA-seq results of the primary VECs showed that the definitive endothelial markers *CDH5* and *PECAMI* were highly expressed (FPKM > 50) while the fibroblast markers *MMP1/3* and *POSTN* as well as cardiomyocyte markers *TNNT1/2* were barely expressed (FPKM < 2). IF results confirmed that almost all cells were CD144 positive. Thus, we determined that the isolated primary hVECs were of high purity (at least rarely contaminated by VICs or other cell types). An average of 16,000 genes in the primary hVECs were identified, which was similar to that of HUVEC. Of which, approximately 6,000 genes were expressed at higher levels (FPKM > 10); 6,000 genes were expressed at medium levels (FPKM 1-10); and the remainder genes were barely or lowly expressed (FPKM < 1) (Supplementary Figure 4a). Heat map analysis of the normalized RNA-seq data showed that day 7 hPSC-derived VELs were globally more similar to the primary VECs than HUVEC,

HAEC, hVICs and H9 (Figure 4b; Supplementary Figure 4d). When the heat map analysis was performed using the G2 genes, a similar result was obtained (Supplementary Figure 4c). We confirmed this by qRT-PCR analysis (Supplementary Figure 4d-e). To further evaluate the similarity, we asked how many highly-expressed genes (FPKM > 10) were shared by day 7 hPSC-derived VECs and the primary hVECs of 9-year old, as highly expressed genes tend to have more important roles than lowly expressed genes. We found that a total of 2,361 genes were expressed at similar levels, representing approximately 44% and 65% of total highly-expressed genes of hPSC-derived VECs and the primary VECs, respectively (Figure 4c). GO analysis of the shared genes showed that they were highly related to terms such as cardiovascular and valve development (Supplementary Figure 4f). KEGG pathway enrichment analysis revealed that TGF- β , Notch and BMP signaling pathways were highly represented (Figure 4d).

Next, the top 100 genes which are highly expressed in both the primary VECs and hPSC-derived VECs (but lowly expressed in HAEC and HUVEC) were screened and subjected to heat map analysis (Figure 4e). The top 100 genes included a subset of G1 and G2 genes such as *NFATc1*, *NRTK2*, *SMAD6*, *BMP4*, *GJA5*, *SELE*, *CD44*, *CDKN1A*, *CCND1*, *NFKB1*, *HEY2*, *HAND2*, *BMP4*, *ID1/2*, *WNT2*, *DKK2/3*, *LDB2*, *ATF3*, *KLFs*, *GATA5*, *THBD*, *PALMD*, *ITM2A*, *FGD5*, *EDN1*, *CXCL12*, *LDB2*, *CDH11*, *CDH13*, *PDGFR α* , *ISLR*, *HMCN1* and *TSPAN8*. The qRT-PCR analysis of the selected genes confirmed the RNA-seq results (Figure 4f). Of which, a few have been shown to be implicated in ECC/VEC formation. For instance, the chemokine

CXCL12 and its receptor CXCR4 are localized to the endocardial cells of the OFT and atrioventricular cushions, and disruption of this signaling causes cardiac defects (Sierro et al., 2007). CDH11 and PDGFRa have been shown to be expressed in valve endocardial cells and are involved in endocardial cushion formation (Cui et al., 2019; El-Rass et al., 2017). Next, we validated these genes as described below. WB results showed that BMP4 was expressed at higher levels in hPSC-derived VELs and the primary VECs than HUVEC (Figure 4g). IF results showed that CXCL12 and FGD5 were highly expressed in both the primary hVECs and hPSC-derived VELs, but lowly or barely expressed in HUVEC/HAEC (Figure 4h). Similar results were observed for FGD5, GALC, ITM2A and LDB2 (Figure 4i). We specially focused on cell surface markers such as CLDN5, CLDN11, and ITM2A. ITM2A, a single-pass type II membrane protein, is of particular interest to us. Flow cytometry results showed that approximately 77% of day 7 hPSC-derived VELs were ITM2A/VE-cad double positive (Figure 4j), which was close to that of NFATc1/VE-cad positive cells (Figure 2i). The suitability of ITM2A as a VEC surface marker is under more investigation in the lab.

Finally, we examined the mRNA expression of oscillatory shear-related genes such as *EDNI*, *BMP4*, *CTSK*, *PPARG* and *THBS1* (Holliday et al., 2011). Both the scRNA-seq and bulk RNA-seq results showed that these genes were expressed at lower levels in day 7 hPSC-derived VELs than in primary VECs. Similar results were observed for general shear stress response genes such as *KLF2*, *CAVI*, *NOS3* and *ICAMI*. This was confirmed by qRT-PCR analysis of selected genes (Supplementary

Figure 4g). Thus, although hPSC-derived VELs resembled the primary VECs, they were still likely in an immature state, presumably due to lack of the hemodynamic stimulus that are exposed to hVECs in normal physiological conditions (see discussion below).

The combined treatment with BMP4 and TGFb1 promotes VEC fate by activating NOTCH signaling and enhancing *ATF3/KLFs*

So far, we have shown that the crosstalk between BMP and TGF- β signaling pathways is important for directing hPSC-derived CPCs to the VEC-like fate. Remarkably, core NOTCH-related genes such as *NOTCH1/4*, *DLL3/4*, *JAG1/2* and *HEY1/2*, as well as NOTCH target genes such as *FOS*, *NR4A2*, *CD44*, *CDKN1A*, *NFKB1*, *CCDC141*, *GATA2* and *HAND2*, were significantly up-regulated during VEC induction (Figure 2c; Figure 3e; Supplementary Figure 3f). NOTCH signaling is absolutely required for valvulogenesis, and disruption NOTCH signaling blocks ECC and heart valve formation (Papoutsi et al., 2018; Wang et al., 2013). As NOTCH genes such as *NOTCH1/4*, *JAG1* and *HEY1/2* have been shown to be targets of TGF- β /BMP signaling (Garside et al., 2013; Hoogaas et al., 2007; Morikawa et al., 2011; Zawadil et al., 2004), we asked whether NOTCH signaling was activated by the combined treatment with BMP4 and TGFb1. When BMP inhibitor LDN and/or TGF- β inhibitor SB were applied, the expression of NOTCH signaling components and its target genes was greatly reduced (Supplementary Figure 5a,b). Flow cytometry results showed that the percentage of NOTCH4 positive cells was greatly decreased in day 7 cell cultures when CPCs were treated with LDN/SB (30% in treated vs 80% in control) (Figure 5a).

Thus, the combined treatment with BMP4 and TGFb1 may induce the VEC fate at least partially by activating NOTCH signaling.

NFATc1 is a key factor for the induction, maintenance and homeostasis of valve endothelial cells (Wu et al., 2011; Wu et al., 2012). In the mouse model, it has been shown that SMAD binding elements (SBEs) in enhancer regions of *Nfatc1* gene are important for its pro-valve endocardial cell expression (Zhou et al., 2004). Besides, a panel of transcription factors such as *ATF3* and *KLFs* were identified as VEC-specific marker genes by scRNA-seq analysis. Of which, *Atf3* has recently been shown to be highly expressed in the OFT where aortic valve is originated (Yin et al., 2020). SMAD transcription factors, including the R-SMADs and the common SMAD (SMAD4), are the mediators of signal transduction by TGF- β superfamily members which include BMP and TGF- β (Mandal et al., 2016). We thus speculated that the combined treatment with BMP4 and TGFb1 may promote VEC fate by inducing *NFATc1* and *ATF3/KLFs*. We identified two SBEs composed of the sequence CAGACA and one SBE in the proximal promoters of the human *NFATc1* and *ATF3* or *KLF9* genes (*KLF9* not shown here) (Figure 5b). The ChIP-PCR results showed that SMAD4 binding was enriched at promoter regions containing the SBEs in day 3 hPSC-derived VELs (Figure 5b). Next, the luciferase reporter plasmids containing -2kb *NFATc1* and *ATF3* promoters were constructed and subsequently transfected into HEK293T cells in the presence and absence of BMP4 and TGFb1 or the inhibitors of the respective signaling pathways. The luciferase reporter analysis showed that BMP4 and TGF β 1 strongly induced while LDN and SB repressed the luciferase activities

(Figure 5c). Consistently, the expression of NFATc1, ATF3 and KLF9 was significantly decreased when LDN and SB were applied during hPSC-derived CPCs differentiation to VEC-like cells (Figure 5d; Supplementary Figure 5c).

Taken together, we concluded that the combined treatment with BMP4 and TGFb1 may induce the VEC fate at least partially by activating NOTCH signaling at early stage and by enhancing *NFATc1/ATF3/KLFs* at late stage.

Functional characterization of hPSC-derived VELs

Our final protocol for hPSC differentiation into VELs is illustrated in Figure 6a. On average, 3 million CPCs could be obtained from 1 million hPSCs in 3 days. After additional 4-7 days of differentiation, 10-20 million VEC-like progenitor cells can be generated depending the hPSC lines. HPSC-derived VELs could be passaged up to 4 times in vitro with commercial EBM2 medium before eventually adopting a fibroblastic morphology (Supplementary Figure 6a).

In addition to cell type-specific marker characterization, functional assays are important determinants of cell identity and cellular maturity. We thus investigated whether hPSC-derived VELs functionally resembled the primary VECs. A hallmark of ECs is the uptake of LDL both for normal metabolism and under pathologic conditions (Holliday et al., 2011). HPSC-derived VELs were split at a 1:3 ratio and re-plated on Matrigel, and fluorescent-acetylated LDL (Dil-Ac-LDL) uptake assay was performed. HPSC-derived VELs adopted an EC cell morphology and formed vascular network-like structures on Matrigel (Figure 6b), and abundantly expressed

the endothelial markers CD31 and VE-cad as well as the newly-identified candidate markers such as CXCL12 and LDB2 (Figure 6c; Supplementary Figure 6b). To assess the LDL uptake, day 7 hPSC-derived VELs and the primary VECs were incubated with Alexa Fluor 594 conjugated to acetylated LDL (Ac-LDL) for 2 hours. The results showed that hPSC-derived VELs were able to robustly incorporate Dil-Ac-LDL and exhibited relatively homogeneous uptake of LDL as indicated by the red fluorescence in each cell (Figure 6d).

During valvulogenesis, valvular interstitial cells (VICs) are mainly derived from endocardial cushion cells through an EndoMT process that is likely induced by signaling molecules (such as TGF- β , BMPs, WNTs and FGFs) (Combs and Yutzey, 2009; Hinton and Yutzey, 2011; Lincoln et al., 2006). We therefore investigated whether hPSC-derived VELs could be converted to VIC-like cells through EndoMT by treating them with higher concentration of TGFb1 and bFGF over a time course of 6 days. The treated cells were collected every 1.5 days and analyzed as described below (Figure 7a; Supplementary Figure 7a). We found that hPSC-derived VELs quickly lose the cobble-stone morphology, and soon displayed the fibroblastic morphology (Figure 7b). The qRT-PCR analysis showed that after 3 days treatment with high concentration of bFGF and TGFb1, VIC-type markers such as *POSTN*, *ACTA2* and *S100A4/FSP1* were strongly induced (Figure 7a; Supplementary Figure 7b). And the expression of EndoMT-related genes such as *SNAIL*, *TWIST1*, *SOX9*, *AGGRECAN*, *TENASCIN* and *SCLERAXIS* was significantly increased (Lincoln et al., 2006) (Supplementary Figure 7c). IF staining and WB analyses of the treated cells

confirmed that they abundantly expressed FSP1, MRTF-A and VIM, albeit to a lesser levels compared to the isolated primary VICs (Figure 7b-c;) (Latif et al, 2017). These data suggested that VIC-like cells were formed by treating hPSC-derived VELs with high concentration of bFGF and TGFb1.

Next, we investigated whether the VIC-like cells expressed extracellular matrix components (ECM). We found that the expression of ECM-related genes such as *COLLAGEN I (COL1A1)* and *III (COL3A1)* was significantly increased when hPSC-derived VELs were treated with bFGF and TGFb for 6 days (Figure 7d). IF staining was performed using antibodies against COLLAGEN I and III. The IF results showed that day 6 treated cells abundantly expressed COLLAGEN I and III (Figure 7e). Finally, flow cytometry analysis of day 6 treated cells revealed that the vast majority of the cells (> 97%) were FSP1 positive (Figure 7f). Thus, hPSC-derived VELs can be converted to valvular interstitial-like cells very efficiently by inducing EndoMT.

Of note, the ability to efficiently generate both VEC-like and VIC-like cells from hPSCs is important, when both hPSC-derived VECs and VICs are needed to make valve organoids or next generation TEVs for the patient.

HPSC-derived VELs interacts with de-cellularized porcine heart valves

De-cellularized bioprosthetic scaffolds, which are widely used to replace the aortic valve, have exhibited promising results for endogenous endothelialization and mechanical durability (Nejad et al., 2016). We have previously made poly(ethylene

glycol) tetraacrylate (PEG-TA) cross-linked de-cellularized porcine aortic valves (PEG-DCVs) (Hu et al., 2013). Although the acellular PEG-DCVs exhibit significantly improved mechanical and anti-calcification properties when compared to the glutaraldehyde crosslinked counterparts, the poor clinical long-term result remains unsatisfactory likely due to the early tissue degeneration (Zhou et al., 2013). Thus, hPSC-based valve organoids or the next generation tissue engineered heart valves (TEVs) that overcome the shortcomings of the current bioprosthetic valves are highly demanded.

To initially evaluate whether hPSC-derived VELs could be used as the potential seed cells for the valve organoids, we studied the growth and adherent properties of the cells seeded on the modified de-cellularized porcine aortic valves (DCVs). We seeded a total of 4×10^5 hPSC-derived VELs on the DCVs in the presence of 100 ng/ml VEGF and 20 ng/ml bFGF, and the cells were monitored for a time course of 7 days. We found that 1 day after seeding, about 50% of hPSC-derived VELs attached to the surface, similar to HUVEC as revealed by IF staining of F-actin, CD31 and VE-cad antibodies (Figure 8a; Supplementary Figure 8a-b). Cell proliferation assay by EdU staining showed that hPSC-derived VELs were highly proliferative, with 40% of cells being EdU positive at day 3 and 80% of cells being EdU positive at day 4 (Figure 8b). In contrast, apoptosis assay by TUNEL staining showed that TUNEL positive cells were greatly reduced (from approximately 19% at day 2 to 4% at day 4) (Figure 8c). Analysis of dynamic growth for a time course of 7 days demonstrated a robust growth of the seeded VELs on the DCVs (Figure 8d). IF staining of day 7 cells

showed that they co-expressed TIE2 and VIM as well as VE-Cad and BMP4 (Figure 8e). BMP4 has been shown to be expressed in hVECs in both physiological and shear stress conditions and is our newly identified VEC marker in this work (Holliday et al., 2011).

To understand the long term interaction between hPSC-derived VELs and the DCVs, we seeded hPSC-derived VELs at a low density and co-cultured them for 3-4 weeks. A monolayer of endothelium was formed on the surface of the valves, as revealed by immunohistochemistry (IHC) staining for CD31 (Figure 8f). IF staining of the co-cultured DCVs showed that NFATc1 and CD144 were abundantly expressed in the surface of the DCVs, confirming the IHC results (Figure 8g). Interestingly, IF staining results showed that hPSC-derived VELs appeared more evenly distributed and more proliferative than the primary VECs. The observations demonstrated that endothelialization occurred and cell proliferated after long term co-culture of DCVs and hPSC-derived VELs, and that hPSC-derived VELs exhibited superior proliferative and clonogenic potential than the primary VECs.

Taken together, we concluded that hPSC-derived VELs could attach, survive and proliferate when seeded on the de-cellularized porcine aortic valves, which demonstrated that they could have potential implications for modeling valve diseases or use for seed cells for making the valve organoids in the future.

Discussion

There are few studies reporting the generation of valve endothelial-like cells from

hPSCs, likely due to insufficient understanding of VEC biology and/or difficulty in obtaining VECs from human embryos. A recent study has reported the generation of pre-valvular endocardial cells (HPVCs) (Neri et al., 2019). However, the cell identity of HPVCs was primarily based on comparative transcriptome analysis between hPSC-derived HPVCs and mouse atrio-ventricular canal (AVC) endocardial cells. Furthermore, the differentiation approach requires cell sorting, the use of mouse fibroblast cells and the knockout serum, which makes the differentiation variable and invokes potential safety problem in the context of regeneration medicine. In this work, we describe a chemically defined xeno-free method for generating VEC-like cells from hPSCs, by a two step-wise differentiation strategy that mimics the embryonic valvulogenesis. The developmental hierarchy of in vitro hPSC VEC differentiation faithfully recapitulates embryonic valve development events. HPSC-derived VELs exhibit morphological, molecular and functional similarities to that of the primary VECs isolated from normal human aortic valves. Importantly, we demonstrated that when seeded onto the surface of the de-cellularized porcine aortic valve (DCV) matrix scaffolds, hPSC-derived VELs exhibit superior proliferative and clonogenic potential than the primary VECs.

The role of TGF β , BMP and NOTCH signaling in cardiac cushion and valve formation has been well discussed using different models (Garside et al., 2013; Kruithof et al., 2012; Timmerman et al., 2017). Despite the great progress made in the field, there are a number of gaps about the induction and formation of ECCs and VECs. For instance, what are the phenotypical and genetic differences between the

endocardial cushion cells (ECCs) compared to the neighboring endocardial cells at a global or single cell levels? How the ECCs are defined and specified within the endocardium? What controls valve endocardial cell fate determination and how the EndoMT is initiated? And which signaling pathways are involved in the process and what are the key downstream targets or mediators? What is the phenotypical and genetic differences between the ECCs and VECs? How the VEC identity is established and maintained throughout lifetime? Answering these key questions will undoubtedly deepen our understanding of valvulogenesis and valve biology, and benefit the treatment or prevention for valve diseases. As our in vitro hPSC VEC differentiation recapitulates embryonic valvulogenesis, it may serve as a unique system to address the above-mentioned outstanding questions. First, we found that the crosstalk or synergy of BMP and TGF- β signaling pathways is important and sufficient for the specification of VEC fate via an intermediate ECC stage (Lincoln et al., 2006). The requirement of BMP and TGF- β signaling pathways for valve endocardium formation has been described using animal models (Garside et al., 2013; Kruithof et al., 2012), however, whether this is true in human VEC formation remains unclear. We demonstrated here that this mechanism is conserved. Second, we precisely dissected the requirement of key signaling pathways and transcription programs for the determination of VEC cell fate. We found that NOTCH signaling is quickly induced at early stage, and WNT/BMP signaling pathways and a panel of previously known TFs such as *NFATc1*, *HEY2* and *HAND2* and newly identified TFs such as *ATF3* and *KLFs* are activated at late stage as a part of VEC formation (Figure

2c, 3e). The result is in line with a recent report based on the analysis of scRNA-seq of cardiac cells of human embryos (Cui et al., 2019). The ECCs and the VECs exhibit tremendous differences in transcription factor regulatory network and signaling pathway network. The ECCs are highly expressing G1 genes and the VECs are highly expressing G2 genes. As NOTCH signaling is activated downstream of TGF β signaling, it may interpret why addition of DLL4 does not augment the expression of ECC genes, in the presence of VAGFA/BMP4/TGF β 1. We propose that the VEC identity is established and maintained by an integrated network consisting of VEC-specific transcription factors (such as NFATC1/HAND2/HEY2/ATF3/KLFs) and key signaling pathways (such as WNT/BMP). Third, by comparative transcriptome assay of hPSC-derived VELs with VECs from embryos of 5-25W and adults, the cell identity and maturity of in vitro hPSC-derived VELs were evaluated. Importantly, we found that our hPSC VEC differentiation largely recapitulates the key events of in vivo valvulogenesis: day 5 hPSC-derived VELs are analogous to endocardial cushion cells of 7-9W embryos, and day 7 hPSC-derived VELs are analogous to VECs of 20-25W embryos. Thus, we are able to generate VEC-like cells from hPSCs with precise cell maturity corresponding to genuine VECs at different developmental stages. We think this is important, which will facilitate the choice of most suitable starting cells for making the valve organoids or drug screening in the future.

An interesting observation in our current protocol is that constant BMP activities are needed throughout hPSC differentiation into VELs (Figure 6A). This is not

unexpected as BMP is one of the most important morphogens patterning cardiogenic mesoderm during embryogenesis (Kruithof et al., 2012; Jiao et al., 2003). *Bmp4* is expressed in E8.0 when AVC is formed and is required for normal septation of the OFT (Jiao et al., 2003; liu et al., 2004). BMP expression in the AVC myocardium is necessary and sufficient to induce cushion formation and EMT of the adjacent endocardium (Palencia-Desai et al., 2015; Sahara et al., 2014; Sriram et al., 2015; Vincent and Buckingham 2010), and attenuating *Bmp* signaling inhibits SHF differentiation and the subsequent endocardial cushion formation (Brade et al., 2013; Combs and Yutzey, 2016; Hinton and Yutzey, 2011; Kattman, 2011; Lee et al., 1994; Lopez-Sanchez et al., 2015; McCulley et al., 2008; Nakano et al., 2016; Palpant et al., 2015; Rochais et al., 2009). BMP target genes *ID1/2*, *MSX*, *TGFb2*, *TBX2* and *TBX20* are known to be expressed in human valve endocardial cells and important for the endocardial cushion formation (Combs and Yutzey, 2009; Papoutsi et al., 2018; Shelton and Yutzey, 2007; Singh et al., 2011). Mechanistically, BMP signaling may function by promoting the earliest cardiac markers *NKX2.5* and *GATA4* as well as the earliest valve endothelial markers such as *NFATc1*, *JAG1* and *HEY1/2* (Bai et al., 2010; Row et al., 2018; Zhou et al., 2004; Wu et al., 2011).

In vitro hPSC-derived VELs may still represent an immature form of VECs, as revealed by expression levels of shear stress response genes such as *KLF2*, *CAV1*, *NOS3* and *ICAM1* (Supplementary Figure 4g). This is likely because hPSC-derived VELs lack of mechanical stimulus that are exposed to hVECs in normal physiological conditions. It has been shown that EC identity could be better maintained under

continuous stimulation with shear stress or cyclic strain by using bio-reactors in vitro or by grafting the vessel into a host organism in vivo (Nejad et al., 2016). Thus, a better strategy to obtain mature VEC-like cells is to stimulate the immature hPSC-derived VELs by mechanical forces (such as bio-reactor) and tissue-engineered materials that can provide spatial and temporal control over the presentation of proper signaling molecules (cytokines or small molecules). Our long term goal is to make autologous stem cell-based valve organoids with self-renewal and self-assembly capacities after transplantation that could substitute the current mechanical and bioprosthetic valves. The ability to generate both VEC-like and VIC-like cells from hPSCs and the proof-of-concept study of this work predict a promising future of making autologous stem cell-based valve organoids.

Acknowledgement

We thank Prof. Donghui Zhang from Hubei University (Wuhan, China) for providing the PGP1 iPSCs. We thank Prof. Ning Wang from Illinois University and Dr. Weihua Qiao from UNION hospital of HUST for the comments of the manuscript. This work was supported by National Key Research and Development Program of China (2016YFA0101100), National Natural Science Foundation of China (31671526) and Hundred Talents Program to YH Sun, and by National Key Research and Development Program of China (2016YFA0101100) and National Natural Science Foundation of China (81930052) to NG Dong.

Author Contributions: LX Cheng and YY Zhang performed the hPSC VEC differentiation and bioinformatics analysis; Yu Song performed the interaction of hPSC-derived VECs with DCVs; WL Xu, Z Wang, L Wang, K Huang, NG Dong and YH Sun supervised the study.

Declaration of Interests: the authors declare no conflict interests.

Materials and Methods

Isolation of human VECs

Healthy aortic valve tissue specimens were harvested from patients undergoing repair of aortic dissection requiring aortic valve replacement. Side-specific human aortic VECs [from the aortic side (VEC-A) and the ventricular side (VEC-V)] were isolated (according to an Institutional Review Board approved protocol at UNION hospital, HUST) using a brief collagenase digestion and gentle scraping method as previously described (Holliday et al., 2011). Briefly, Human aortic VECs from 7-, 9-, 20-, 30-,

40-, 50-year old were isolated and cultured with ECGM or EBM-2 medium (Lonza) for 1-2 days to examine the cell morphology. To keep the intact features of the isolated VECs, the cells were not passaged and were directly used for RNA-sequencing. The quality of isolated hVECs was evaluated by three criteria. First, the primary VECs were checked morphologically under the microscope. The batch of the isolated VECs with significant contamination with fibroblast-like cells (likely the VICs) was not used for RNA-sequencing. The vast majority of the primary VECs (> 99%) adopted a cobblestone morphology, suggesting that the isolated VECs were not significantly contaminated by the VICs. Second, to further reduce the possibility that the isolated VECs were contaminated by the VICs or other non-valvular cell types, cells with fibroblastic morphology were manually removed. Third, the RNA-seq data were used to double-check the quality of the isolated primary VECs. The RNA-seq results showed that the definitive EC markers *CDH5* and *PECAMI* were highly expressed while the fibroblast markers *SI00A4* and *POSTN* as well as cardiomyocyte markers *TNNT1/2* were barely detectable (RPKM < 5; $P < 0.05$).

Human endothelial cell line HUVEC (#CRL-1730) was purchased from the American Type Culture Collection (Rockville, MD, USA). Human aortic endothelial cell line HAEC (#6100) was purchased from Shanghai Cell Bank, CAS (Shanghai, China).

Maintenance of human PSCs

Human PSCs including human induced pluripotent stem cells (Colunga et al., 2019) and PGP1 human induced pluripotent stem cells (kindly provided by Prof. Zhang

from Hubei University, Wuhan, China), and human ESC lines (H8 and H9 lines, Wicell, WI, USA) were used for this study.

HPSCs were maintained with mTsSR1 medium (STEMCELL Technologies, Canada) or E8 medium (Life Technologies, USA), in feeder-free plates coated with Matrigel (Corning) as previously described (Berger et al., 2016). HPSCs were treated with Accutase (Gibco) for 4 min, and passaged every four days (Singh et al., 2012; 2015). Briefly, single hPSCs were centrifuged at 400 g for 4 min, and seeded onto the Matrigel-coated 6-well plates at 30,000 cell/cm² in mTeSR1 supplemented with 0.1 μM ROCK inhibitor Y-27632 (Tocris, USA).

CPC differentiation

We have previously described the method for the generation of CPCs from hPSCs (Berger et al., 2016). To optimize the generation of ISL1⁺ KDR⁺ CPCs, we further modified the method. HPSCs were passaged as described above and reseeded at 5× 10⁵ cells/cm² (H9) or 8× 10⁴ cells/cm² (H8 and iPSCs) onto the Matrigel coated plates with Essential 6 medium (Gibco) supplemented with 25 ng/ml WNT3a (5036-WN, R&D Systems) and 100 ng/ml BMP4 (314-BP, R&D Systems) for 1 day. Next, cells were cultured in E6 medium supplemented with 50 ng/ml BMP4 and 20 ng/ml bFGF for 3 days with daily medium change.

CPCs to VEC-like cells

HPSC-derived day 3 CPCs were dissociated and seeded at 1× 10⁵ cells/cm² onto cell culture dishes. Cells were cultured for additional 3-9 days in E6 medium

supplemented with 100 ng/ml VEGF, 10 ng/ml BMP4 and 10 ng/ml TGF β 1. The medium was changed every day.

Bulk RNA-sequencing and heat map analysis

HAEC, HUVEC, H9 cells, HFF, the primary VICs, the primary VECs and hPSC-derived VELs were collected and lysed with 1ml Trizol (Transgen Biotech, China). RNA sample quality was checked by the OD 260/280 value using the Nanodrop 2000 instrument. When necessary, hPSC-derived VELs were sorted with VE-cad or CD31 magnetic beads (Miltenyi Biotec, GmbH, Germany) before RNA-sequencing. RNA samples were sent to the BGI China where RNA-sequencing libraries were constructed and sequenced by a BGI-500 system. RNA-seq experiments were repeated at least 2 times. Differentially expressed genes (DEGs) were defined by $FDR < 0.05$ and a Log_2 fold change > 1 was deemed to be DEGs. The heat map was constructed based on the commonly expressed genes in different cell types, and the top 100 DEGs were listed as part of the heat map. Gene ontology (GO) analysis for differentially expressed genes (DEGs) and heat maps were generated from averaged replicates using the command line version of deepTools2.

Single cell RNA-sequencing analysis

Two healthy aortic valve specimens of 40-year old were processed according to the manufacturer's instructions (Document CG00055, 10X genomics) and single-cell gene expression profiles determined by Chromium Single Cell 3' (v2 Chemistry). Single Cell 3' v2 libraries were generated using Single Cell 3' v2 Reagent Kits according to the manual. The libraries were sequenced on the Illumina HiSeq Xten

platform. Data were processed using Cell Ranger (v2.0.1) software. Cell counts were then used to map the reads to a reference genome (hg19) using STAR Aligner (v2.5.1b43). A digital gene expression matrix was constructed from the raw sequencing data as described above. Downstream analyses were performed using Monocle 2 v.2.6.023 software. Statistical analysis was performed using GraphPad Prism (version 8.0) software. All data were analysed and expressed as the mean \pm standard deviation (SD). Differences among groups were statistically compared by analysis of variance (ANOVA). A p -value < 0.05 was considered statistically significant.

Quantitative real-time PCR

Total RNA for cells was extracted with a Total RNA isolation kit (Omega, USA). 1 μ g RNA was reverse transcribed into cDNA with TransScript All-in-One First-Strand cDNA synthesis Supermix (Transgen Biotech, China). Quantitative real-time PCR (qRT-PCR) was performed on a Bio-Rad qPCR instrument using Hieff qPCR SYBR Green Master Mix (Yeasen, China). The primers used for RT-qPCR are listed in Table 2. All experiments were repeated for three times. The relative gene expression levels were calculated based on the $2^{-\Delta\Delta C_t}$ method. Data are shown as means \pm S.D. The Student's t test was used for the statistical analysis. The significance is indicated as follows: *, $p < 0.05$; **, $p < 0.01$; ***, $p < 0.001$.

Western blot analysis

WB analysis was done as previously described (Berger et al., 2016). Briefly, cells

were lysed on ice in SDS lysis buffer (50 mM Tris-HCl, 150 mM NaCl, 5 mM EDTA, 1% TritonX-100, 0.5% Na-Deoxycholate, 1× Protein inhibitor, 1× DTT) for 30 min, shaking for 30s every 5 min. Protein samples were resolved by SDS-PAGE (EpiZyme) and transferred to the PVDF membranes. The blots were incubated overnight at 4°C with primary antibodies against Anti-CD31 (Abcam, ab28364, 1:500), Anti-VE-cadherin (Abcam, ab33168, 1:1000), Anti-NFATc1 (Abcam, ab2796, 1:2000), Anti-ISLET1 (Abcam, ab20670, 1:1000), FSP1 (Abcam, ab124805, 1:1000), anti-TBX2 (Proteintech, 22346-1-AP, 1:200), Anti-BMP4 (Abcam, ab39973, 1:1000) and Anti-GAPDH (Santa Cruz, sc-25778, 1:1000), followed by incubation with a HRP-conjugated goat anti-rabbit IgG (GtxRb-003-DHRPX, ImmunoReagents, 1:5000), a HRP-linked anti-mouse IgG (7076S, Cell Signaling Technology, 1:5000) for 1 hour at room temperature. Western blotting was detected by ECL substrate (Advansta, K-12045-D20) and visualized by LAS4000 mini luminescent image analyzer (GE Healthcare Life Sciences, USA).

Flow cytometry assay

Cells were washed twice with DPBS (BI, China), and digested with Trypsin (BI) for 1 min, followed by wash with DPBS containing 0.5% BSA (0.5% PBSA). Next, cells were centrifuged and washed once with 0.5% PBSA. The resuspended cells in 200 µl 0.5% PBSA were passed through the flow tube to obtain single cells. After that, cells were incubated with the antibodies for 30 min at room temperature. The antibodies used are Anti-NFATc1 (Abcam, ab2796); Anti-ISL1 (Abcam, ab178400); Anti-VE-cadherin (Abcam, ab33168), Anti-CD31 (R&D, FAB35679), Anti-KDR (R&D, FAB3579),

Anti-CDH5 (BD Horizon, 561569), Anti-SOX9 (Proteintech, 67439-1-Ig, 1: 200), Anti-HEY1 (Proteintech, 19929-1-AP, 1: 200), Anti-JAG1 (Proteintech, 668909-1-Ig, 1: 200) or (Invitrogen, PA5-86057), Anti-NOTCH1 (Proteintech, 20687-1-AP, 1: 200), Anti-NOTCH4 (Abcam, ab225329, 1:100), Anti-P-SELECTIN (Proteintech, 60322-1-Ig, 1: 200) and the isotype control antibodies: mouse IgG (R&D, C002P) and rabbit IgG (Invitrogen, 10500C). After 3 times washing, cells were treated with secondary antibodies at room temperature for 15 min. Finally, cells were washed twice and resuspended with 300-500 μ l 0.5% PBSA, and then analyzed by Accuri C6 flow cytometer (BD Biosciences, USA).

Immunofluorescence

Cells were fixed in 4% paraformaldehyde (PFA) for 15 min at room temperature, then were washed 3 times with DPBS containing 5% Triton X-100 for 10 min. Following the incubation with blocking buffer (5% normal horse serum, 0.1% Triton X-100, in PBS) at room temperature for 1 hour, cells were incubated with primary antibodies at 4°C overnight. The primary antibodies used were: ISL1 (Abcam, ab178400, 1:300), CD31 (Abcam, ab28364, 1:80), NOTCH4 (Abcam, ab225329, 1:100), DLL4 (Abcam, ab7280); VE-cadherin (Abcam, ab33168, 1:300), CDH5 (proteintech, 66804-4-Ig, 1:200), NFATc1 (Abcam, ab2796, 1:100), Endomucin (Abcam, ab106100, 1:50), HEY1 (Proteintech, 19929-1-AP, 1: 200), LDB2 (Abcam, ab3627, 1:100), GATA4 (Proteintech, 19530-1-AP, 1:100) , Anti-PROX1 (Proteintech, 11067-2-AP, 1: 200) and NESTIN (Abcam, ab22035, 1:200). After three-times washing with PBST, the cells were incubated with secondary antibodies (1: 500 dilution in antibody buffer,

Alexa Fluor-488 or -555, ThermoFisher) at room temperature for 1 hour in the dark. The nuclei were stained with DAPI (D9542, Sigma, 1:1000). After washing with PBS twice, the slides were mounted with 100% glycerol on histological slides. Images were taken by a Leica SP8 laser scanning confocal microscope (Wetzlar, Germany).

Quantification of immunofluorescence staining was done by ImageJ software. When measuring the number of positive cells, 3-4 random fields per coverslip were counted. DAPI-positive cells (a total of appropriately 500 cells) were counted as the total number of cells. The proportion of cells positive for specific markers was calculated with respect to the total number of DAPI-positive cells, and the results were expressed as the mean \pm s.e.m. of cells in 5-6 fields taken from 3 to 4 cultures of three independent experiments. Differences in means were statistically significant when $p < 0.05$. Significant levels are: * $p < 0.05$; ** $P < 0.01$.

Chromatin Immunoprecipitation (ChIP)

ChIP experiments were performed according to the Agilent Mammalian ChIP-on-chip manual as described (Sun et al., 2020). Briefly, 1×10^8 cells were fixed with 1% formaldehyde for 10 min at room temperature. Then the reactions were stopped by 0.125 M Glycine for 5 min with rotating. The fixed chromatin were sonicated to an average of 500-1,000bp (for ChIP-qPCR) using the S2 Covaris Sonication System (USA) according to the manual. Then Triton X-100 was added to the sonicated chromatin solutions to a final concentration of 0.1%. After centrifugation, 50 μ l of supernatants were saved as input. The remainder of the chromatin solution was incubated with Dynabeads previously coupled with 10 μ g ChIP grade antibodies

(SMAD4, #9515, CST) overnight at 4°C with rotation. Next day, after 7 times washing with the wash buffer, the complexes were reverse cross-linked overnight at 65°C. DNAs were extracted by hydroxybenzene-chloroform-isoamyl alcohol and purified by a Phase Lock Gel (Tiangen, China). The ChIPed DNA were dissolved in 100 µl distilled water. Quantitative real-time PCR (qRT-PCR) was performed using a Bio-Rad qPCR instrument. The enrichment was calculated relative to the amount of input as described. All experiments were repeated at least two times. The relative gene expression levels were calculated based on the $2^{-\Delta\Delta C_t}$ method. Data were shown as means \pm S.D. The Student's t test was used for the statistical analysis. The significance is indicated as follows: *, $p < 0.05$; **, $p < 0.01$; ***, $p < 0.001$.

Low-density lipoprotein uptake assay

HPSC-derived VELs, HUVEC and H9 ESCs (as negative control) were cultured to a confluency of 30-40%. After serum starve of the cells for 12 hours, cells were incubated at a final concentration of 15 ng/ml of Alexa Fluor 594 AcLDL (Invitrogen) for 4 hours at 37°C. The cells were rinsed twice with DPBS and were fixed with 4% PFA for 10 min at room temperature. The nuclei were stained with DAPI (D9542, Sigma, 1:1000). Images were taken by a Leica SP8 laser scanning confocal microscope (Wetzlar, Germany).

In vitro tube formation assay

HPSC-derived VELs, HUVEC and the isolated VECs were cultured on a Matrigel (Corning) coated 96-well plate (Matrigel, #356234, Corning, USA) in EBM-2

medium (Lonza). Images were taken 24 hours later after plating under a phase-contrast microscope.

Interaction between the de-cellularized porcine valves and the VELs

De-cellularized porcine aortic valves were prepared as previously described (Hu et al., 2013; Zhou et al., 2013). Approximately 5×10^5 hPSC-derived VELs, the isolated primary VECs and the control HUVEC were added to the apical surface of the DCV constructs and allowing attachment for 24 hours in a CO₂ incubator. Then the medium was removed and tissue constructs were carefully turned over using sterile forceps, and cells seeding procedure was repeated on the opposite surface of the constructs. The constructs were maintained in culture for a week with medium changed daily or 3-4 weeks to study the long term interaction between the seeded hPSC-derived VELs and the de-cellularized porcine aortic valves.

Transwell assay

HPSC-derived VELs and the isolated VECs were washed twice with PBS. A total of 8×10^4 cells were suspended in 200 μ l serum-free EBM-2 and seeded in the upper chamber of a transwell system (3422, Corning, USA). The lower chamber was filled with 600 μ l EBM-2 containing supplements and growth factors. Cells were allowed to migrate for 6 hours before membranes were fixed with 4% PFA for 10 min and stained with 0.5% crystal violet dyes for 2 hour. The cells on the upper chambers was scraped with a cotton swab. Random fields were photographed under a microscope and cells were counted.

TUNEL staining assay

HPSC-derived VELs and the isolated primary VECs were seeded onto a 96-well plate. After washing twice with PBS, cells were treated with H₂O₂ (200 μM) for 24h. Then TUNEL staining was performed using a TUNEL detection kit (Vazyme biotech Co. Ltd., China) according to the manufacturer's instructions. The microscopic areas were randomly selected and the TUNEL-positive cells were calculated by Image-Pro Plus.

EdU incorporation analysis

HPSC-derived VELs, the isolated primary VECs and HUVEC were seeded on the de-cellularized porcine aortic valves. The EBM-2 culture medium or our home made medium (VEGFA+ BMP4+ TGFb1) was added with 5-ethynyl-2-deoxyuridine (EdU, Ribobio, China). Cells were fixed at 72h and 96h after plating and processed for immunofluorescence by using the Cell-Light EdU Apollo567 In Vitro Kit (C10310-1, Ribobio, China). Images were captured and the number of EdU positive nuclei was counted manually by using Image-Pro Plus software.

Cell viability analysis

HPSC-derived VELs, the isolated VECs and HUVEC were seeded the de-cellularized porcine aortic valves, and seeded at the density of 7×10^3 cells/well. At day 1, 3, 5, and 7 after plating, cells were rinsed with PBS and cultured in 100 μl EBM-2, followed by the addition of 20 μl MTS solution (Promega, USA). A triple number of wells were set for each time point. Cell viability was measured with a spectrophotometer at an absorbance of 490 nm after 1h incubation.

Data availability

All RNA-seq data have been deposited into the database at <https://bigd.big.ac.cn/>. The accession number is PRJCA002549. All other related data will be available upon reasonable request.

Figure Legends

Figure 1. PSCs to cardiogenic mesoderm expressing KDR and ISL1. **a** Schematic of differentiation hPSCs to CPCs, VEC-like cells, and VIC-like cells. X indicates the future cytokines or small molecules for phase 2; Y indicates the future cytokines or small molecules for phase 3. **b** The qPCR analysis of day 3 hPSC-derived CPCs for the indicated markers. **c** IF staining of day 3 CPCs showing that the majority of cells were ISL1 positive. Scale bar: 50 μ m. **d** Quantification analysis of IF staining of panel (c) by ImageJ. Bar graph represents percentage of ISL1 positive cells \pm S.D of three independent experiments. **e** WB analysis of day 3 CPCs using the indicated antibodies. **f** Flow cytometry analysis showing the percentage of KDR and ISL1 positive cells, respectively. **g** The representative morphology of cells during hPSC differentiation to CPCs. All experiments were repeated 3 times. Significant levels are: * p < 0.05; ** P < 0.01; *** P < 0.001. Shown are representative data.

Figure 2. One step differentiation of CPCs to VELs. **a** Schematic of differentiation hPSC-derived CPCs to VEC-like cells. **b** The qRT-PCR analysis of the selected ECC genes for day 6 hPSC-derived cells. Note that the combined treatment with VEGF, BMP4 and TGF β 1 leads to a marked up-regulation of ECC genes. **c** Time-course gene

expression analysis of the indicated genes during hPSCs differentiation to CPCs and CPC to VEC-like cells. The ECC-enriched genes are highlighted by a red box, and the VEC-enriched genes are highlighted by a blue box. **d** IF staining of day 6 hPSC-derived cells, showing double positive cells for NOTCH4/VE-cad, DLL4/VE-cad and CD31/JAG1, respectively. Scale bar: 25 μ m. **e** Percentage of NOTCH4/VE-cad-, DLL4/VE-cad- and CD31/JAG1-double-positive cells of panel (d), quantified by ImageJ. Bar graph represents double positive cells \pm S.D of three independent experiments. **f** Flow cytometry analysis showing the percentage of JAG1/VE-cad double positive cells. Left: epitope controls; Right: JAG1/VE-cad antibodies. **g** IF staining of day 8 hPSC-derived VELs, showing double positive cells for HEY2/VE-cad, PROX1/VE-cad and TBX2/VE-cad, respectively. Scale bar: 25 μ m. **h** WB analysis for day 3 hPSC-derived CPCs and day 8 hPSC-derived VELs, with the indicated antibodies. **i** Flow cytometry analysis showing the percentage of NFATc1/VE-cad and TBX2/VE-cad double positive cells, after treating CPCs with VEGFA/BMP4/TGFb1 for 5 days. All experiments were repeated 3 times. Significant levels are: * p < 0.05; ** P < 0.01; *** P < 0.001. Shown are representative data.

Figure 3 Analysis of the primary VECs at single cell level. **a** The t-distributed stochastic neighbor embedding (t-SNE) showing unbiased clustering results of endothelial cells. **b** Pseudotime trajectory showing the distribution of cardiac endothelial cells. Cells are colored with developmental times. Black arrows show the direction of pseudotime across trajectories. **c** Heat map illustrating the dynamic gene expression patterns of group 1 (G1) and 2 (G2) genes. Note: G1 genes are highly

expressed at early stages; while G2 are highly expressed at later stages. **d** Cartoon showing the dynamic expression of the representative G1 (*Dll4*) and G2 (*WNT2*) genes, based on developmental timing. **e** Heat map illustrating the dynamic gene expression patterns of the indicated signaling pathway genes (top panel) and transcription regulatory genes (bottom panel) identified in G2. Black arrows pointing to TFs with well-known function in VEC induction and/or formation. **f** Heat map showing expression of a panel of G1 and G2 genes in day 3 and day 7 hPSC-derived VEC-like cells. **g** The t-distributed stochastic neighbor embedding (t-SNE) showing unbiased clustering results of the filtered cells ($n = 3,600$) of 40-year-old. **h** 14 major clusters were identified for cardiac valves, based on the well-known marker genes. **i** t-SNE showing the second-level clustering of cluster 11 in (h) into two subclusters, as subcluster 0 and 1. **j** Violin plots showing the expression of indicated genes for subcluster 0 and 1, suggesting that subcluster 0 may represent ventricular side specific VECs and subcluster 1 represents aortic side specific VECs. **k** Validation of the expression of selected G2 genes, showing they are expressed much higher in VECs than HAEC and HUVEC. VEC-A and VEC-V represent VECs isolated from the aortic side and the ventricular side of valves, respectively. qRT-PCR were repeated three times. Significant levels are: $*p < 0.05$; $**P < 0.01$; $***P < 0.001$.

Figure 4. Transcriptome comparison between the VELs and the primary VECs. a

A cartoon showing the design of RNA-seq experiments. HPSC-derived VELs at three time points (CPCs treated with VEGFA/TGFb1/BMP4 for 1, 3 and 6 days) were sequenced. Each time points had at least three experimental repeats. The sampling

information for the primary VECs of different ages is shown in Table 1. **b** Heat map showing the relationships among H9, HAEC, HUVEC, the primary VICs and VECs of 7-year old, and day 7 hPSC-derived VELs. Note that day 7 hPSC-derived VELs are more similar in gene expression to the primary VECs than H9, HAEC, HUVEC and the primary VICs. **c** The pie chart showing number of shared highly-expressed genes between hPSC-derived VELs and the isolated primary VECs of 7-year old (after normalized). **d** KEGG analysis of the shared genes between hPSC-derived VELs and the primary VECs, showing the enrichment of TGF- β , WNT, BMP and NOTCH signaling pathways. **e** Heat map analysis showing that the top 100 genes were highly expressed in the primary VECs and hPSC-derived VELs, but lowly in HAEC/HUVEC. **f** Validation of the selected top-100 genes by qRT-PCR analysis. **g** WB analysis showing that BMP4 was expressed at much higher levels in day 7 hPSC-derived VELs than HUVEC. **h** IF staining results showing that FGD5 and CXCL12 are abundantly expressed in the primary VECs and day 7 hPSC-derived VELs, but lowly expressed in HUVEC and HAEC. **i** IF staining results showing that the expression levels of the indicated markers was much higher in day 7 hPSC-derived VELs than in HUVEC. Scale bar: 100 μ m. **j** Flow cytometry analysis of ITM2A/VE-cad double positive cells in day 7 hPSC-derived VELs, indicating that ITM2A might be a useful VEC surface marker. Left: isotype control. All experiments were repeated 3 times. Significant levels are: * p < 0.05; ** P < 0.01; *** P < 0.001. Shown are representative data.

Figure 5. BMP4 and TGF β 1 induce VEC-like fate by promoting NFATc1. a Flow

cytometry analysis of day 7 hPSC-derived VELs in the presence and absence of SB and LDN, showing the percentage of NOTCH4 positive cells. **b** ChIP experiments showing the enrichment of SMAD4 at *NFATc1* and *ATF3* promoter regions. **c** Luciferase reporter assay showing *NFATc1* and *ATF3* promoter activities in the presence and absence of LDN and SB. **d** WB showing the expression levels of NFATc1 and ATF3 in CPCs that treated with VEGF/BMP4/TGFb1 or VEGF/SB/LDN for 3 days. All experiments were repeated 3 times. Significant levels are: * $p < 0.05$; ** $P < 0.01$; *** $P < 0.001$. Shown are representative data.

Figure 6. Functional characterization of VELs. **a** Cartoon depicting the protocol that is used to differentiate hPSC to VELs in 9 days. **b** Tube formation assay of day 7 hPSC-derived VELs. **c** IF staining showing that hPSC-derived VELs express VE-cad and CD31, similar to the primary VECs. Scale bar: 25 μm . **d** Fluorescence signals showing that hPSC-derived VELs could uptake Ac-LDL, similar to the primary VECs. All experiments were repeated 3 times. Significant levels are: * $p < 0.05$; ** $P < 0.01$; *** $P < 0.001$. Shown are representative data.

Figure 7. HPSC-derived VELs to VIC-like cells by inducing EndoMT. **a** The qPCR analysis of the indicated VIC markers for hPSC-derived VELs that were treated with the indicated signaling molecules for 3-6 days. **b** IF staining of hPSC-derived VIC-like cells showing the expression of the indicated VIC markers. The primary VICs were used as positive controls. Scale bar: 100 μm . **c** WB analysis showing the expression levels of FSP1 in hPSC-derived VEC-like cells and VIC-like cells. **d** The qRT-PCR analysis of type I collagen marker *COL1A1* and type III collagen marker

COL3A1 in hPSC-derived VIC-like cells. The primary VICs were used as positive controls. **e** IF staining showing the expression levels of COLLAGEN I and III in hPSC-derived VIC-like cells, with and without membrane breaking treatment. **f** Flow cytometry analysis showing the percentage of FSP1 positive cells in hPSC-derived VIC-like cells. All experiments were repeated 3 times. Significant levels are: * $p < 0.05$; ** $P < 0.01$; *** $P < 0.001$. Shown are representative data.

Figure 8. HPSC-derived VECs seeded on de-cellularized porcine heart valves. a

IF staining of F-actin showing the morphology of hPSC-derived VECs and HUVEC seeded onto the de-cellularized porcine heart valves. Scale bar: 25 μm . **b** Left panel: the EdU staining of hPSC-derived VELs that have been seeded onto the de-cellularized porcine heart valves for 72 and 96 hours. Right panel: the percentage of EdU positive cells at 72h and 96h. **c** Right panel: TUNEL assay for hPSC-derived VELs seeded onto the de-cellularized porcine heart valves. Right panel: the percentage of TUNEL positive cells at 48h and 72h. **d** A 7-day growth curve of hPSC-derived VELs seeded onto the de-cellularized porcine heart valves. **e** IF staining showing BMP4/VE-Cad and VIM/TIE2 double signals in hPSC-derived VELs seeded onto the surface of the de-cellularized porcine heart valves. Bar: 50 μm . **f** The IHC result showing the lining of the DCVs with hPSC-derived VELs after 3 weeks of co-culturing. Lateral view of the representative DCV. Left: the aortic side of the valve; Right: the ventricular side of the valve. **g** IF staining showing NFATc1 and VE-cad signals in hPSC-derived VELs that have been seeded on the surface of the de-cellularized porcine heart valves for 3 weeks. The primary VECs were used as

controls. Scale bar: 100 μ m. All experiments were repeated 3 times. Significant levels are: * $p < 0.05$; ** $P < 0.01$; *** $P < 0.001$. Shown are representative data.

Table 1 The primary VECs isolated from normal human aortic valves

Age (year-old)	numbers	Aortic side VEC (VEC-A) (Yes/ No)	Ventricular side VEC (VEC-V)(Yes/ No)	VICs (Yes/ No)
7	1	Yes	Yes	Yes
9	1	Yes	Yes	Yes
19	1	No	Yes	Yes
20	1	Yes	Yes	Yes
30	2	Yes	Yes	Yes
43	2	Yes	Yes	Yes
50	2	Yes	Yes	Yes
51	1	Yes	Yes	Yes
59	1	Yes	Yes	Yes

Table 2 The primers used for qRT-PCR analysis

genes	Forward (5'-3')	Reverse (5'-3')
<i>GAPDH</i>	TGTTGCCATCAATGACCCCTT	CTCCACGACGTACTIONCAGCG
<i>NANOG</i>	TCCTGAACCTCAGCTACAAACA	GGTAGGTGCTGAGGCCTTCT
<i>POU5F1</i>	GTGGGGGCAGGGGAGTTTGG	AGTGTGTCTATCTACTGTGTCCCAGGC
<i>T</i>	GGGTGGCTTCTTCCTGGAAC	TTGGAGAATTGTTCCGATGAG
<i>CXCR4</i>	CGCCTGTTGGCTGCCTTA	ACCCTTGCTTGATGATTTCCA
<i>PDGFα</i>	GATTAAGCCGGTCCCAACCT	GGATCTGGCCGTGGGTTT
<i>PDGFβ</i>	TGGCAGAAGAAGCCACGTT	GGCCGTCAGAGCTCACAGA
<i>GATA4</i>	TCCAAACCAGAAAACGGAAGC	GCCCGTAGTGAGATGACAGG
<i>VEGFR2</i>	CGGCTCTTTCGTTACTGTT	TCCTGTATGGAGGAGGAGGA
<i>SOX1</i>	GCGGTAACAACCTACAAAAACTTGTAA	GCGGAGCTCGTCGCATT
<i>NKX2.5</i>	CCAAGGACCCTAGAGCCGAA	ATAGGCGGGGTAGGCGTTAT
<i>MEF2C</i>	ATGGATGAACGTAACAGACAGGT	CGGCTCGTTGTACTCCGTG
<i>ISL1</i>	GCAAATGGCAGCGGAGCCCA	AGCAGGTCCGCAAGGTGTGC
<i>FOXF1</i>	GTACCCGCACCACGACAGCTC	ATACCGCGGGATGCCTTGACG
<i>PECAMI</i>	GCAACACAGTCCAGATAGTCGT	GACCTCAAACCTGGGCATCAT
<i>ETV2</i>	AACACCAGCTGGGACTGTTC	GAGGTTTGACCGGGAATTTT
<i>NFATc1</i>	GCATCACAGGGAAGACCGTGTC	GAAGTTCAATGTCCGAGTTTCTGAG
<i>eNOS</i>	CCAGCTAGCCAAAGTCACCAT	GTCTCGGAGCCATACAGGATT
<i>POSTN</i>	CTGCCAAACAAGTTATTGAGCTGGC	AATAATGTCCAGTCTCCAGGTTG

<i>a-SMA/ACTA2</i>	TTTCCGCTGCCAGAGAC	GTCAATATCACACTTCATGATGCTGT
<i>CDH5</i>	TGTTACGCATCGGTTGTTT	ACTTGGTCATCCGGTTCTGG
<i>S100A4/FSP1</i>	GATGAGCAACTTGGACAGCAA	CTGGGCTGCTTATCTGGGAAG
<i>VIMENTIN</i>	GAAGGCGAGGAGAGCAGGATT	CAAGGTCATCGTGATGCTGAG
<i>HAND2</i>	TACCAGCTACATCGCCTACCT	TCACTGCTTGAGCTCCAGGG
<i>CXCL12</i>	GGGCTCCTGGGTTTTGTATT	GTCTGAGAGTCCTTTTGCG
<i>GATA5</i>	CCTGCGCCTCTACCACAA	GGCGCGCGGGACGAGGAC
<i>CD34</i>	CAACCAGGGGAGCTCAAGTT	AAGACACTACTCGGCTTGGC
<i>JAG1</i>	TCAGTCGGGAGGCAAAT	GCCACCGTTTCTACAAGG
<i>MCAM</i>	TCTCCCAGTCCCAAGGC	CTCCCCAGGTTTCGTCT
<i>JAG2</i>	GACACCAATCCCAACGACT	TAGGCATCGCACTGGAAC
<i>GJA4</i>	CGACCAGTACGGCAACAA	TCATCGCAGAACCCTCCCT
<i>HEY2</i>	TGGGGAGCGAGAACAAT	TCAAAAGCAGTTGGCACA
<i>TNNT1</i>	GCTGGAAGTGAGGATGCC	GCTACCGATGGGACAAACA
<i>IGFBP3</i>	AGCGGGAGACAGAATATGG	TTTGGAAGGGCGCACT
<i>FGF13</i>	TCTGCGAGTGGTGGCTA	CCTGACTGCTGCTGACG
<i>PITX1</i>	TGTCGTCGCAGTCCATGTT	GGAGCCGGTGAGGTTGTT
<i>vWF</i>	CCTTGAATCCAGTGACCCTGA	GGTCCGAGATGTCCTCCACAT
<i>SMAD6</i>	CACTGAAACGGAGGCTACCAAC	CCTGGTCGTACACCGCATAGAG
<i>COL1A1</i>	GATTCCCTGGACCTAAAGGTGC	AGCCTCTCCATCTTTGCCAGCA
<i>TGFb</i>	TACCTGAACCCGTGTGCTCTC	GTTGCTGAGGTATCGCCAGGAA
<i>TGFb2</i>	AAGAAGCGTGCTTTGGATGCGG	ATGCTCCAGCACAGAAGTTGGC
<i>CTSK</i>	GAGGCTTCTCTTGGTGTCCATAC	TTACTGCGGAATGAGACAGGG
<i>EMCN</i>	ACAATTCAGAAAACACCTCA	CACATTCGGTACAAACCCA
<i>MESPI</i>	CTCTGTTGGAGACCTGGATG	CTCAAACCTGCTTGCGTG
<i>EDN1</i>	CTACCTCACCTATATTGCACT	GACCAGACTTCTACGAGGCTA
<i>NES</i>	TCCTACAGCTCCATTCTT	GCAGCACTCTTAACTTACG
<i>NOTCH4</i>	AGTGGCAGAAATAGGAGGG	ATTCCCACTGCCTCCAGAC
<i>DDR1</i>	AGCTCCTGGTCAGATTCCAC	GATCCACCTGCAAGTACTCCT
<i>NFATC4</i>	TCCCTTCAGCATCGGCAAC	AAGCCTTCTGATAGGTAAGGAGT
<i>TAL1</i>	CGATCCCAGTTGGAGGGTTC	CCAGTCCAGGGAATCGCAA
<i>GAL</i>	GTGCTGTAACCTGAAGTCA	ACAGGAATGGCTGACTCT
<i>DLL4</i>	GGACCAGGAGGATGGCT	GCTCAAGGTGCTGTGTTCA
<i>LEFTY1</i>	GCCCTGAATTTGCTTCTC	GACACATTGGGCTTTCTGC
<i>BMP4</i>	CTGGTCTTGAGTATCCTGAGCG	TCACCTCGTTCTCAGGGATGCT
<i>LDB2</i>	TTCCACCAGCAGCACTTCCAAC	TCAGAGTTGGCTCTCCTACCAC
<i>FGD5</i>	CCTTGTCATCGCACAGGAACTG	CTCTGCCTTCATGGTCCATGTC
<i>BGN</i>	TTGAACCTGGAGCCTTCGATGG	TTGGAGTAGCGAAGCAGGTCTT

Supplementary Figure 1. Related to Figure 1. **a** The qRT-PCR analysis of *T* and *MIXL1* for hPSCs treated with BMP4 and Wnt3a for a time course of 3 days. **b** Day 1 hPSC-derived T positive cells were treated with bFGF and BMP4 for a time course of 6 days, and dynamic expression of the indicated genes were examined daily. **c** The qRT-PCR analysis of hPSC-derived day 3 CPCs for the indicated markers. **d** IF staining of day 3 hPSC-derived CPCs for protein expression of NKX2.5. All experiments were repeated 3 times. Significant levels are: * $p < 0.05$; ** $P < 0.01$; *** $P < 0.001$. Shown are representative data.

Supplementary Figure 2. Related to Figure 2. **a** The qRT-PCR analysis of the indicated genes for CPCs that treated with NOTCH inhibitor DAPT or activator DLL4 for 3 days. **b** The qRT-PCR analysis of the indicated genes for CPCs that treated with FGF inhibitor PD or bFGF for 3 days. **c** The qRT-PCR analysis of the indicated genes for CPCs that treated with BMP4 or BMP inhibitor LDN for 3 days. **d** The qRT-PCR analysis of the indicated genes for CPCs that treated with TGF β 1 or TGF inhibitor SB for 3 days. **e** The qRT-PCR analysis of the indicated genes, showing that DLL4 addition did not augment the expression of ECC genes, in the presence of VEGFA/BMP4/TGF β 1. **f** The representative morphology of hPSC-derived CPCs treated with VEGFA, TGF β 1 and BMP4 for a time course of 12 days. **g** Flow cytometry analysis showing the percentage of GATA4/VE-cad double positive cells in day 5 hPSC-derived VELs. **h** IF staining of day 8 hPSC-derived VELs showing the expression of VEC-specific marker NFATc1. Scale bar: 25 μ m. Significant levels are: * $p < 0.05$; ** $P < 0.01$; *** $P < 0.001$. Shown are representative data.

Supplementary Figure 3. **a** Left panel: a tSNE map indicating expression of the indicated VEC marker genes, showing that they are highly expressed in the identified VEC cluster; right panel: violin plots showing the distribution of expression for the indicated genes. **b** Left: a tSNE map indicating expression of the indicated ECC marker genes, showing that they are highly expressed in the identified endocardium; right panel: violin plots showing the distribution of expression for the indicated genes. **c** Pseudotime trajectory showing the distribution of endocardial cells and valvular endothelial cells. Cells are colored with cell types. Black arrows show direction of pseudotime across trajectories. **d** KEGG analysis of G1 and G2 genes. **e** GO analysis of G1 and G2 genes. **f** Dynamic expression of representative G1 and G2 genes in their respective branches for endocardial cells and VECs at different developmental stages. Note that the representative G1 genes are expressed in endocardium of early developmental stage, and the representative G2 genes are expressed in VECs of late stage. **g** a tSNE map indicating expression of the indicated G2 marker genes, showing that they are highly expressed in the two VEC subclusters.

Supplementary Figure 4. Related to Figure 4. **a** Representative image showing the gene numbers and gene expression levels of HUVEC and the primary VECs isolated from aortic valves of different ages. For instance, hVEC-30-1 and hVEC-30-2 are human aortic valve endothelial cells isolated from two 30-year-old individuals. **b** Heat map showing the relationship among HAEC, HUVEC, the primary VECs from different ages and day 7 hPSC-derived VELs. Note that day 7 hPSC-derived VELs is more similar to the primary VECs than HUVEC and HAEC. **c** Heat map of G2 genes

in hPSC-derived VELs (day 3 and 7), the primary VECs, H9 and HAEC, showing G2 genes are expressed higher in VEL and VECs than in HAEC. **d** The qRT-PCR analysis of the selected marker genes for (c). **e** The qRT-PCR analysis of a panel of selected genes for (c). hVEC-A and hVEC-V stand for the primary VECs isolated from the aortic side and the ventricular side of valves, respectively. **f** KEGG analysis of shared genes between day 7 hPSC-derived VELs and the primary hVECs of 9-year old. **g** The qRT-PCR analysis of selected oscillatory shear-related genes, showing that they are expressed at lower levels in day 7 hPSC-derived VELs than in primary VECs. All experiments were repeated 3 times. Significant levels are: $*p < 0.05$; $**P < 0.01$; $***P < 0.001$. Shown are representative data.

Supplementary Figure 5. Related to Figure 5. **a** qRT-PCR analysis of a panel of selected NOTCH-related genes. Note that expression of NOTCH-related genes was decreased when BMP signaling was inhibited by addition of LDN. **b** The qRT-PCR analysis of the indicated genes in various signaling conditions. Note that expression of *NFATc1/HEY2/HAND2/EDN1* was greatly decreased when TGF β signaling was inhibited by addition of SB. **c** The expression of KLF9 in the indicated condition. Significant levels are: $*p < 0.05$; $**P < 0.01$; $***P < 0.001$. ns: not significant. All experiments were repeated 3 times.

Supplementary Figure 6. Related to Figure 6. **a** The morphology of hPSC-derived VELs that have been passaged for 5 times. Note that cells began to show fibroblastic morphology. **b** IF staining of the newly identified markers (Figure 4 h-i) for day 7 hPSC-derived VELs. Scale bar: 25 μ m. All experiments were repeated 3 times. Shown

are representative data.

Supplementary Figure 7. Related to Figure 7. **a** A cartoon diagram showing the experimental design for converting hPSC-derived VELs to VIC-like cells. **b** IF staining of VE-cad and FSP1 of hPSC-derived VIC-like cells. Scale bar: 100 μm . **c** The qRT-PCR analysis of the indicated VIC markers for hPSC-derived VELs that are under the combined treatment with high concentration TGFb1 and bFGF for 4.5 days. All experiments were repeated 3 times. Significant levels are: * $p < 0.05$; ** $P < 0.01$; *** $P < 0.001$. Shown are representative data.

Supplementary Figure 8. Related to Figure 8. **a** IF signals of CD31 in hPSC-derived VELs seeded on the DCVs. **b** IF staining of VE-cad of hPSC-derived VELs after seeded on the DCVs. Scale bar: 20 μm . All experiments were repeated 3 times. Shown are representative data.

References

- Andersen, P., Tampakakis E. , Jimenez, D. V., Kannan, S., Miyamoto, M., Shin, H. K., Saberi, A., Murphy, S., Sulistio, E., Chelko, S. P. & Kwon C. L.** (2018). Precardiac organoids form two heart fields via Bmp/Wnt signaling. *Nat. commun.* **9**, 3140-3154
- Bai, H., Gao, Y. X., Arzigian, M., Wojchowski, D. M., Wu, W. S. and Wang, Z. Z.** (2010). BMP4 Regulates Vascular Progenitor Development in Human Embryonic Stem Cells Through a Smad-Dependent Pathway. *J Cell Biochem.* **109**, 363–374. doi:10.1002/jcb.22410.
- Baron, M., Gao, M. and Lough, J.** (2000). Requirement for BMP and FGF Signaling During Cardiogenic Induction in Non-Precardiac Mesoderm Is Specific, Transient, and Cooperative. *Dev. Dynamic.* **218**, 383–393
- Berger, R. P., Sun, Y. H., Kulik, M., Lee, J. K., Nairn, A. V., Moremen, K. W., Pierce, M., Dalton, S.** (2016). ST8SIA4 dependent polysialylation is part of a developmental program required for germ layer formation from human pluripotent stem cells. *Stem Cells.* **34**(7): 1742–1752.
- Brade, T., Pane, L. S., Moretti, A., Chien, K. R. and Laugwitz, K. L.** (2013). Embryonic Heart Progenitors and Cardiogenesis. *Cold Spring Harb Perspect Med* **3**, a013847
- Colunga, T., Hayworth, M., Kreß, S., Reynolds, D. M., Chen, L. M., Kristopher, L., Baur, J., Singh, A. M., Loring, J. F., Metzger, M. and Dalton, S.** (2019). Human

Pluripotent Stem Cell-Derived Multipotent Vascular Progenitors of the Mesothelium Lineage Have Utility in Tissue Engineering and Repair. *Cell Reports* **26**, 2566–2579

Combs, M. D. and Yutzey, K. E. (2009). Heart Valve Development Regulatory Networks in Development and Disease. *Circ. Res.* **105**, 408-421.

Cui, Y. L., Zheng, Y. X., Liu, X. X. (2019). Single-Cell Transcriptome Analysis Maps the Developmental Track of the Human Heart. *Cell Reports* **26**, 1934–195.

Di Bernardini, E., Campagnolo, P., Margariti, A., Zampetaki, A., Karamariti, E., Hu, Y. H., Xu, Q. B. (2014). Endothelial Lineage Differentiation from Induced Pluripotent Stem Cells Is Regulated by MicroRNA-21 and Transforming Growth Factor β 2 (TGF- β 2) Pathways. *J Biol Chem.* **289**(6): 3383–3393.

EI-Ras, S. et al. (2017). Disruption of *pdgfra* alters endocardial and myocardial fusion during zebrafish cardiac assembly. *Biol. Open* **6**, 348-357

Frank, D. U., Fotheringham, L. K., Brewer, J. A., Muglia, L. J., Tristani-Firouzi, M., Capecchi, M. R. and Moon, A. M. (2002). An *Fgf8* mouse mutant phenocopies human 22q11 deletion syndrome. *Development* **129**, 4591-4603

Garside, V. C., Chang, A. C., Karsan, A. and Hoodless, P. A. (2013). Co-ordinating NOTCH, BMP, and TGF- β Signalling During Heart Valve Development. *Cell Mol Life Sci.* **70**, 2899–2917.

Harris I. S. and Black B. L. (2010). Development of the Endocardium. *Pediatr Cardiol* **31**, 391–399

Hinton, R. B. and Yutzey, K. E. (2011). Heart Valve Structure and Function in Development and Disease. *Annu. Rev. Physiol.* **73**, 29-46.

Holliday, C. J., Ankeny, R. F., Jo, H. J. and Nerem, R. M. (2011). Discovery of shear- and side-specific mRNAs and miRNAs in human aortic valvular endothelial cells. *Am J Physiol Heart Circ Physiol* **301**, 856–867

Hu, X. J., Dong, N.G., Shi, J. W., Deng, C., Li, H.D., Lu C. F. (2013). Evaluation of a novel tetra-functional branched poly(ethylene glycol) crosslinker for manufacture of crosslinked, decellularized, porcine aortic valve leaflets. *J Biomed Mater Res Part B*. 00B, 1–15.

Hoogaars, W.M.H., Barnett, P., Moorman, A.F.M. et al. (2007). Cardiovascular development: towards biomedical applicability. *Cell. Mol. Life Sci.* **64**, 646-660

Hulin, A., Hortells, L., Gomez-Stallons, M. V., O'Donnell, A., Chetal, K., Adam, M., Lancellotti, P., Oury, C., Potter, S. S., Salomonis, N., Yutzey K. E. (2019). Maturation of heart valve cell populations during postnatal remodeling. *Development* **146**, dev173047

Jiao, K., Kulesa, H., Tompkins, K., Zhou, Y. N., Batts, L., Baldwin, H. S. and Hogan, B. L. (2003). An essential role of Bmp4 in the atrioventricular septation of the mouse heart. *Gene. & Dev.* **17**, 2362–2367

Kattman, S., Witty, A. D., Gagliardi, M., Dubois, N. C., Niapour, M., Hotta, A., Ellis, J. and Keller, R. G. (2011). Stage-specific optimization of activin/Nodal and BMP signaling promotes cardiac differentiation of mouse and human pluripotent stem cell lines. *Cell Stem Cell* **8**, 228–240

Kruithof, B. P., Duim, S. N., Moerkamp, A. T., Goumans, M. J. (2012). TGF β and BMP signaling in cardiac cushion formation: Lessons from mice and chicken.

Differentiation **84**, 89–102

Laforest, B. and Nemer M. (2012). Genetic insights into bicuspid aortic valve formation. *Cardiology Research and Practice*. doi:10.1155/2012/180297

Lamouille, S., Xu, J. and Derynck, R. (2014). Molecular mechanisms of epithelial–mesenchymal transition. *Nat. Rev. Mol. Cell Biol.* **15**(3), 178–196.

Latif, N., Quillon, A., Sarathchandra, P., McCormack, A., Lozoski, A., Yacoub, M. H., Chester A. H. (2015) Modulation of human valve interstitial cell phenotype and function using a fibroblast growth factor 2 formulation. *PLoS ONE* **10**(6), e0127844. doi:10.1371/journal.pone.0127844

Lincoln, J., Alfieri, C. M., Yutzey, K. E. (2006). BMP and FGF regulatory pathways control cell lineage diversification of heart valve precursor cells. *Dev. Biol.* **292**, 290–302

Liu, W., Selever, J., Wang, D. G., Lu, M. F., Moses, K. A., Schwartz, R. J. and Martin, J. F. (2004). Bmp4 signaling is required for outflow-tract septation and branchial-arch artery remodeling. *PNAS* **101**, 4489–4494

Lui, K. O., Zangi, L., Silva, E. A., Bu L., Sahara, M., Li, R. A., Mooney, David, Chien, K. R. (2013). Driving vascular endothelial cell fate of human multipotent Isl1+ heart progenitors with VEGF modified mRNA. *Cell Res.* **23**, 1172-1186

Lyer, D., Gambardella, L., Bernard, W. G., Serrano, F., Mascetti, V. L., Pedersen, R. A., Talasila, A. and Sinha, S. (2015). Robust derivation of epicardium and its differentiated smooth muscle cell progeny from human pluripotent stem cells *Development* **142**, 1528-1541

Marques, S. R., Lee, Y., Poss, K. D., Yelon, D. (2008). Reiterative roles for FGF signaling in the establishment of size and proportion of the zebrafish heart. *Dev. Biol.* **321**, 397-406.

McCulley, D. J., Kang, J. O., Martin, J. F. and Black B, L. (2008). BMP4 Is Required in the Anterior Heart Field and Its Derivatives for Endocardial Cushion Remodeling, Outflow Tract Septation, and Semilunar Valve Development, *Dev. Dynamics* **237**, 3200–3209

Milgrom-Hoffman, M., Harrelson, Z., Ferrara, N., Zelzer, E., Evans, S. M. and Tzahor, E. (2011). The heart endocardium is derived from vascular endothelial Progenitors. *Development* **138**, 4777-4787

Misfeldt, A. M., Boyle, S. C., Tompkins, K. L., Bautch, V. L., Labosky, P. A., Baldwin, H. S. (2009). Endocardial cells are a distinct endothelial lineage derived from Flk1+ multipotent cardiovascular progenitors. *Dev. Biol.* **333**, 78–89

Monaghan M. G., Linneweh M., Liebscher S., Van Handel B., Layland S. L. and Schenke-Layland K. (2016). Endocardial-to-mesenchymal transformation and mesenchymal cell colonization at the onset of human cardiac valve development. *Development* **143**, 473-482

Moretti, A., Caron, L., Nakano, A., Lam, J. T., Bernshausen, A., Chen, Y. H., Ouyang, Y. B., Bu, L., Sasaki, M., Martin-Puig, S., Sun, Y. F., Evans, S. M., Laugwitz, K. L. and Chien, K. R. (2006). Multipotent embryonic Isl1+ progenitor cells lead to cardiac, smooth muscle and endothelial cell diversification. *Cell* **127**, 1151–1165

Muhamud et al. GATA2 controls lymphatic endothelial cell junctional integrity and lymphovenous valve morphogenesis through miR-126. (2019). *Development* **146**, dev184218. doi:10.1242/dev.184218.

Morikawa, M., Koinuma, D., Tsutsumi, S., Vasilaki, E., Kanki, Y., Heldin, C., Aburatani, H. and Miyazono, K. (2011). ChIP-seq reveals cell type-specific binding patterns of BMP-specific Smads and a novel binding motif. *Nucleic Acids Res.* **39**, 8712 – 8727

Nakano, A., Nakano H., Smith, K. A., Palpant, N. P. (2016). The developmental origins and lineage contributions of endocardial endothelium. *Biochimica. et Biophysica. Acta.* **1863**, 1937 – 1947

Nejad, S. P., Blaser, M. C., Santerre, J. P., Christopher, Caldarone, A., Simmons, C. A. (2016). Biomechanical conditioning of tissue engineered heart valves: Too much of a good thing? *Adv. Drug Delivery Rev.* **96**, 161 – 175

Neri, T., Hiriart, E., van Vliet, P. P., Faure, E., A., Norris, R., Farhat, B., Jagla B., Lefrancois, J., Sugi, Y., Moore-Morris, T., Stéphane Zaffran, R. S., Faustino, A. C. et al. (2019). Human pre-valvular endocardial cells derived from pluripotent stem cells recapitulate cardiac pathophysiological valvulogenesis. *Nat. Commun.* **10**:1929

Nolan, D. J., Ginsberg, M., Israely, E., Palikuqi, B., Poulos, M. G., James, D., Ding, B. S., Schachterle, W., Liu, Y., Rosenwaks, Z., Butler, J. M., Xiang, J., Rafii, A., Shido, K. et al. (2013). Molecular Signatures of Tissue-Specific Microvascular Endothelial Cell Heterogeneity in Organ Maintenance and Regeneration. *Dev Cell.* **26**(2), 10

Palencia-Desai, S., Rost, M. S., Schumacher, J. A., Ton, Q. V., Craig, M. P., Baltrunaite, K., Koenig, A. L., Wang, J. H., Poss, K. D., Chi, N. C., Stainier, D. Y., Sumanas, S. (2015). Myocardium and BMP signaling are required for endocardial differentiation. *Development* **142**(13), 2304–2315.

Palpant, N. J., Pabon, L., Rabinowitz, J. S., Hadland, B. K., Stoick-Cooper, C. L., Paige, S. L., Bernstein, I. D., Moon, R. T. and Murry, C. E. (2013). Transmembrane protein 88: a Wnt regulatory protein that specifies cardiomyocyte development. *Development* **140**, 3799-3808

Papoutsis, T., Luna-Zurita, L., Prados, B., Zaffran, S. and de la Pompa J. L. (2018). Bmp2 and NOTCH cooperate to pattern the embryonic endocardium. *Development* **145**: dev163378, doi: 10.1242/dev.163378

Park, E. J., Watanabe, Y., Smyth, G., Miyagawa-Tomita, S., Meyers, E., Klingensmith, J., Camenisch, T., Buckingham, M. and Moon, A. M. (2008). An FGF autocrine loop initiated in second heart field mesoderm regulates morphogenesis at the arterial pole of the heart. *Development* **135**, 3599-3610

Patsch, C., Challet-Meylan, L., Thoma, E. C., Urich, E., Heckel, T., O’Sullivan, J. F., Grainger, S. J., Kapp, F. G., Sun, L., Christensen, K., Xia, Y. L., Florido, M. H. C., He, W., Pan, W., Prummer, M. et al. (2015). Generation of vascular endothelial and smooth muscle cells from human pluripotent stem cells. *Nat. Cell. Biol.* **17**(8): 994–1003

Pucéat, M. (2013). Embryological origin of the endocardium and derived valve progenitor cells: From developmental biology to stem cell-based valve repair.

Biochimica et Biophysica Acta **1833**, 917–922

Rochais, F., Mesbah, K., Kelly R. G. (2009). Signaling pathways controlling second heart field development. *Circ Res.* **104**, 933-942.

Row, R. H., Pegg, A., Kinney, B. A., Farr, G. H., Maves, L., Lowell, S., Wilson, V. and Martin, B. L. (2018). BMP and FGF signaling interact to pattern mesoderm by controlling basic helix-loop-helix transcription factor activity. *Elife*, **7**, e31018

Sahara, M., Hansson, E. M., Wernet, O., Lui, K. O., Später, D., Chien, K. R. (2014). Manipulation of a VEGF-NOTCH signaling circuit drives formation of functional vascular endothelial progenitors from human pluripotent stem cells. *Cell Res.* **24**, 820-841.

Sierro, F. et al. (2017). Disrupted cardiac development but normal hematopoiesis in mice deficient in the second CXCL12/SDF-1 receptor, CXCR7. *PNAS* **104**, 14759-14764.

Shelton E. L. and Yutzey, K. E. (2007). Tbx20 Regulation of Endocardial Cushion Cell Proliferation and Extracellular Matrix Gene Expression. *Dev. Biol.* **302**, 376–388.

Singh, A. M., Reynolds, D., Cliff, T., Ohtsuka, S., Mathyses, A., Sun, Y. H., Menendez, L., Kulik, M., Dalton, S. (2012). Signaling network cross-talk in human pluripotent cells: a Smad2/3-regulated switch that controls the balance between self-renewal and differentiation. *Cell Stem Cell.* **10**(3): 312–326

Singh, A. M., Sun, Y. H., Li, L., Zhang, W. J., Wu, T. M., Zhao, S. Y., Qin, Z. H., Dalton, S. (2015). Cell-Cycle Control of Bivalent Epigenetic Domains Regulates the Exit from Pluripotency. *Stem Cell Reports.* **5**(3): 323–336.

Singh R., Hoogaars, W. M., Barnett, P., Grieskamp, T., Sameer Rana, M., Buermans H., Farin H. F., Petry M., Heallen T., Martin, J. F., Moorman, A. F. M., 't Hoen, P. A. C., Kispert, A. (2012). Tbx2 and Tbx3 induce atrioventricular myocardial development and endocardial cushion formation. *Cell. Mol. Life Sci.* **69**, 1377–1389

Sriram, G., Tan, J. Y., Islam, I., Rufaihah, A. J. and Cao, T. (2015). Efficient differentiation of human embryonic stem cells to arterial and venous endothelial cells under feeder- and serum-free conditions. *Stem Cell Res. & Ther.* **6**, 261-278

Sun, X. Y., Peng, X. X., Cao, Y. Q., Zhou, Y., Sun, Y. H. (2020). ADNP promotes neural differentiation by modulating Wnt/ β -catenin signaling. *Nat. Commun.* **11**, 2984-2999. <https://doi.org/10.1038/s41467-020-16799-0>

Tan, J. Y., Sriram, G., Rufaihah, A. J., Neoh, K. G. and Cao T. (2013). Efficient Derivation of Lateral Plate and Paraxial Mesoderm Subtypes from Human Embryonic Stem Cells Through GSKi-Mediated Differentiation. *Stem Cells Dev.* **22**(13): 1893–1906

VanDusen, N. J., Casanovas, J., Vincentz, J. W., Firulli, B. A., Osterwalder, M., Lopez-Rios, J., Zeller, R., Zhou, B., Grego-Bessa, J., Pompa, J. L., Shou, W. N. and Firulli, A. B. Hand2 is an essential regulator for two NOTCH-dependent functions within the embryonic endocardium. (2014). *Cell Reports* **9**, 2071–2083

Wang, Y., Wu, B., Chamberlain, A. A., Lui, W., Koirala, P., et al. (2013) Endocardial to Myocardial NOTCH-Wnt-Bmp Axis Regulates Early Heart Valve Development. *PLoS ONE* **8**(4): e60244. doi:10.1371/journal.pone.0060244

White, M. P., Rufaihah, A. J., Liu, L., Ghebremariam Y. T., Ivey, K. N., Cooke, J. P., Srivastava, D. (2013). Limited Gene Expression Variation in Human Embryonic Stem Cell and Induced Pluripotent Stem Cell Derived Endothelial Cells. *Stem Cells*. **31**(1): 92–103

Wilson, H. K. Canfield, S. G. Shusta, E. V. Palecek, S. P. (2014). Concise Review: Tissue-Specific Microvascular Endothelial Cells Derived From Human Pluripotent. *Stem Cells* **32**, 3037 – 3045

Wu, B. R., Zhang, Z., Lui, W., Chen, X. J., Wang, Y. D., Chamberlain, A. A., Moreno-Rodriguez, R. A., Markwald, R. R., O'Rourke, B. P., Sharp, D. J., Zheng, D. Y., Lenz, J., Baldwin, H. S., Chang, C. P., Zhou, B. (2012). Endocardial cells form the coronary arteries by angiogenesis through myocardial-endocardial VEGF signaling. *Cell* **151**, 1083–1096

Wu, B. R., Wang, Y. D., Lui, W., Langworthy, M., Tompkins, K. L., Hatzopoulos, A. K., Baldwin, H. S., Zhou, B. (2011). Nfatc1 Coordinates Valve Endocardial Cell Lineage Development Required for Heart Valve Formation. *Circ Res*. **109**, 183-192

Yamagishi, T., Ando K., Nakamura H. (2009). Roles of TGFb and BMP during valvulo–septal endocardial cushion formation. *Anat. Sci. Int.* **84**, 77–87

Yang, B., Zhou, W., Jiao, J. et al. (2017). Protein-altering and regulatory genetic variants near GATA4 implicated in bicuspid aortic valve. *Nat. Commun.* **8**, 15481-15490

Yin, H. et al. (2020). Activating transcription factor 3 coordinates differentiation of cardiac and hematopoietic progenitors by regulating glucose metabolism. *Sci. Adv.* **6** :

eaay9466

Zavadil, J., Cermak, L., Soto-Nieves, N. and Bottinger, E. P. (2004). Integration of TGF- β /Smad and Jagged1/NOTCH signalling in epithelial-to-mesenchymal transition. *The EMBO Journal* **23**, 1155–1165

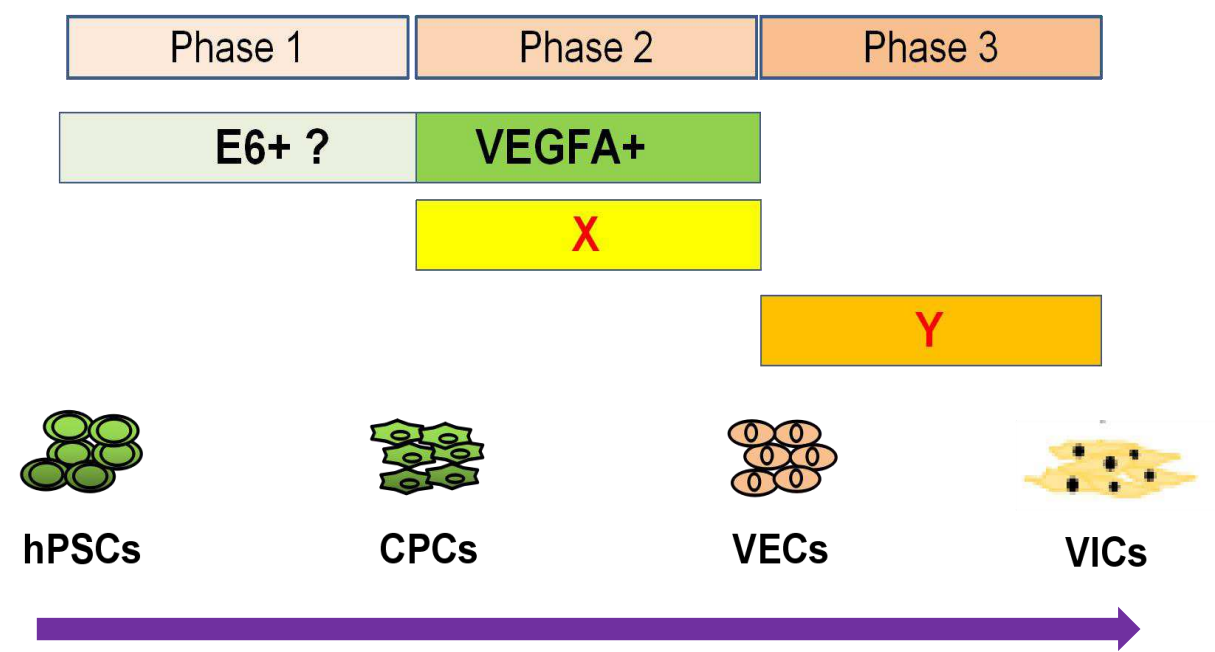
Zhang, J., Chang, Y. F., Huang, Y. Q., Lin, X., Luo, Y. D., Schwartz, R. J., Martin, J. F. and Wang, F. (2010). The FGF-BMP signaling axis regulates outflow tract valve primordium formation by promoting cushion neural crest cell differentiation. *Circ Res.* **107**(10), 1209–1219

Zhou, B., Wu, B.R., Baldwin, H. S. (2004). Characterization of Nfatc1 regulation identifies an enhancer required for gene expression that is specific to pro-valve endocardial cells in the developing heart. *Development* **132**, 1137-1146

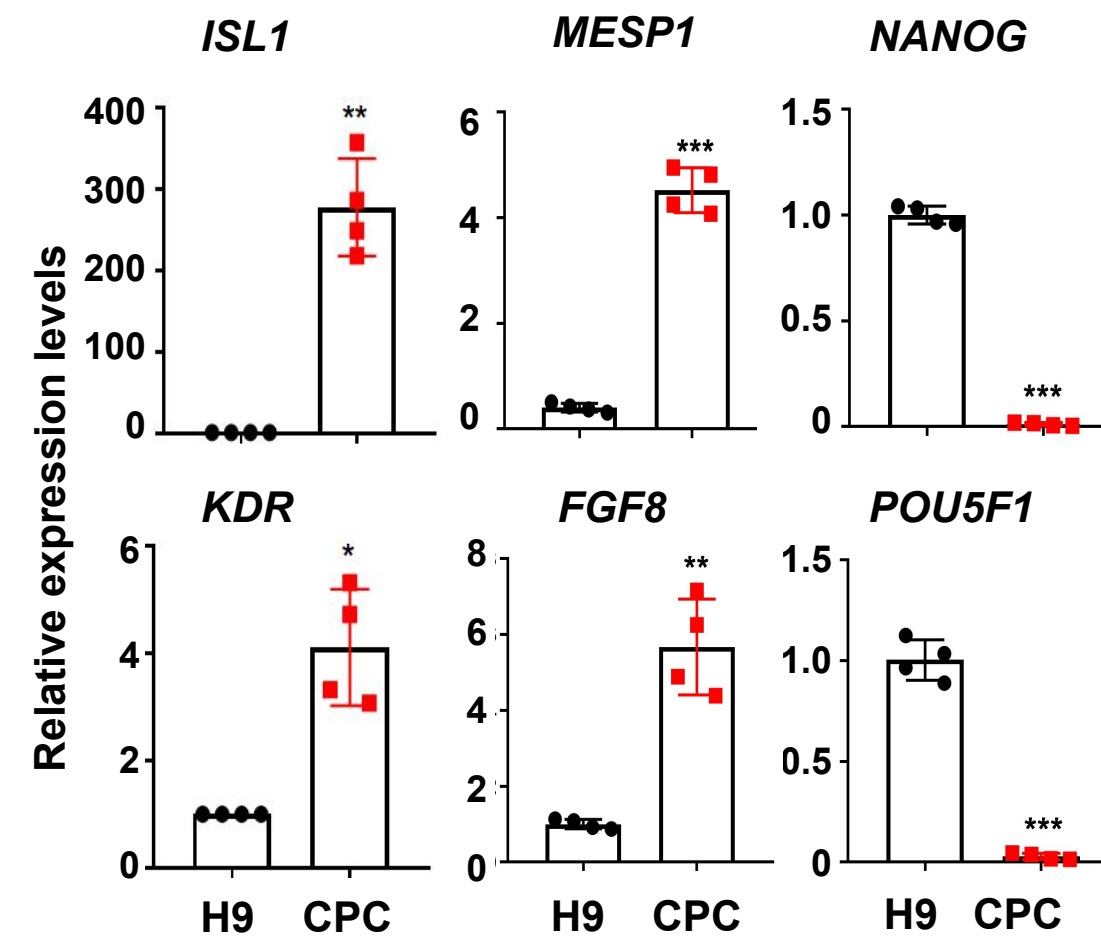
Zhou, J. L., Hu, S. D., Ding, J. L., Xu, J. J., Shi, J. W. and Dong, N. G. (2013). Tissue engineering of heart valves: PEGylation of decellularized porcine aortic valve as a scaffold for in vitro recellularization. *BioMedical. Eng. Online.* **12**, 87-97

Figure 1 PSCs to cardiogenic mesoderm cells (CPCs) expressing *KDR* and *ISL1*

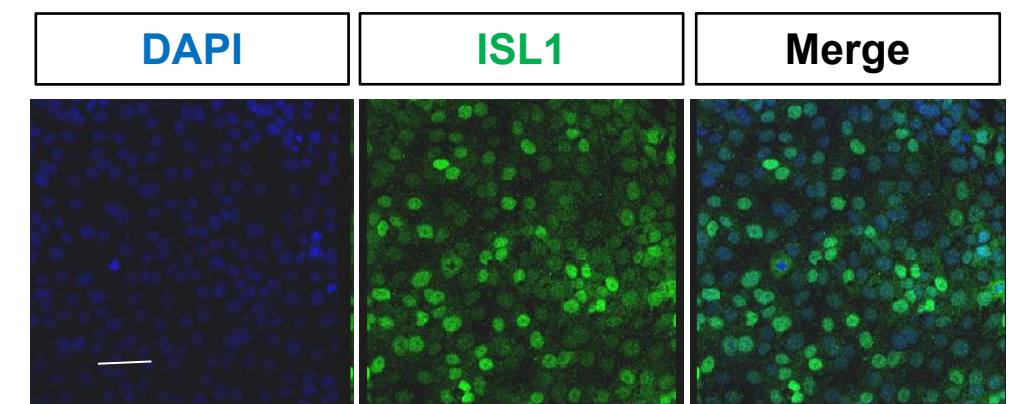
a



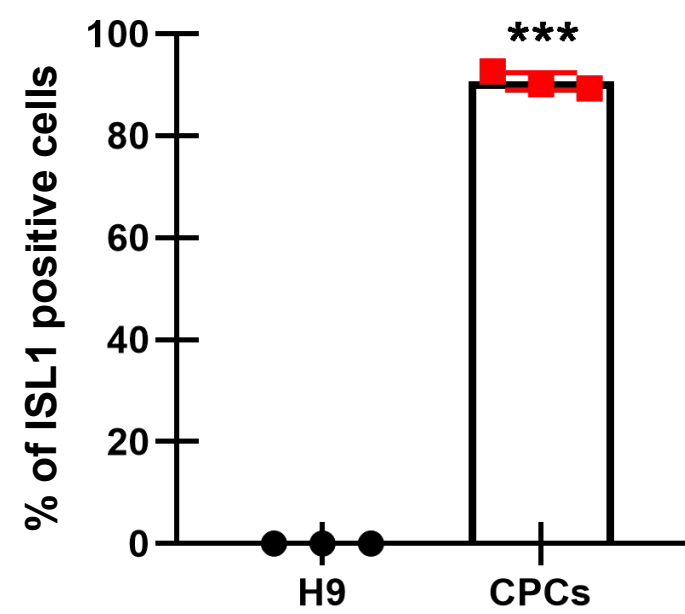
b



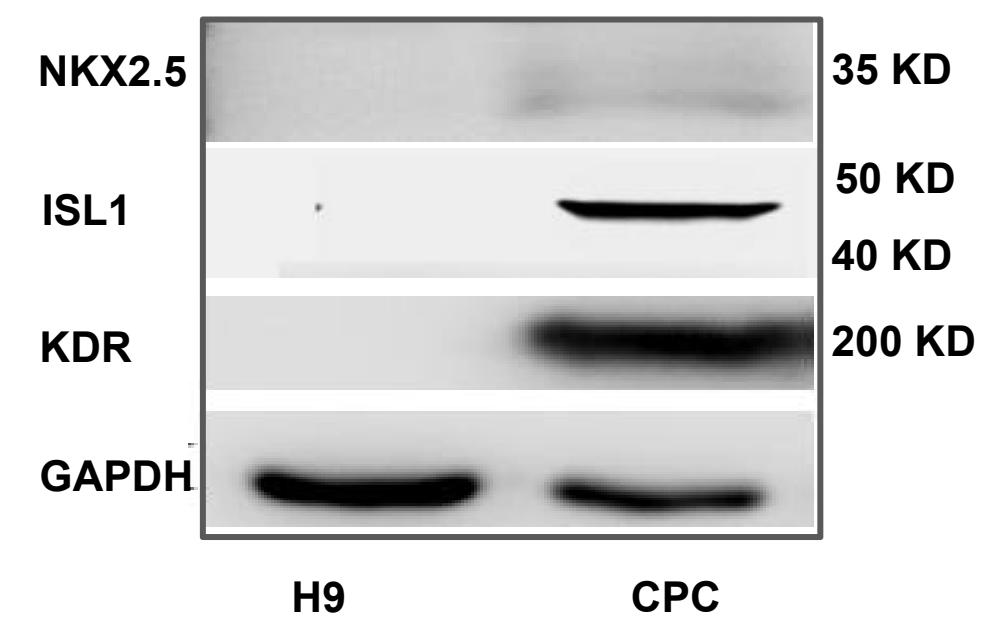
c



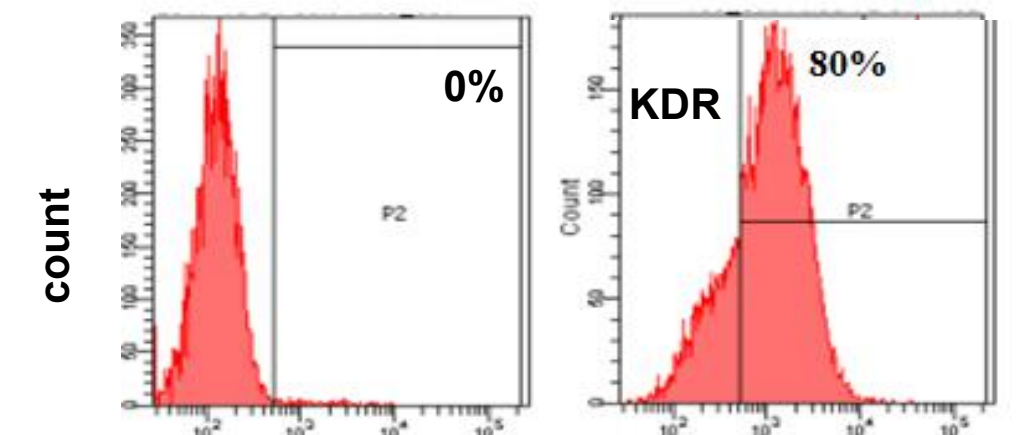
d



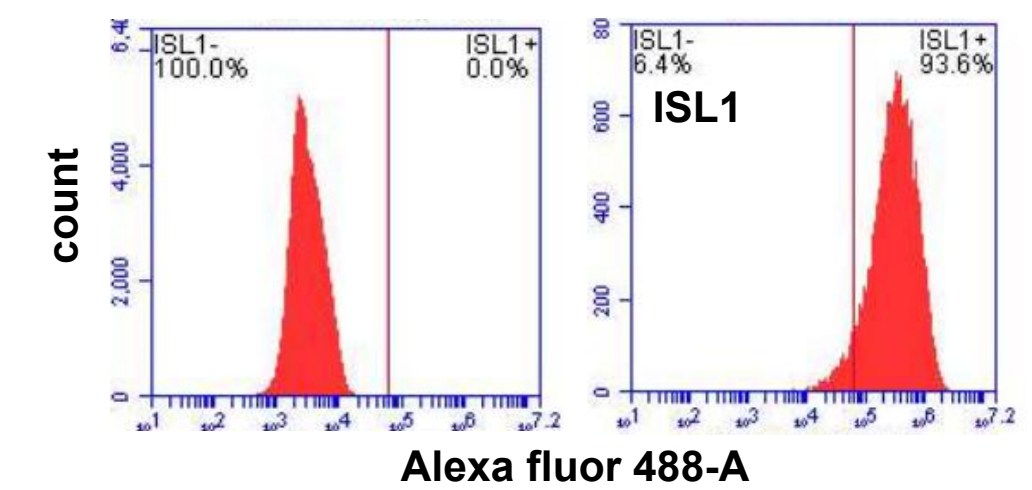
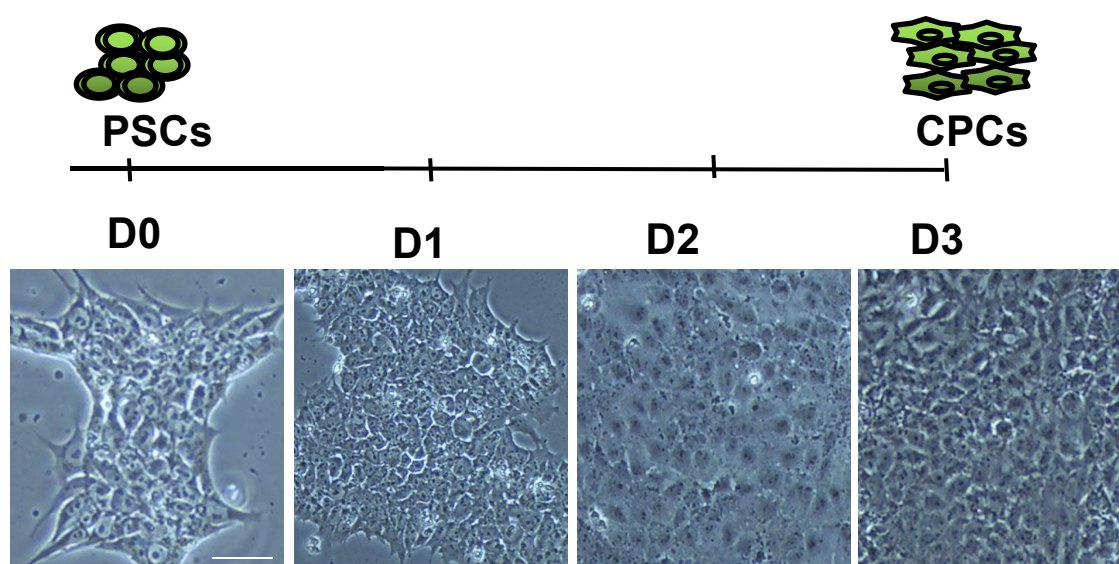
e



f



g



Supplementary Figure 1

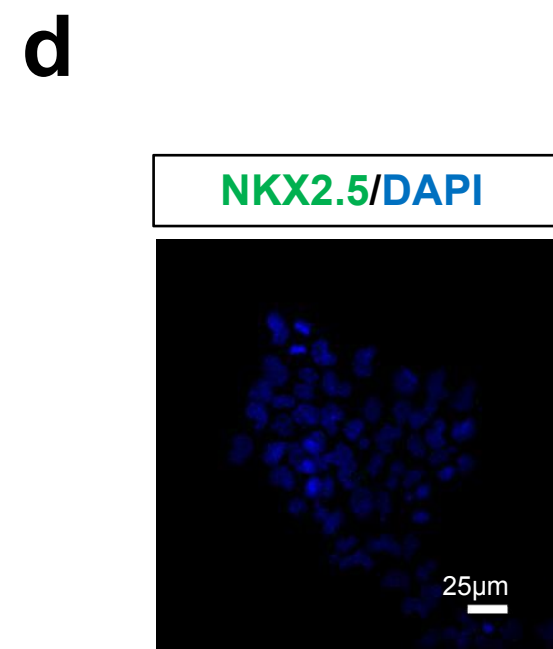
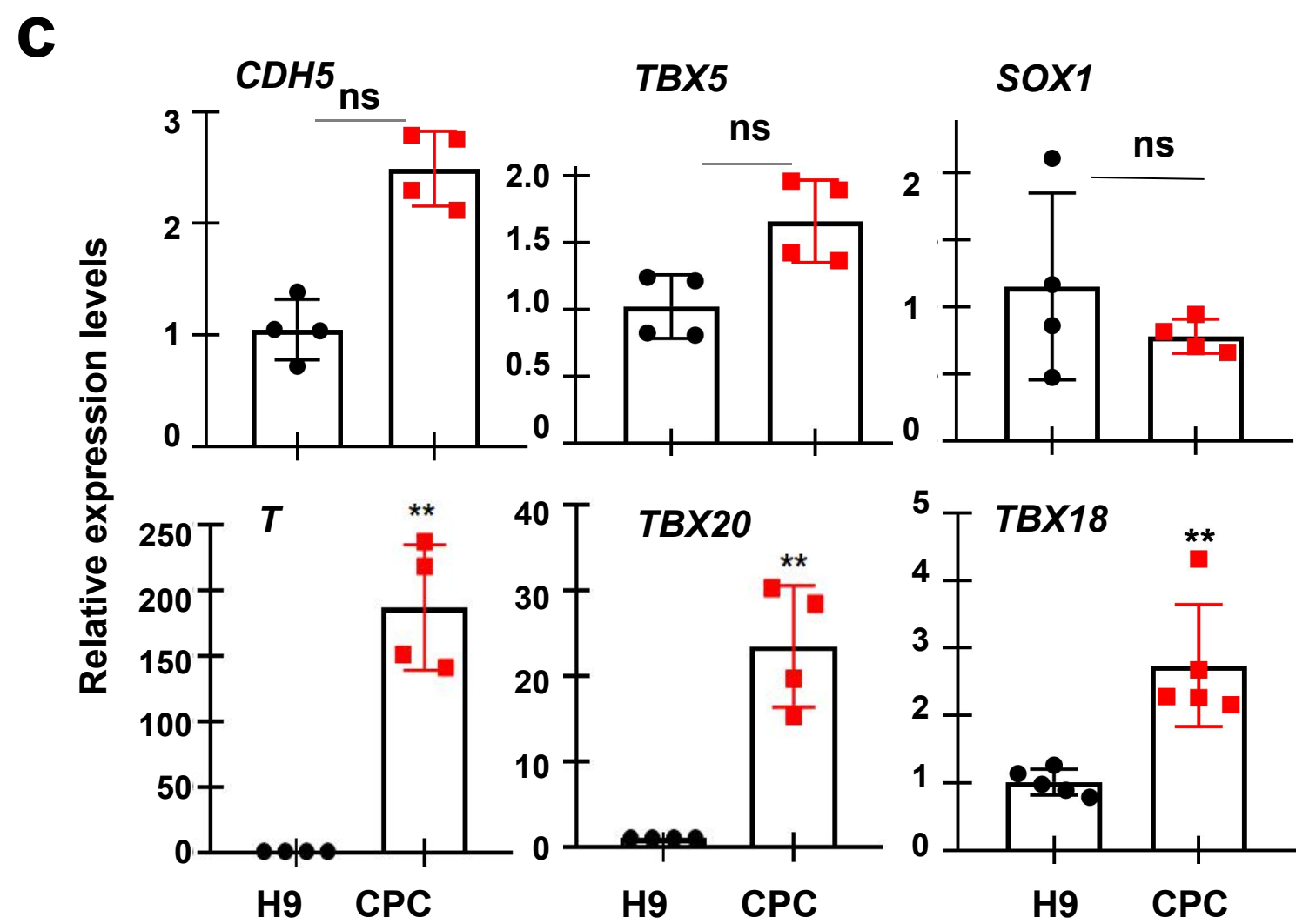
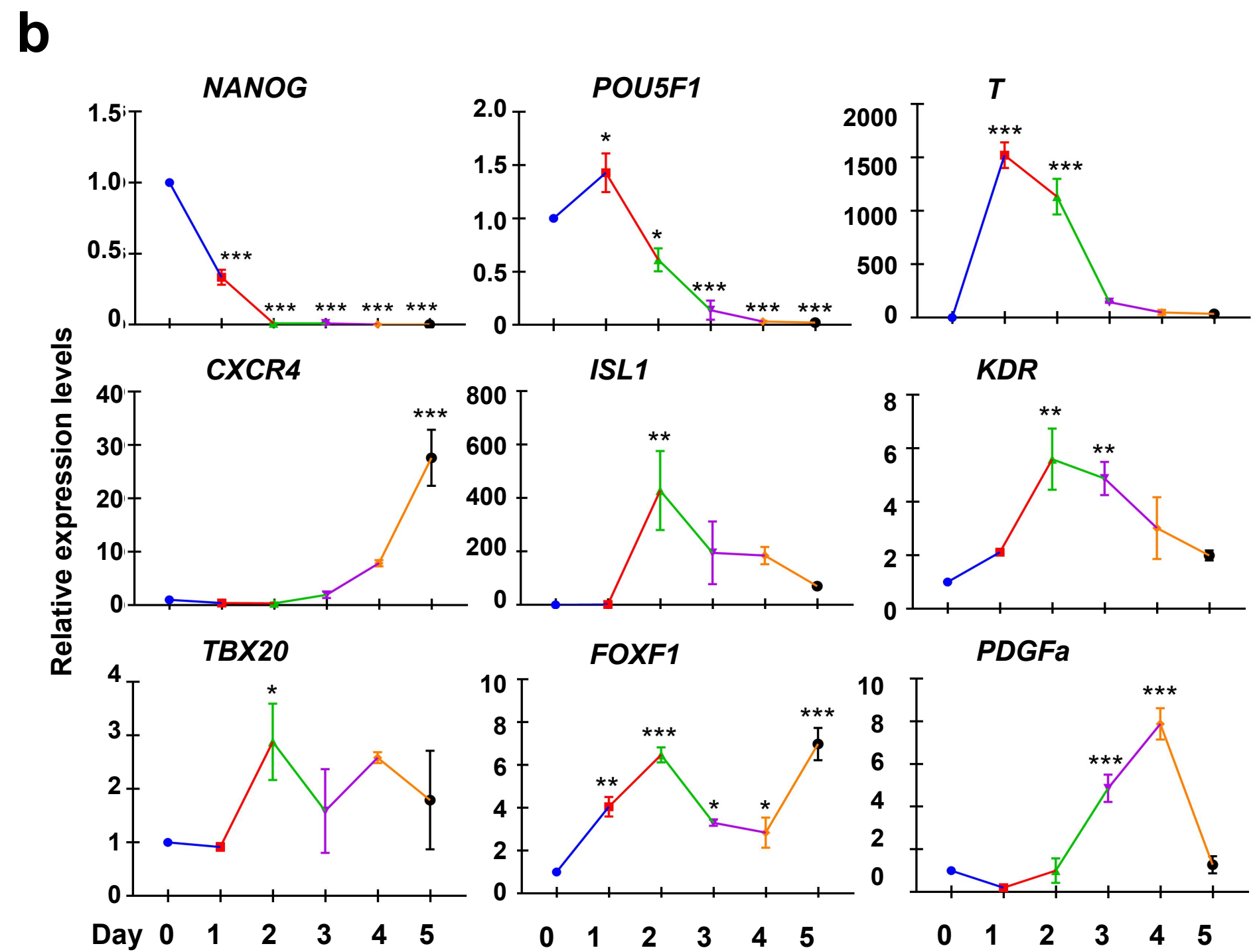
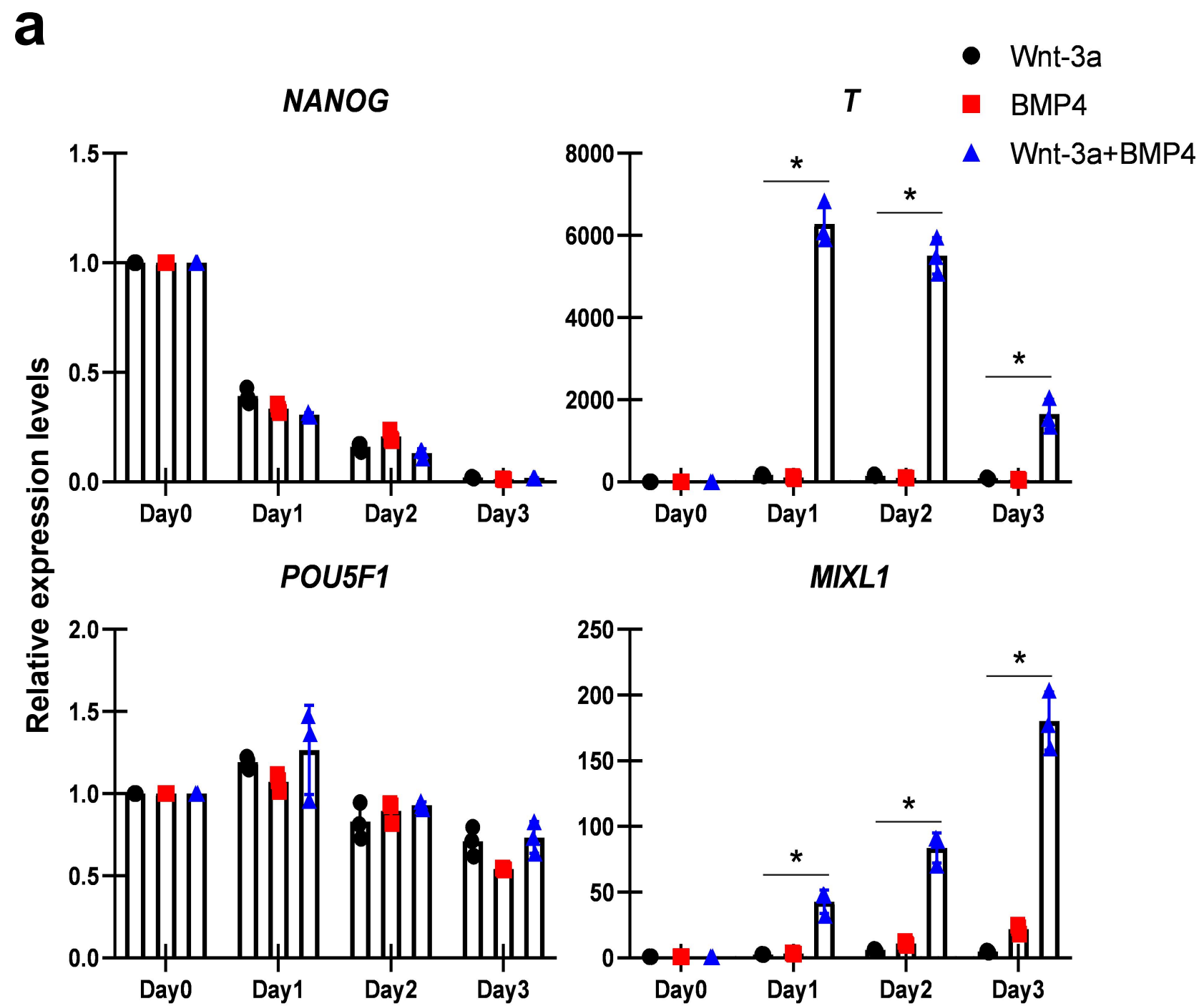
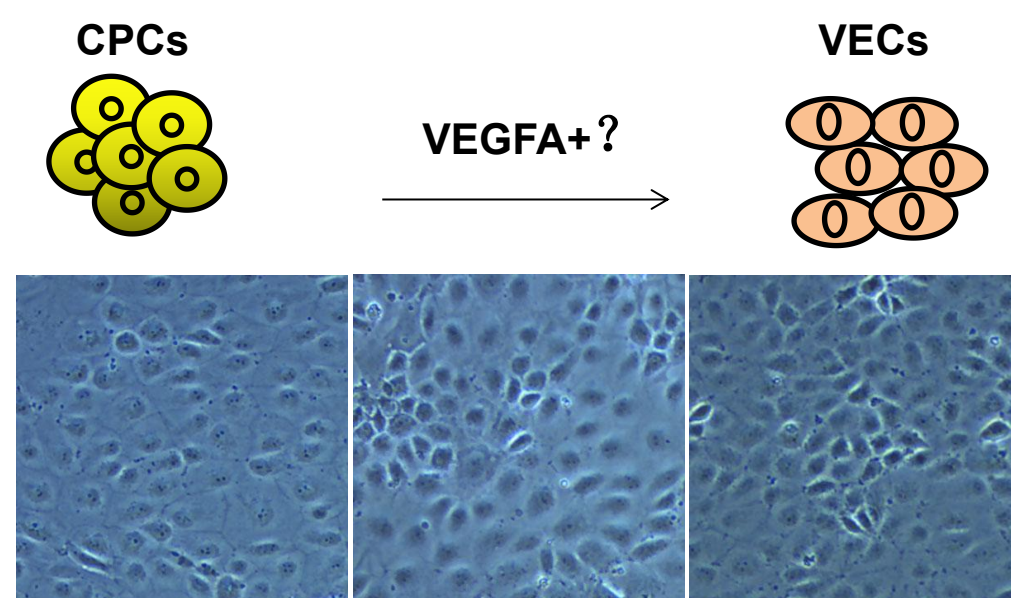
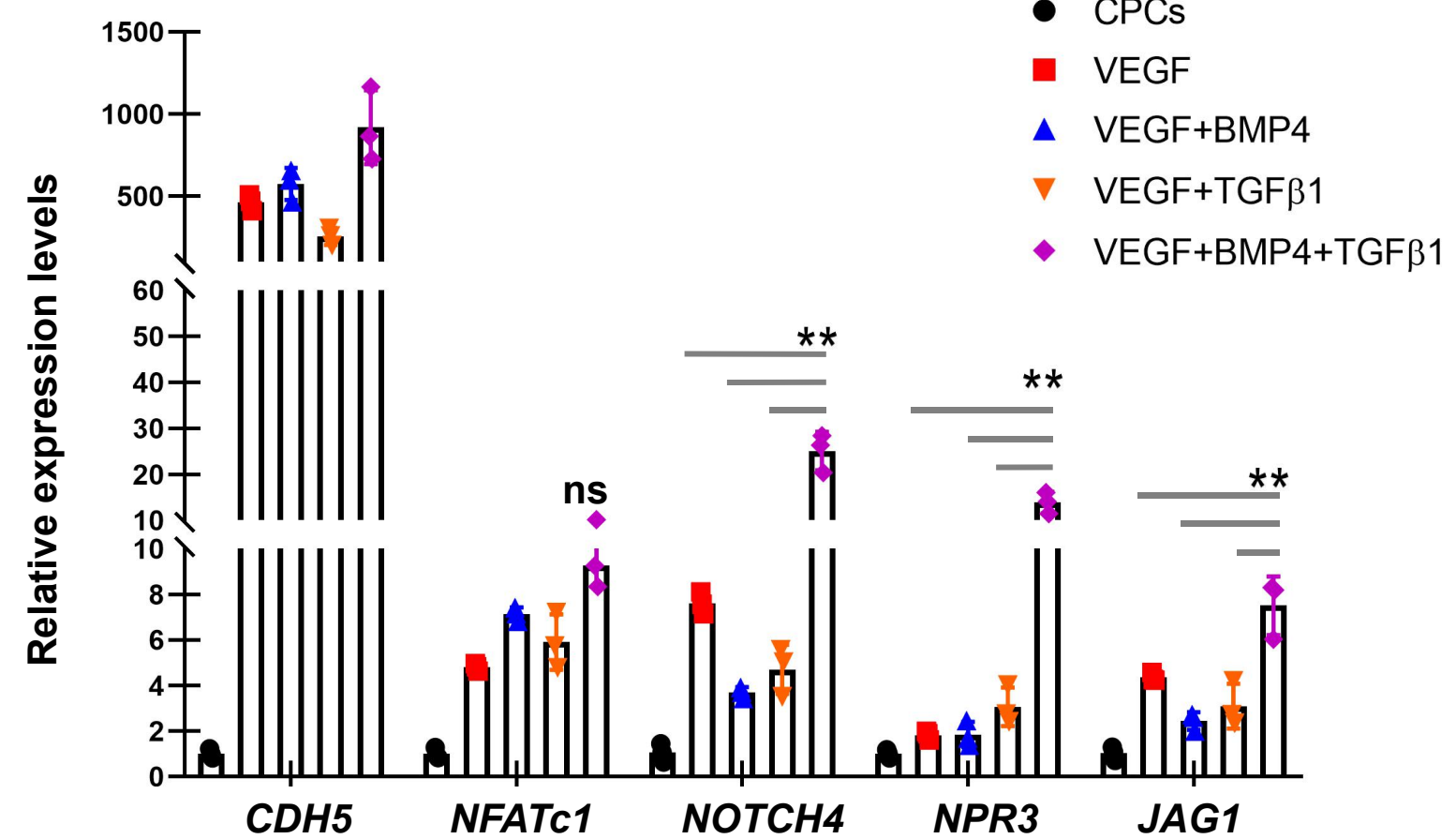


Figure 2 CPCs to VEC-like cells

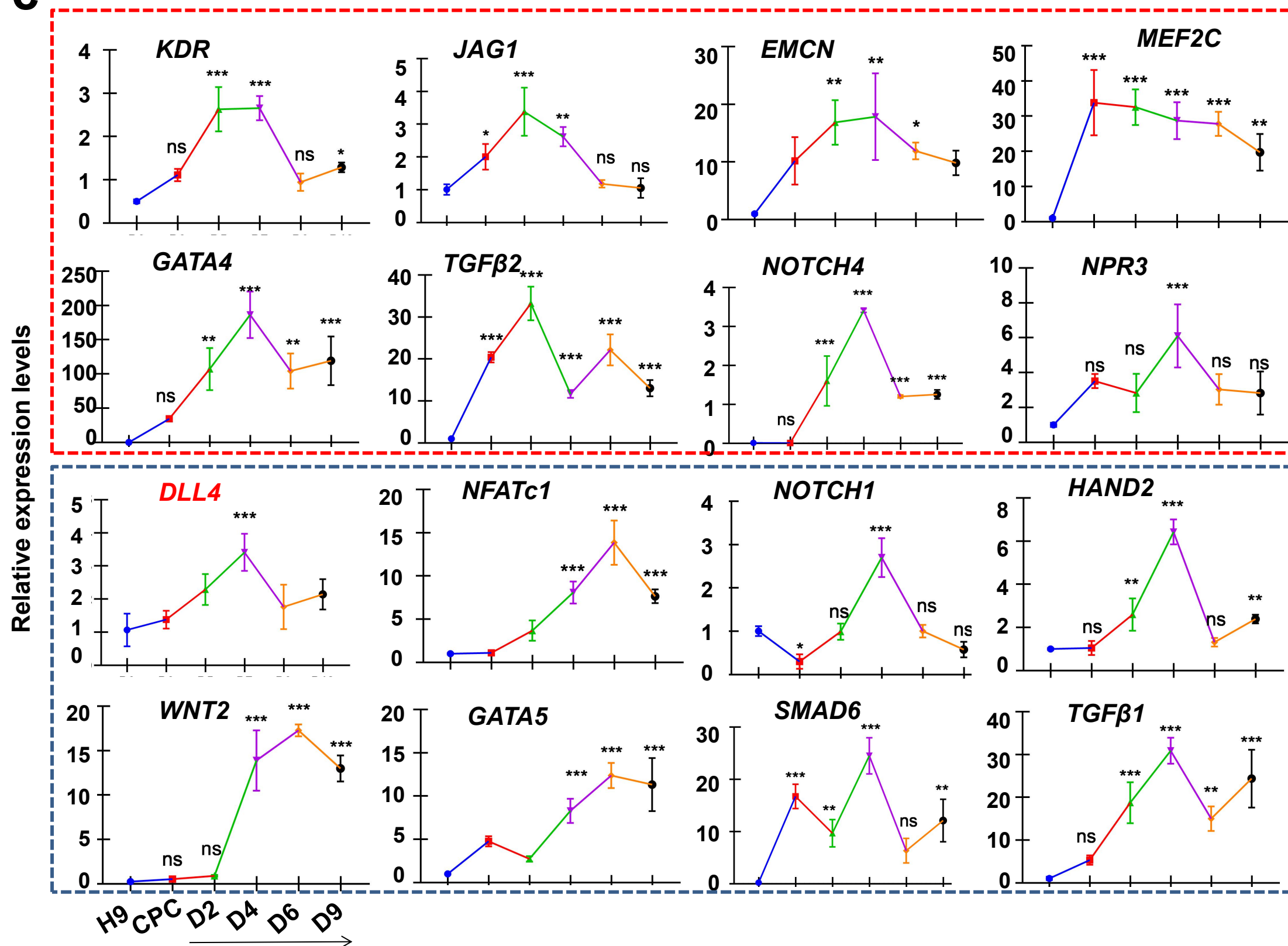
a



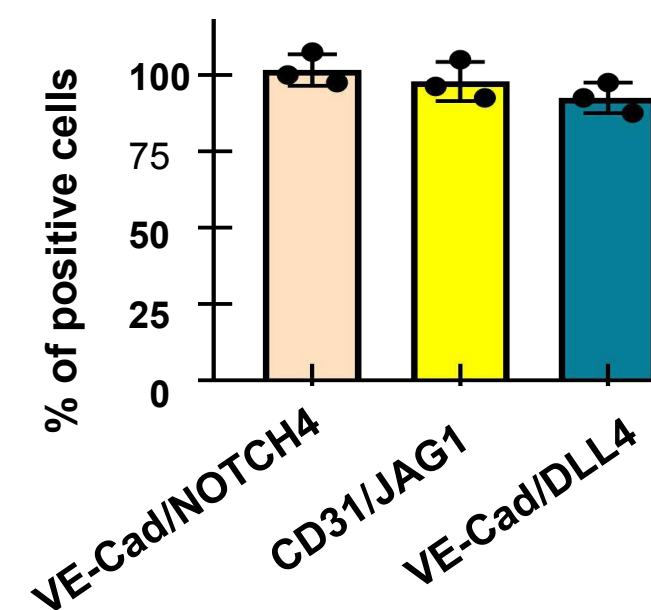
b



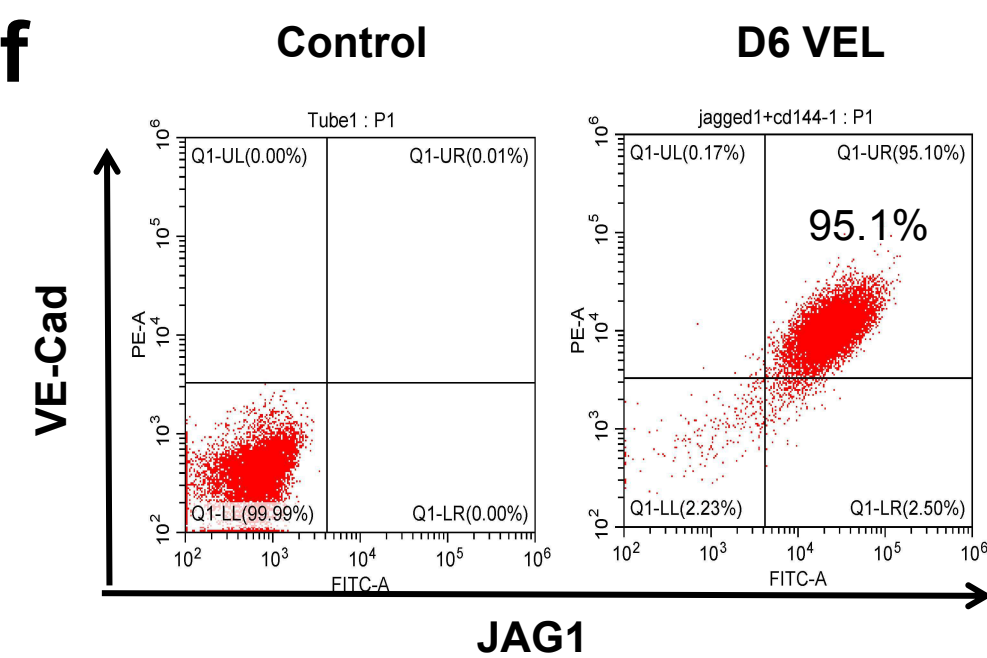
c

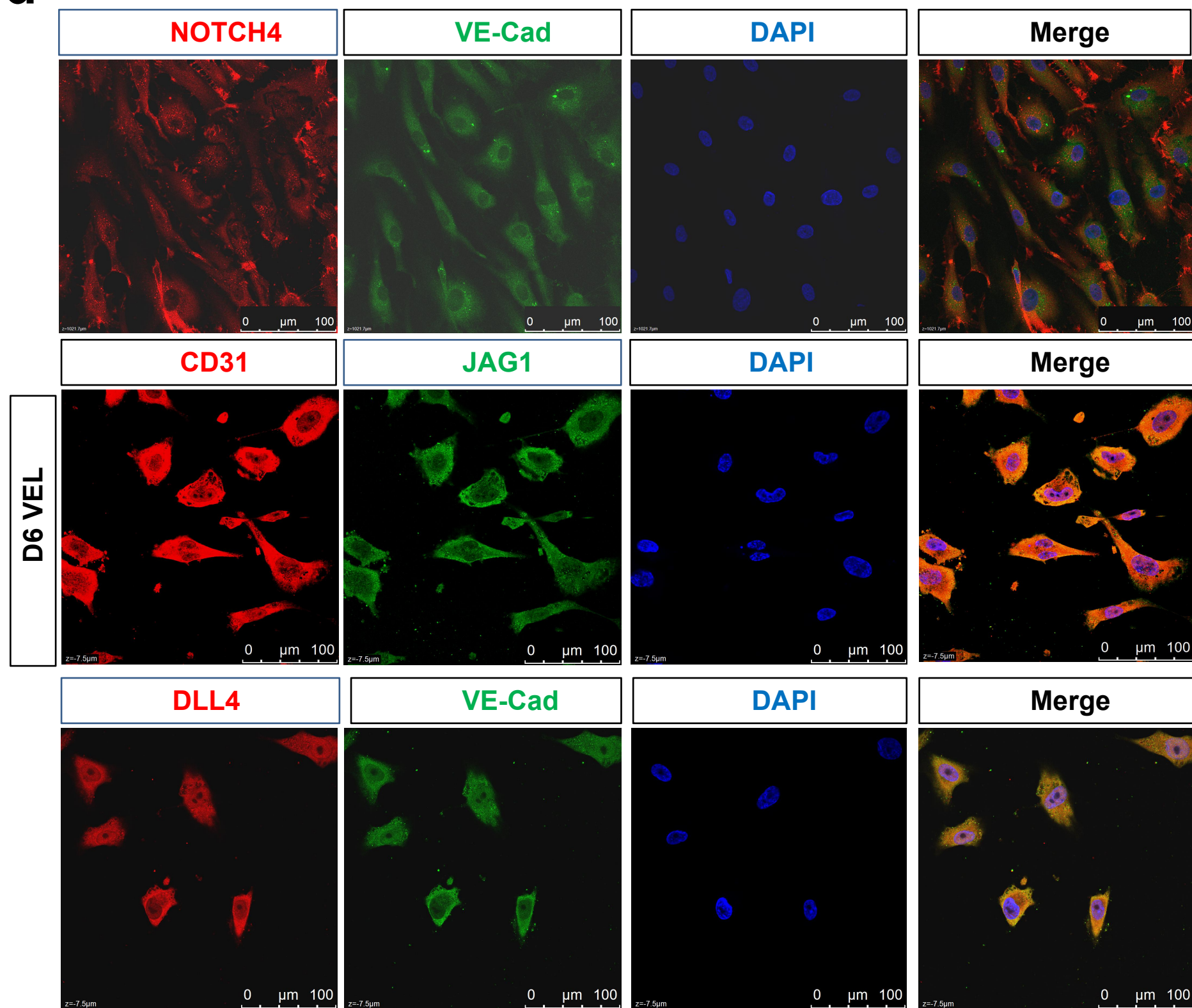
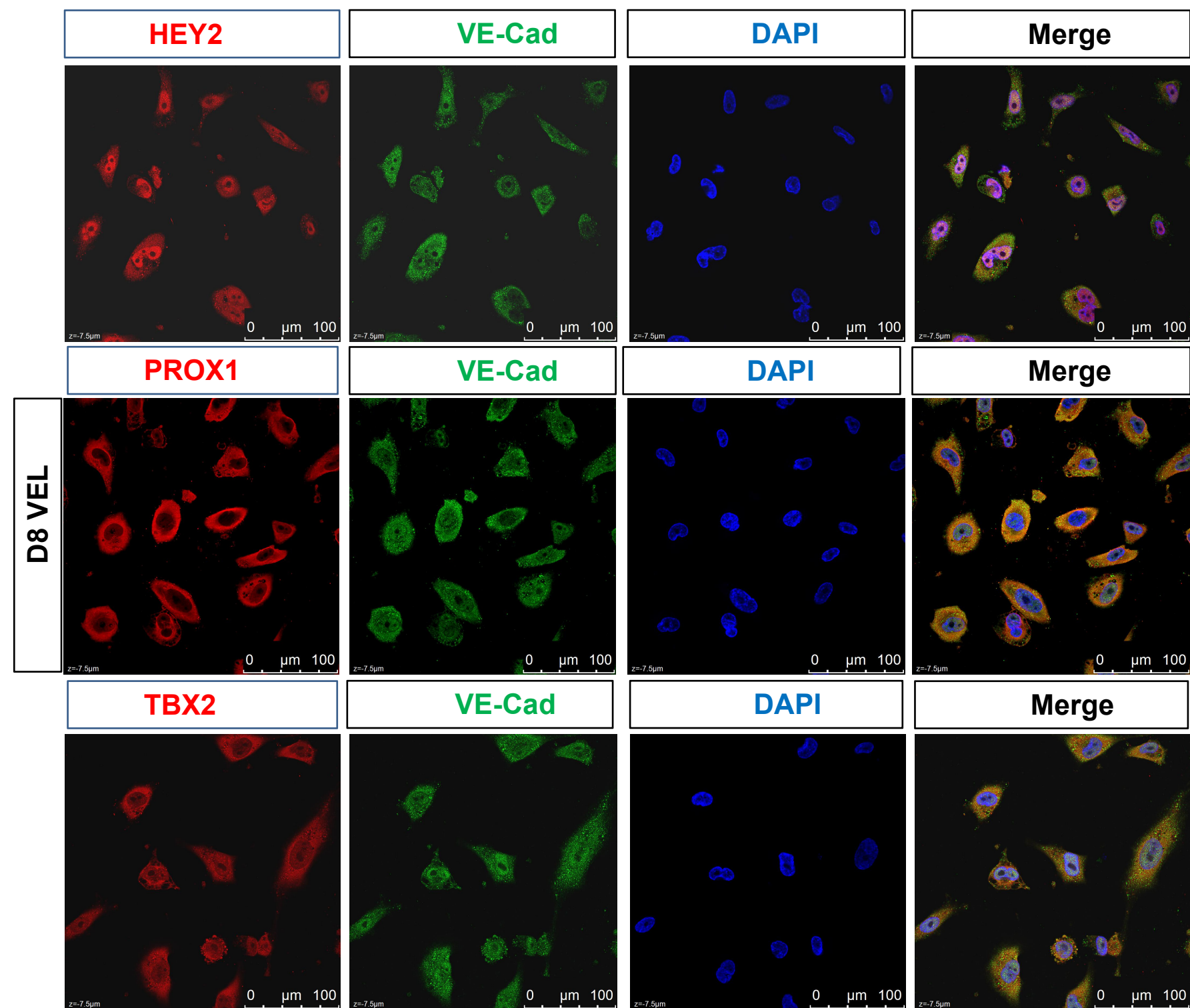
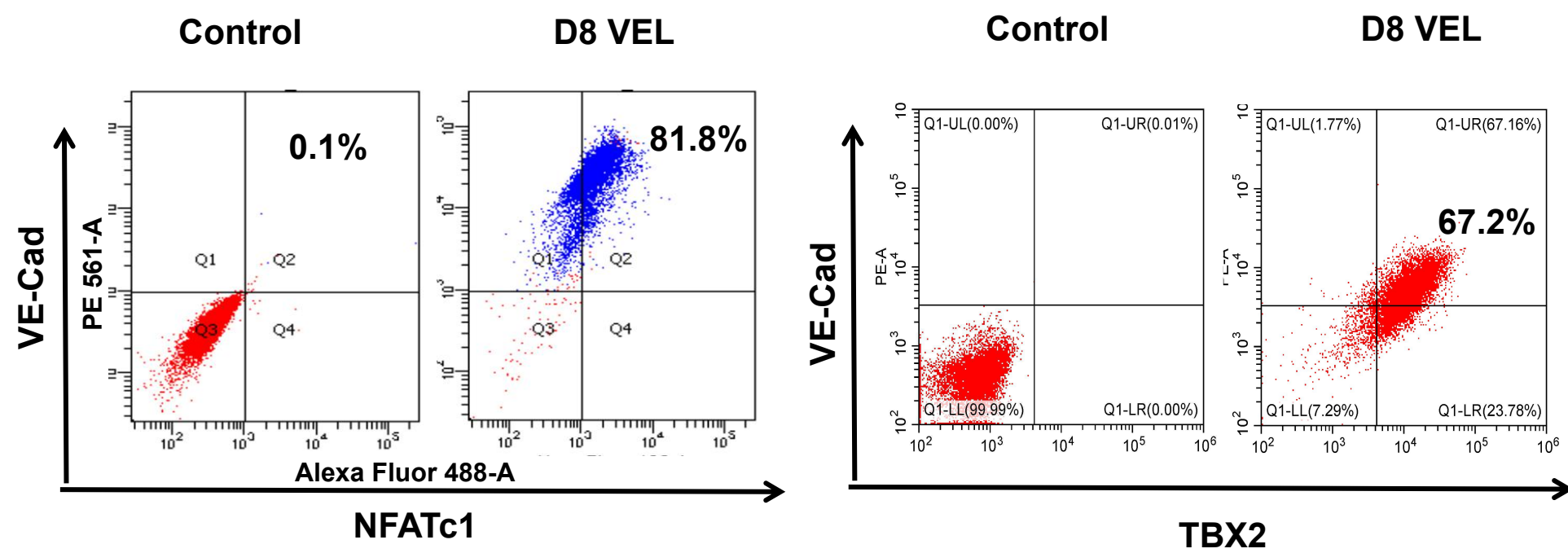
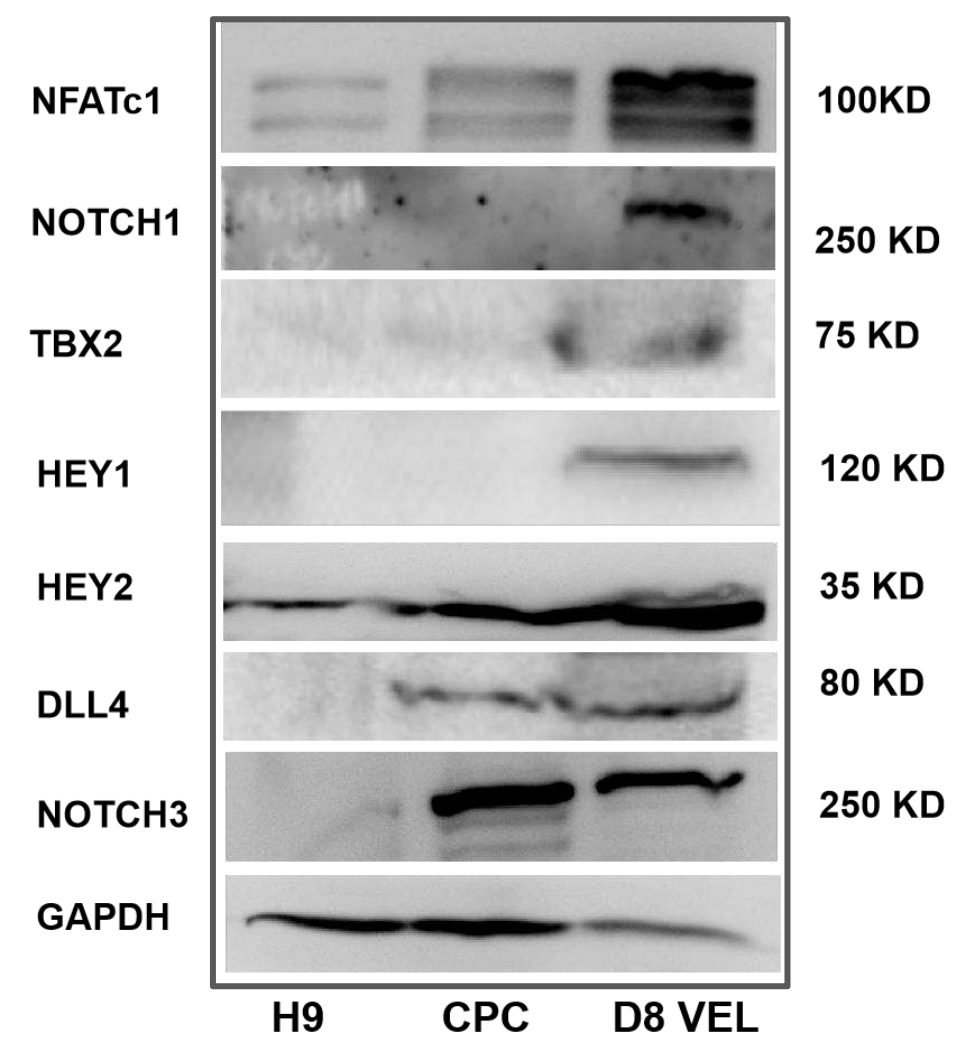


e



f



d**g****i****h**

Supplementary Figure 2

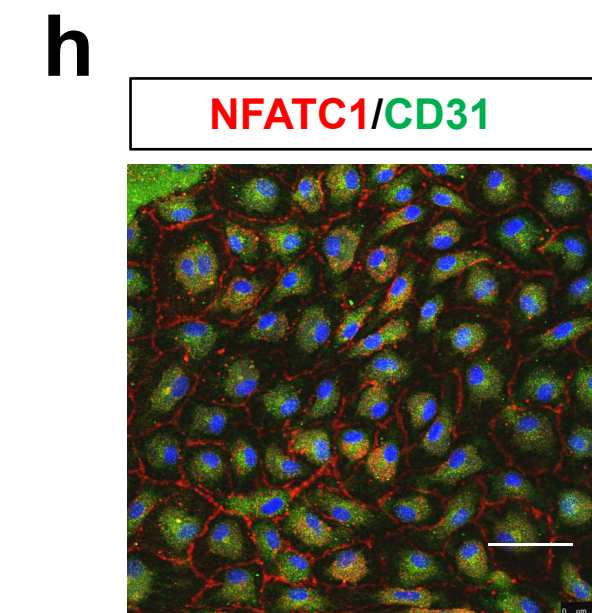
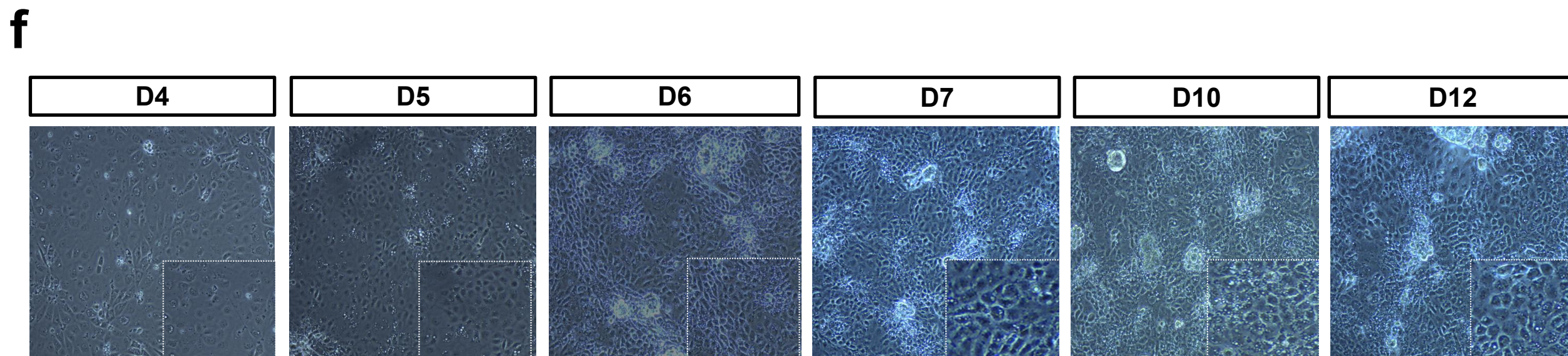
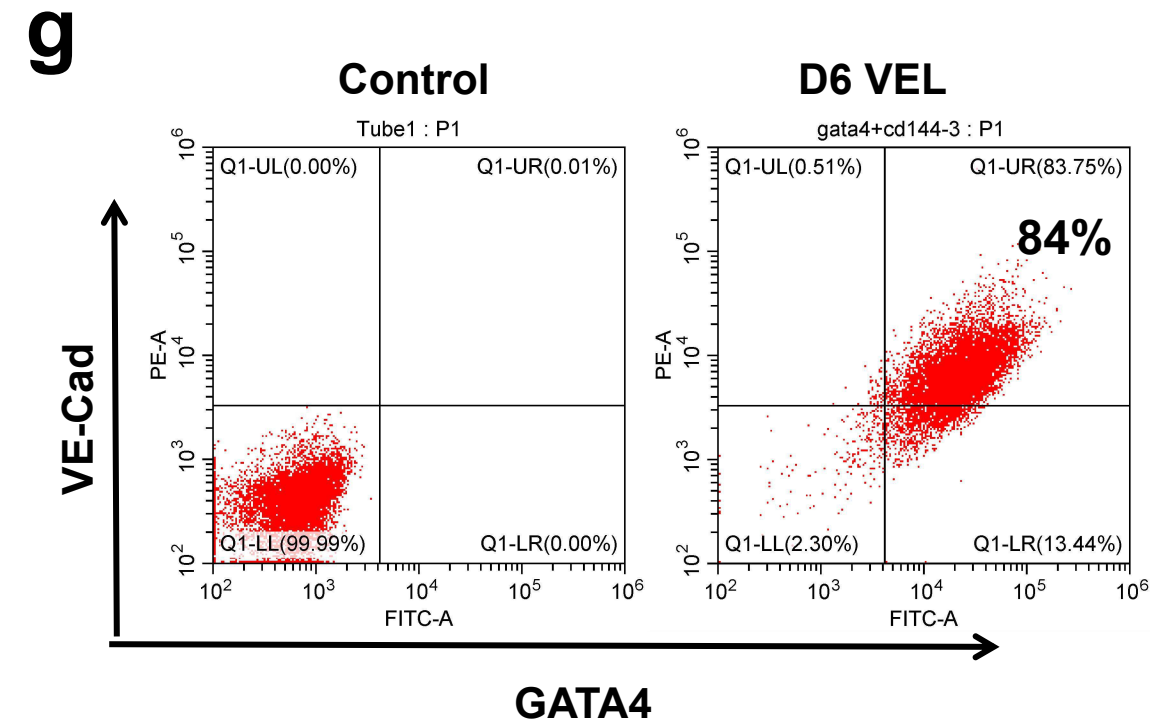
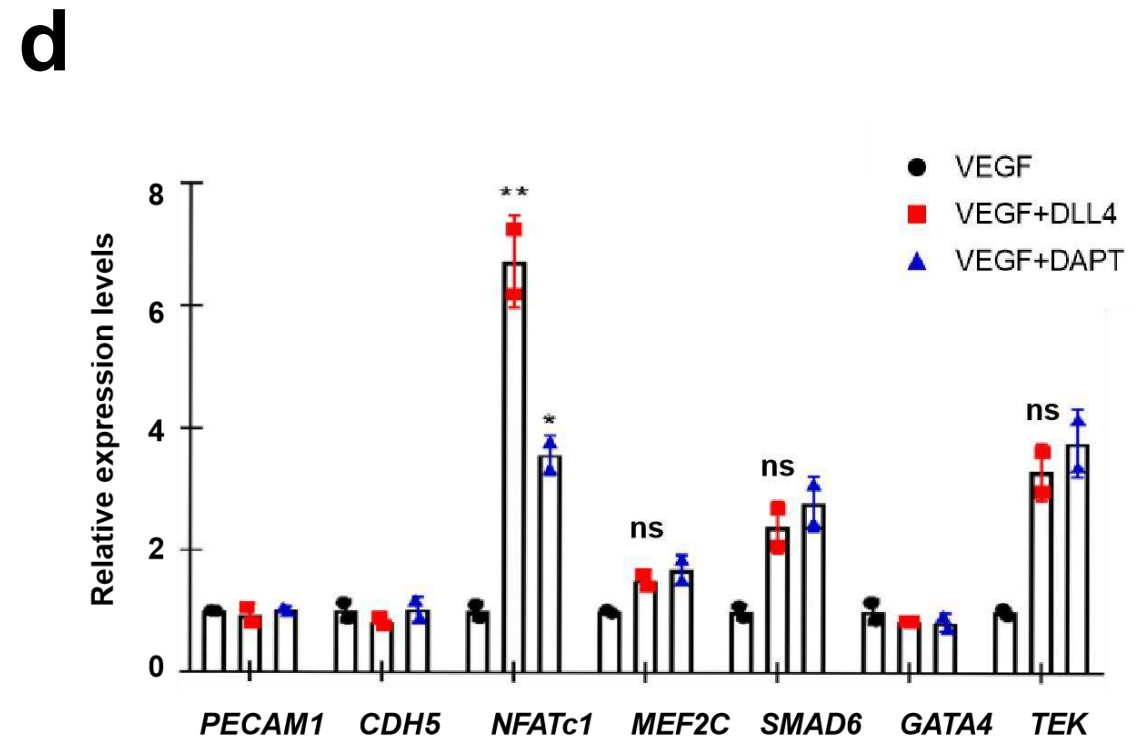
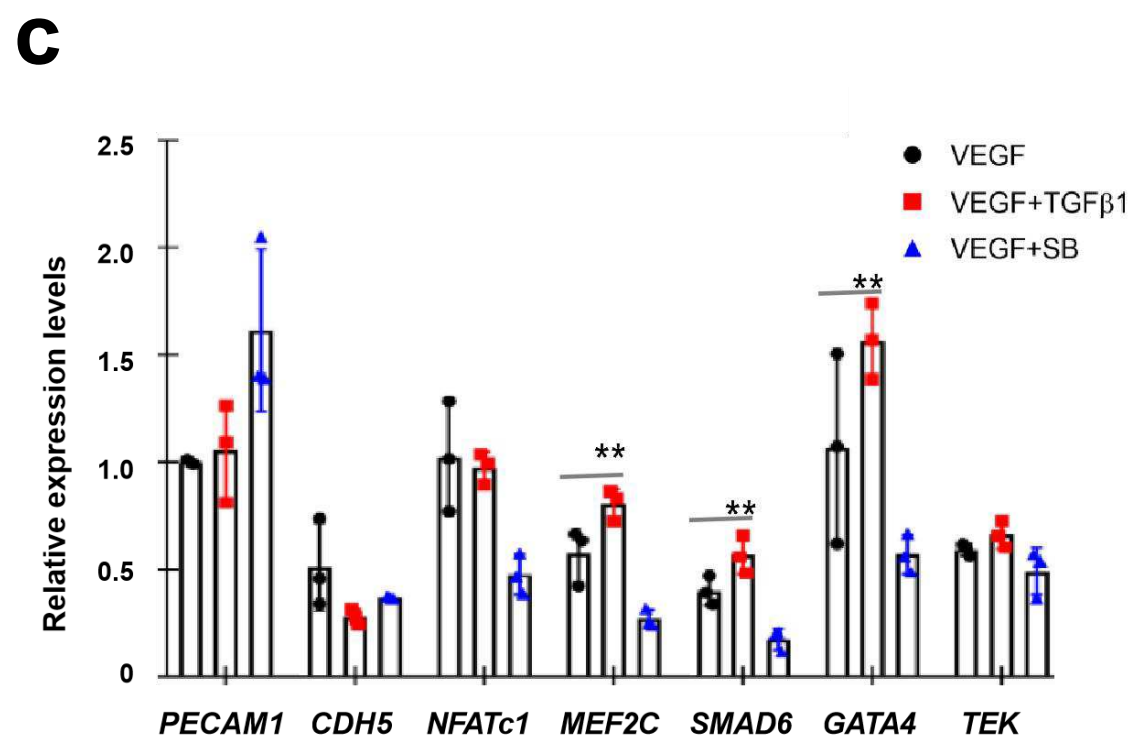
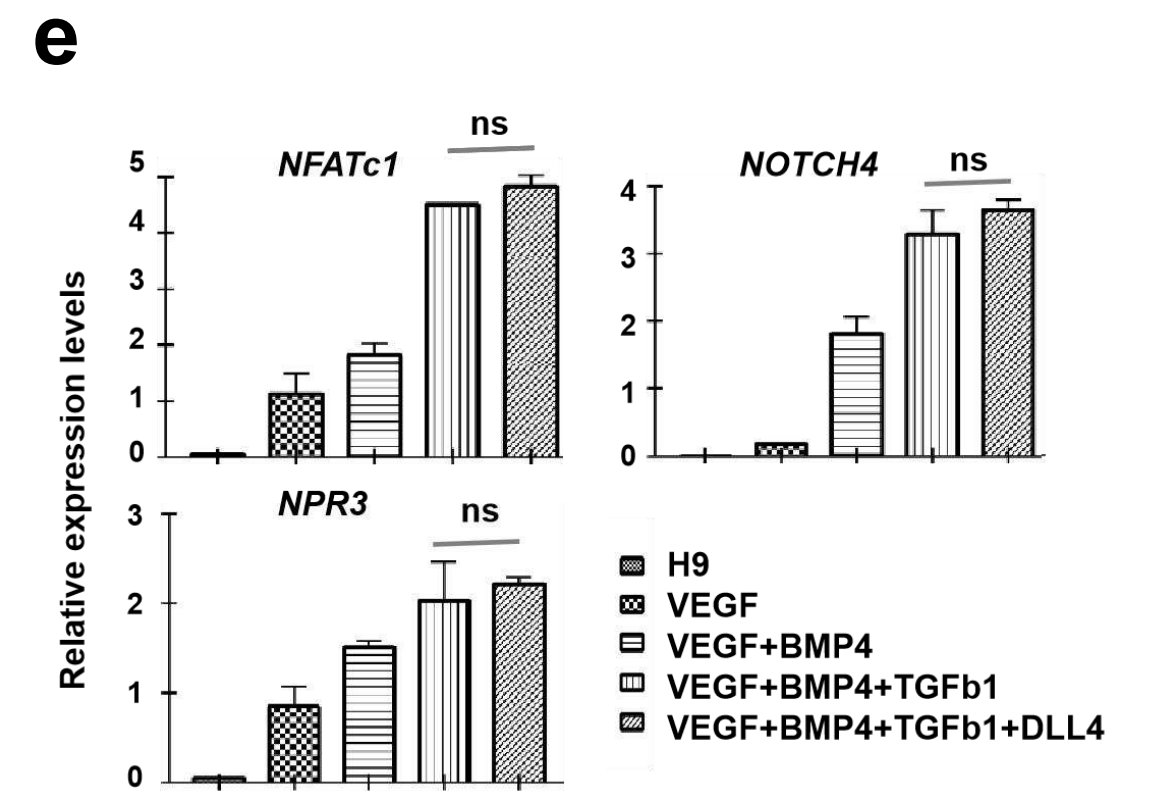
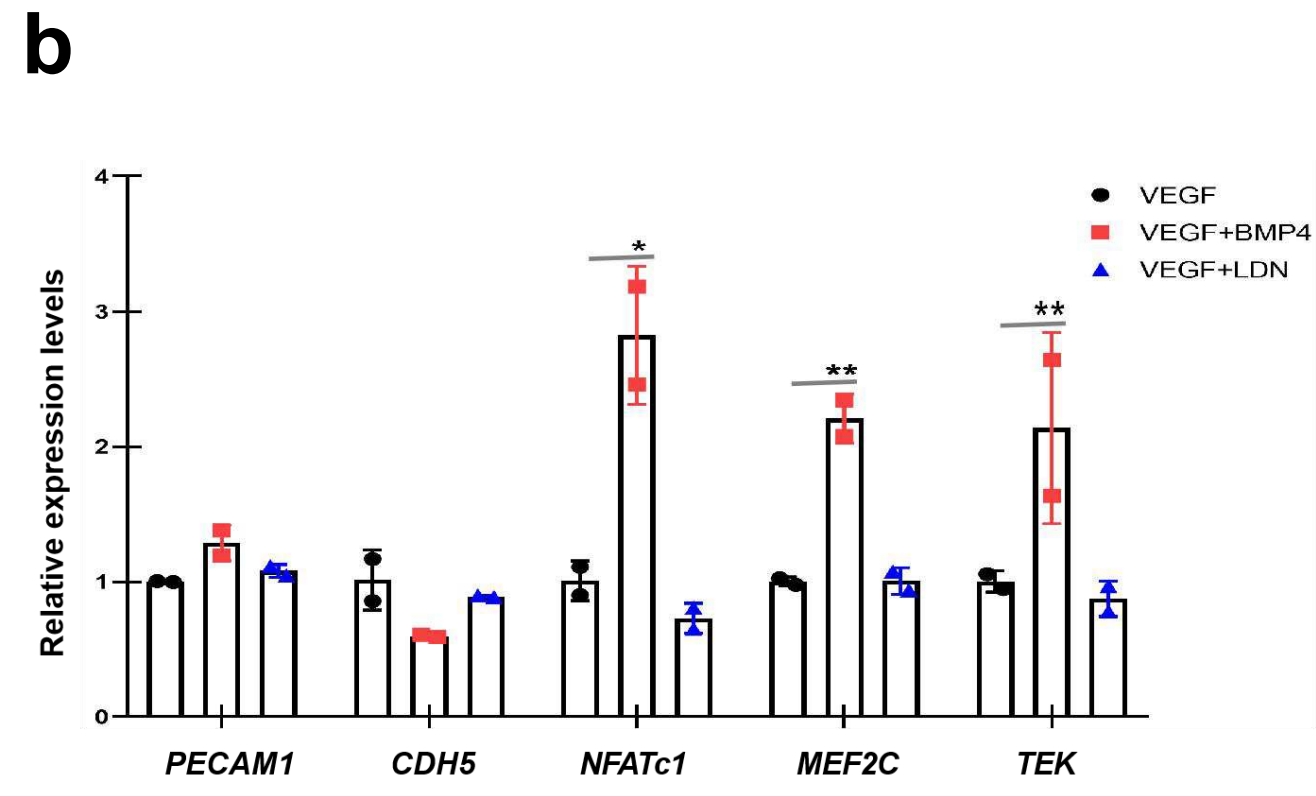
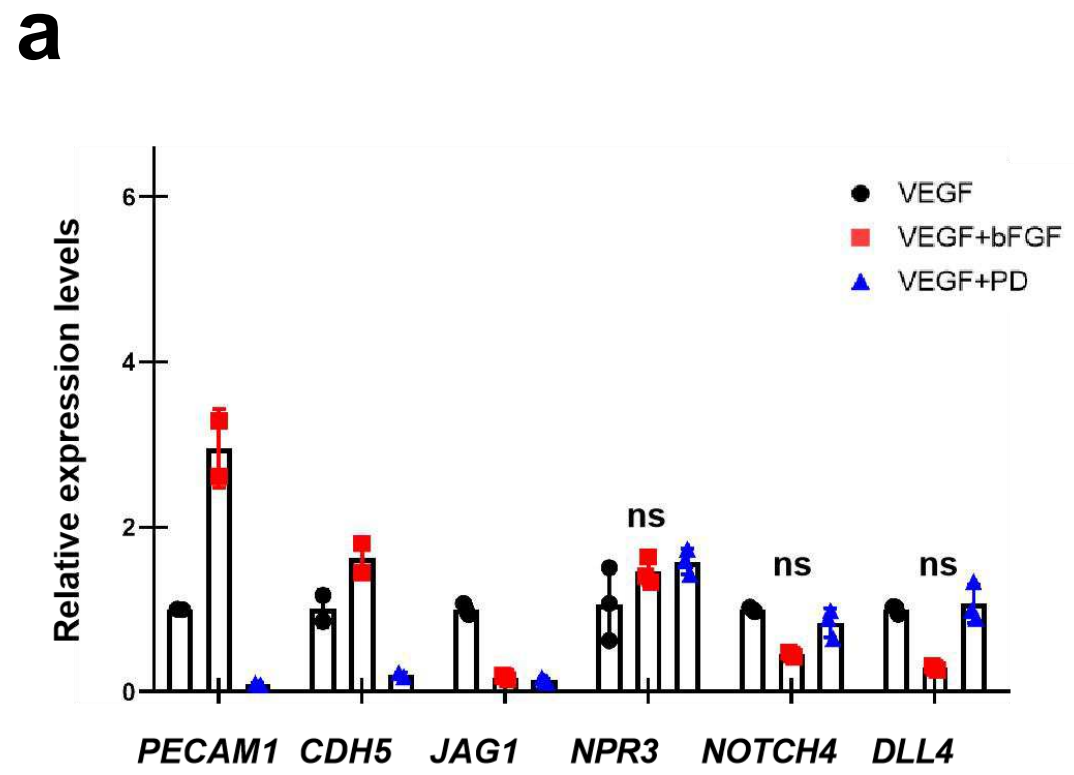
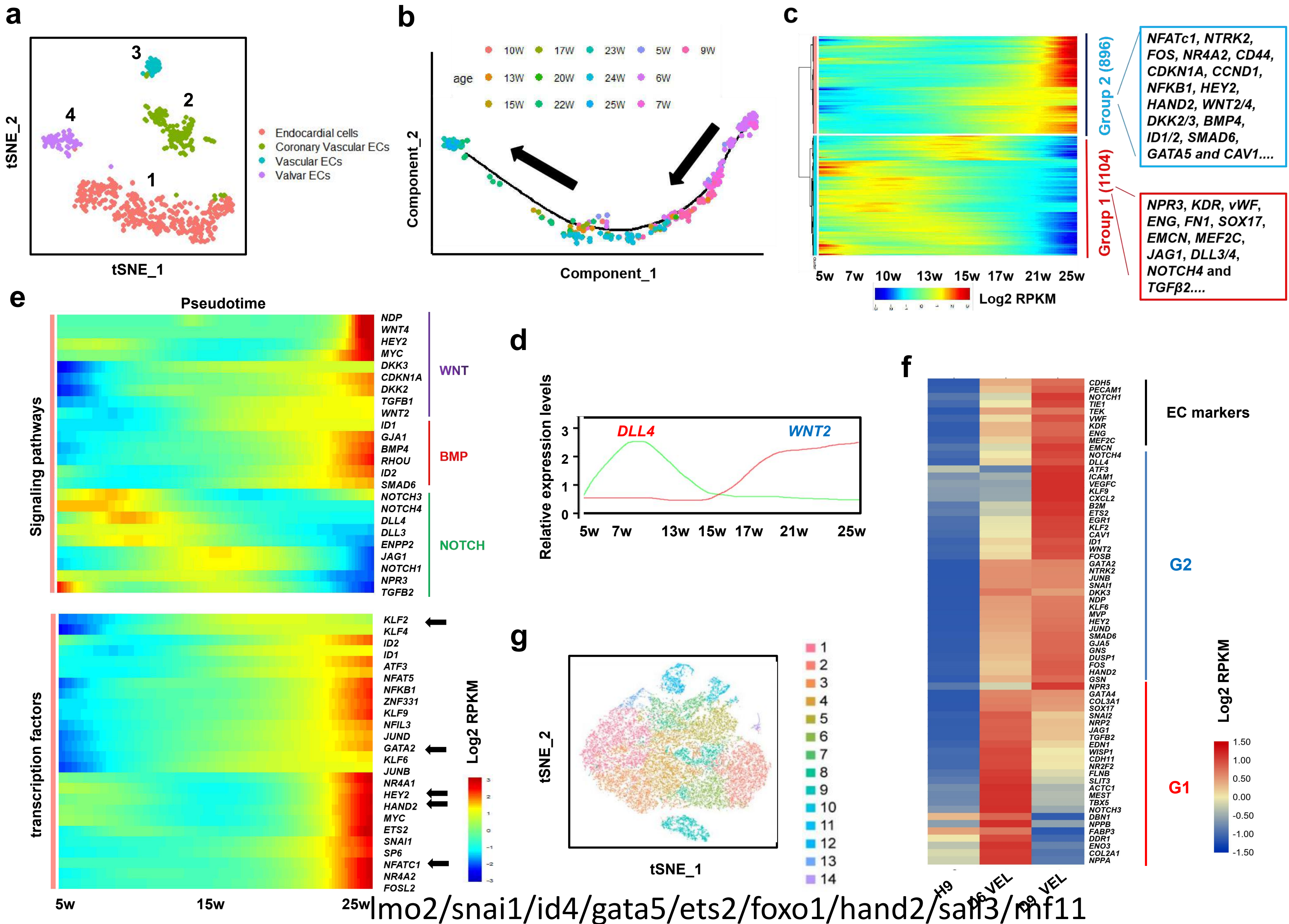
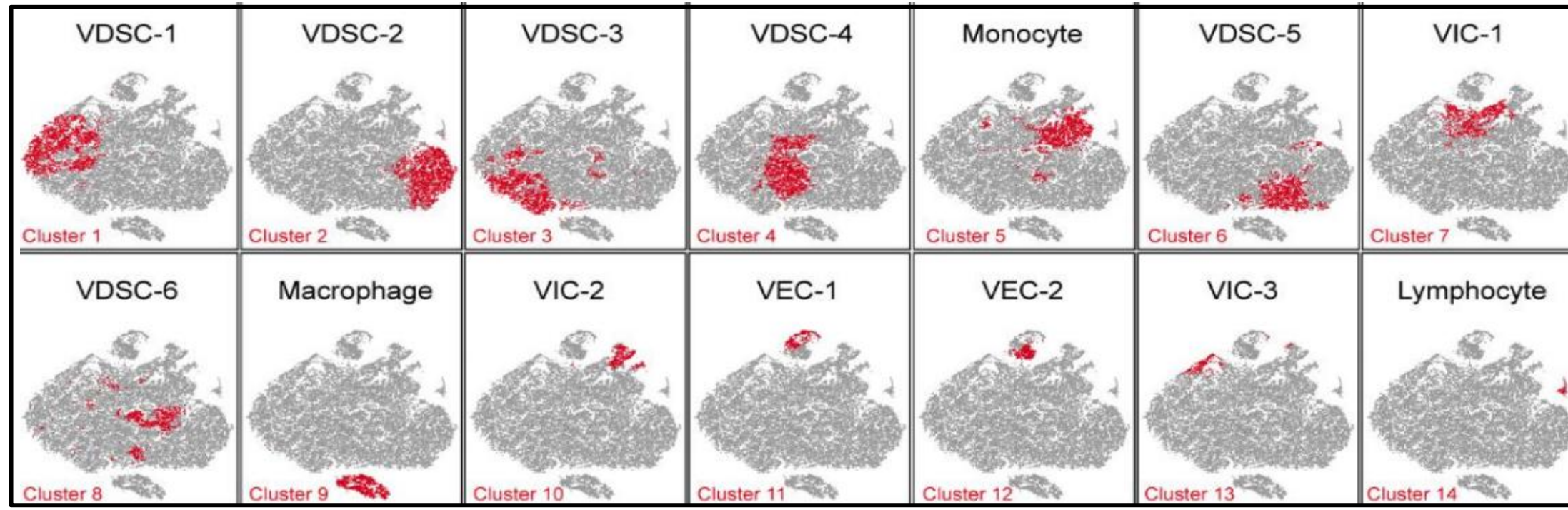
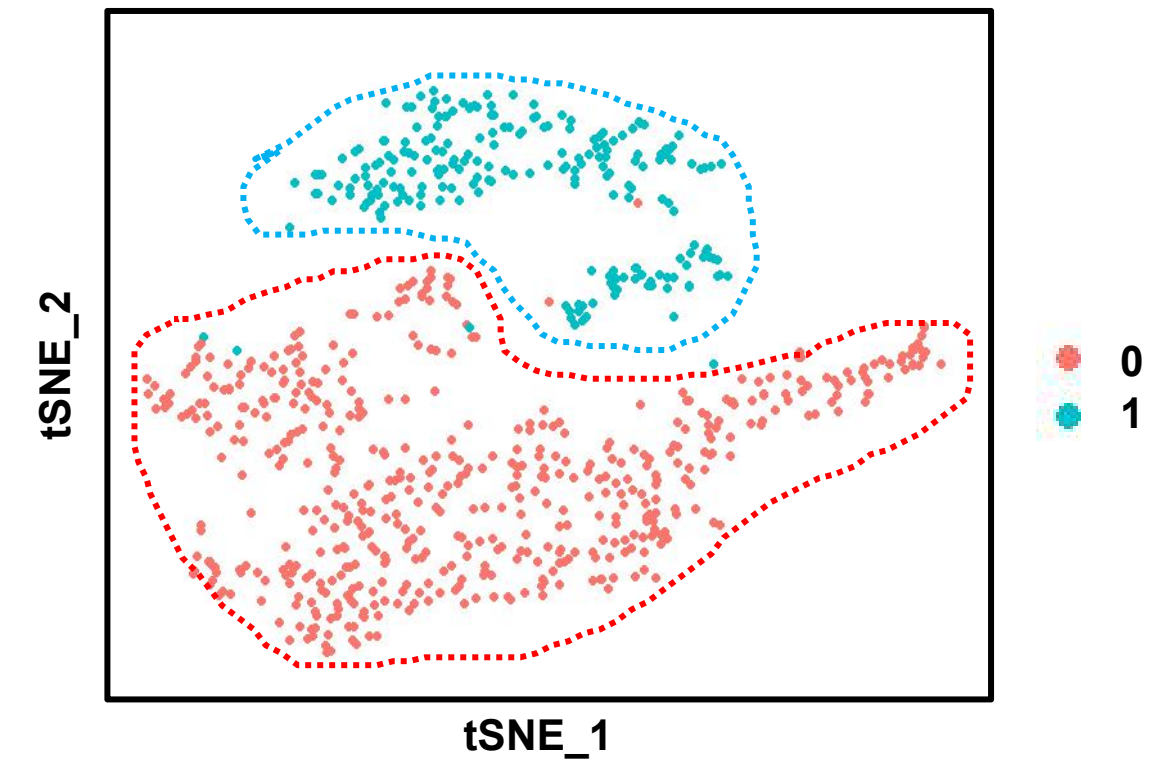
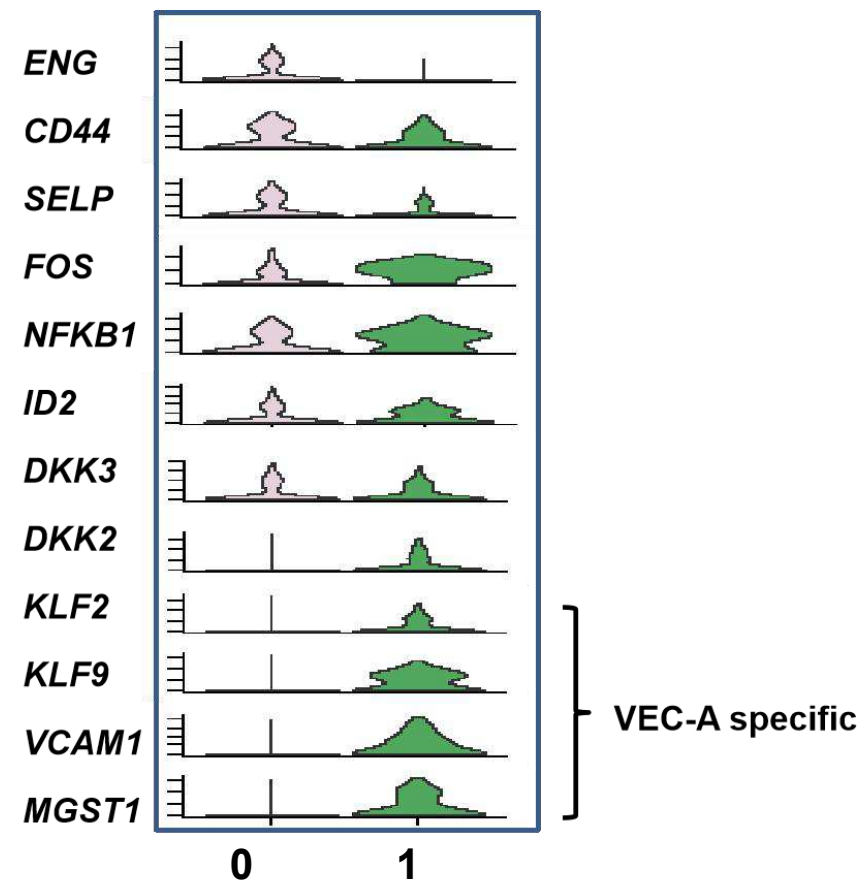
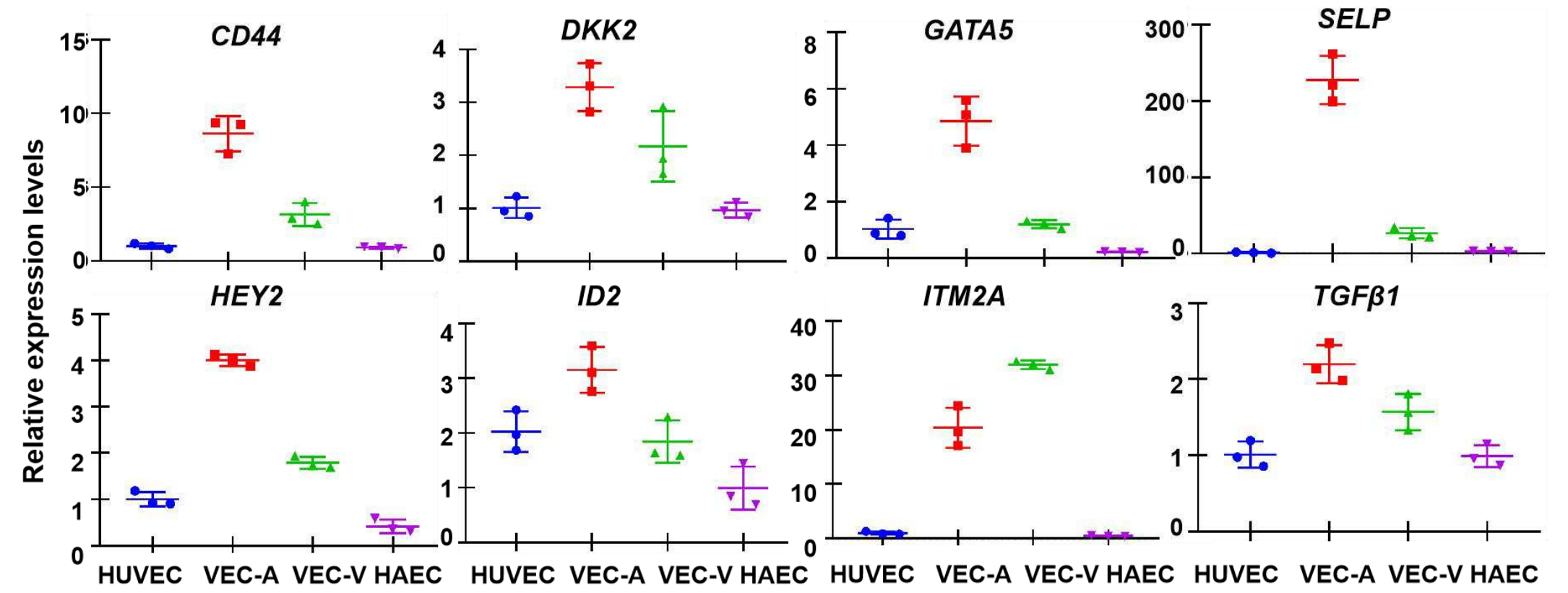


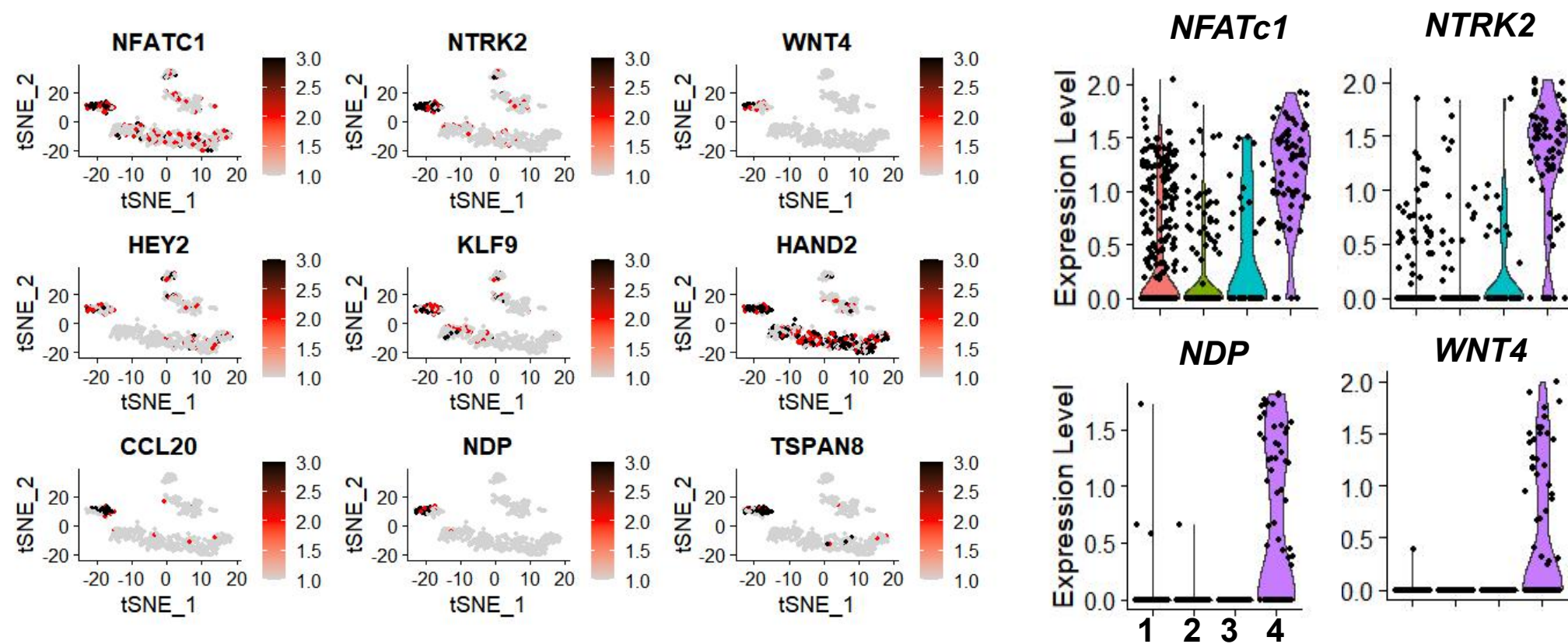
Figure 3 Analysis of genuine VECs at single cell level



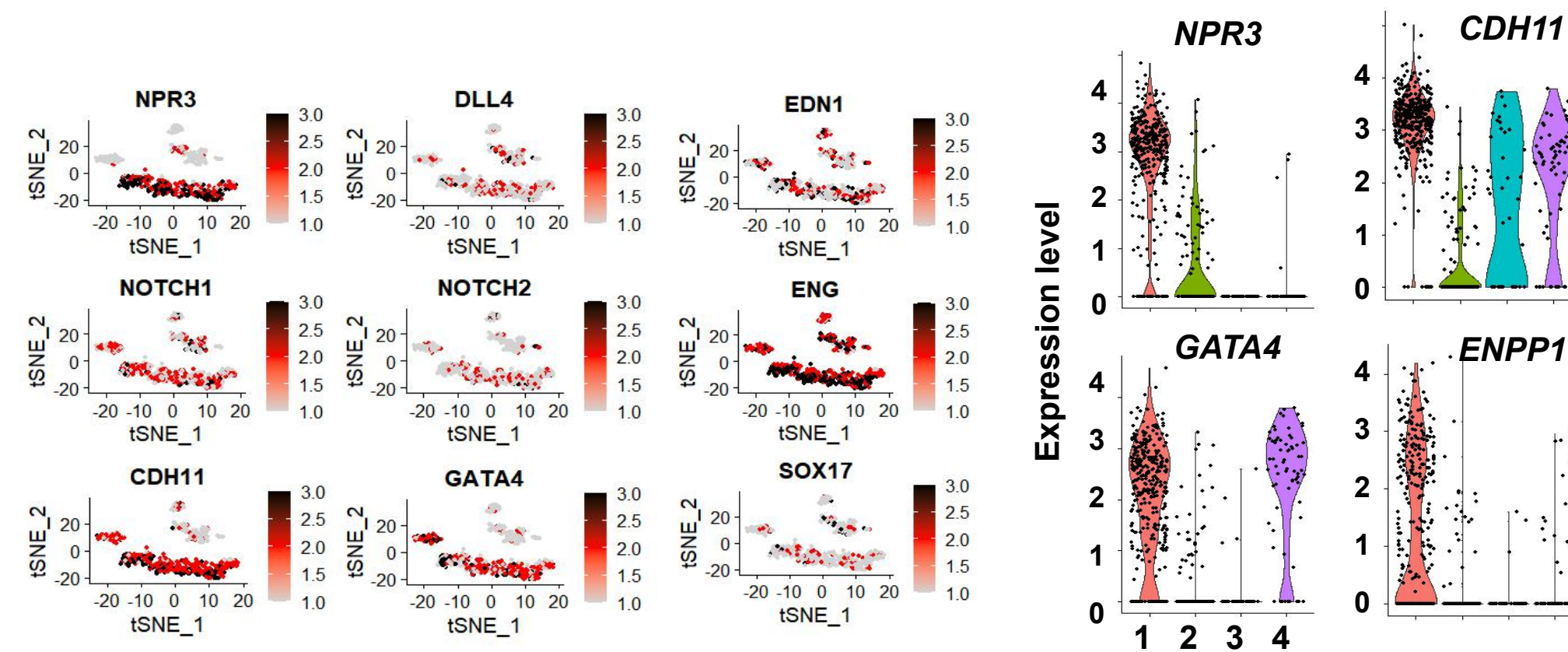
h**i****j****k**

Supplementary Figure 3

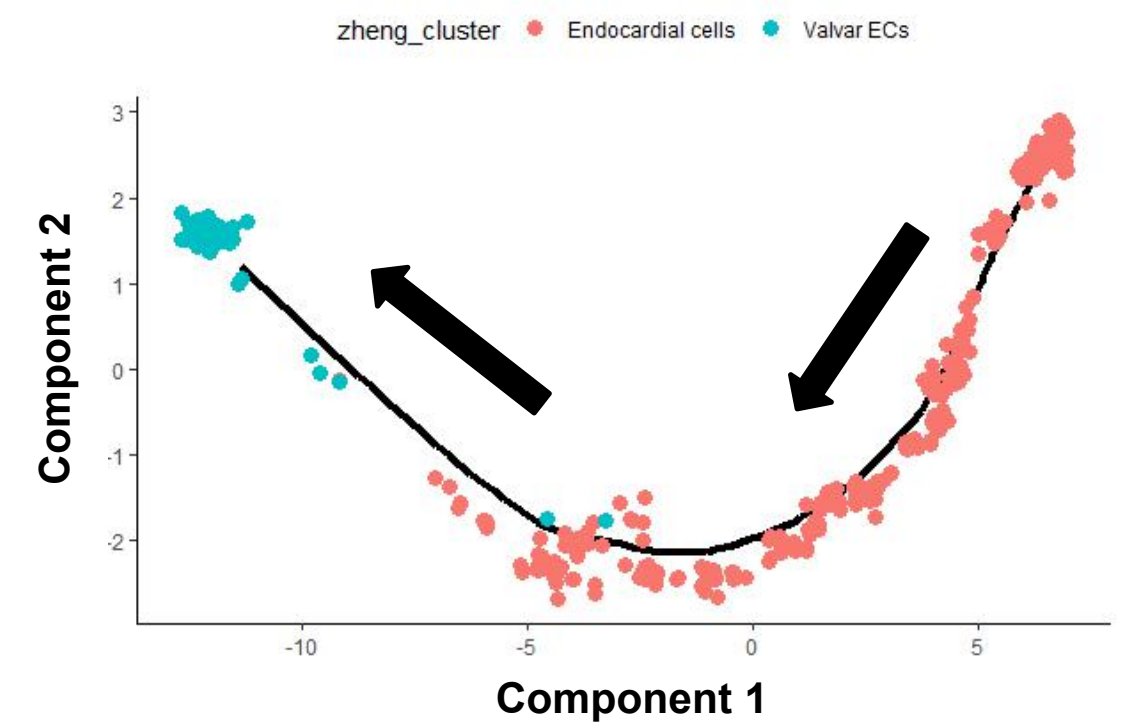
a



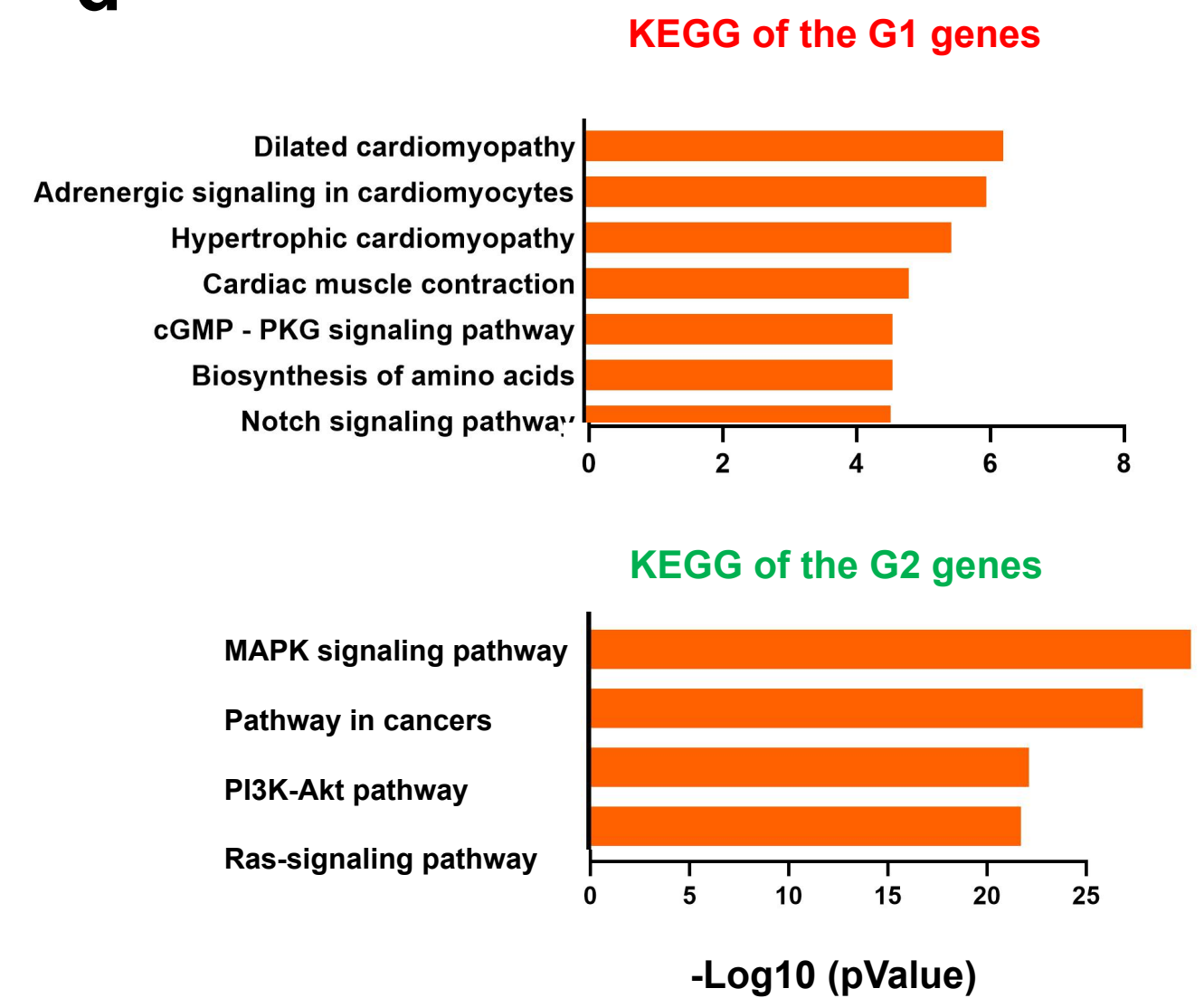
b



c



d



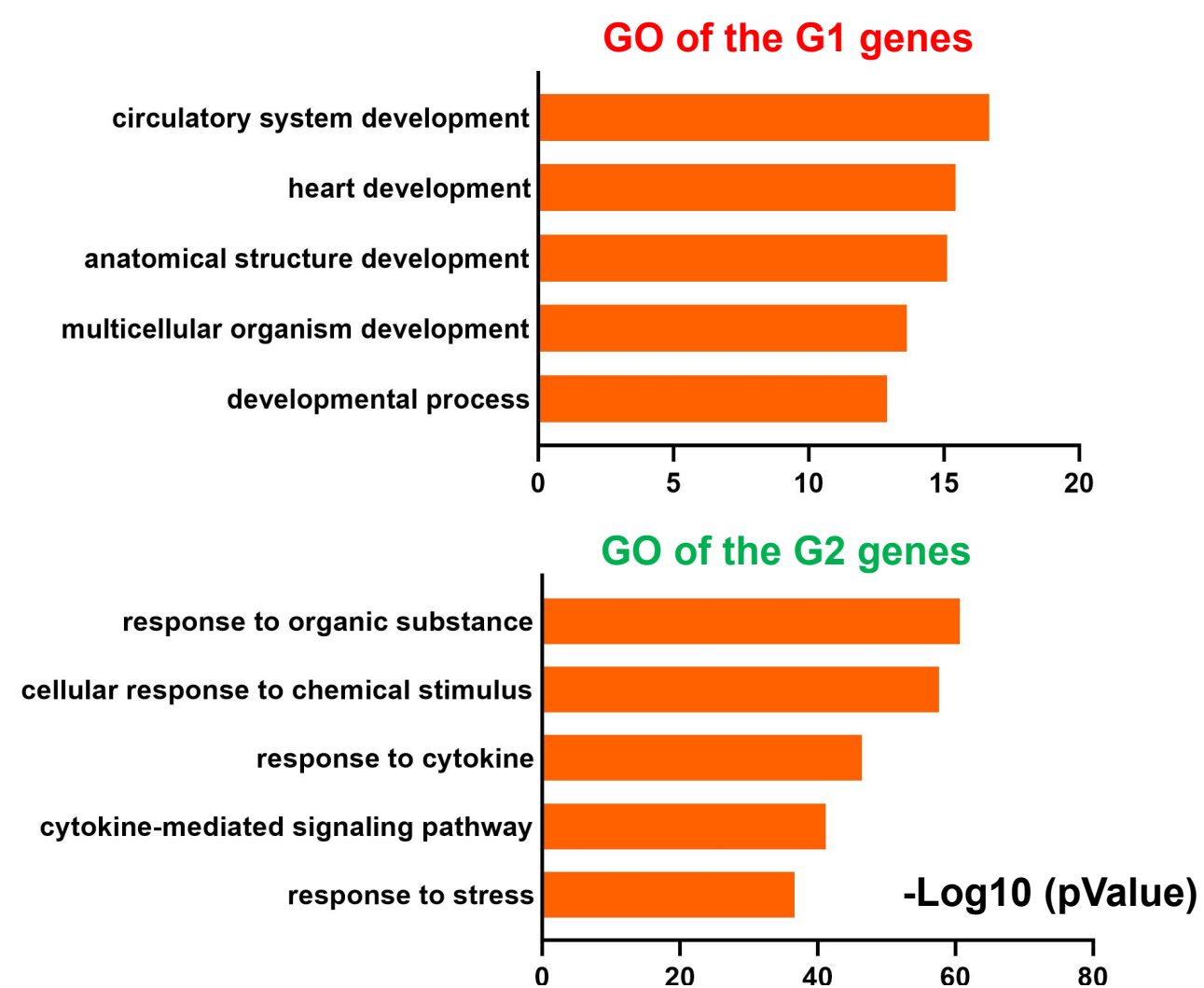
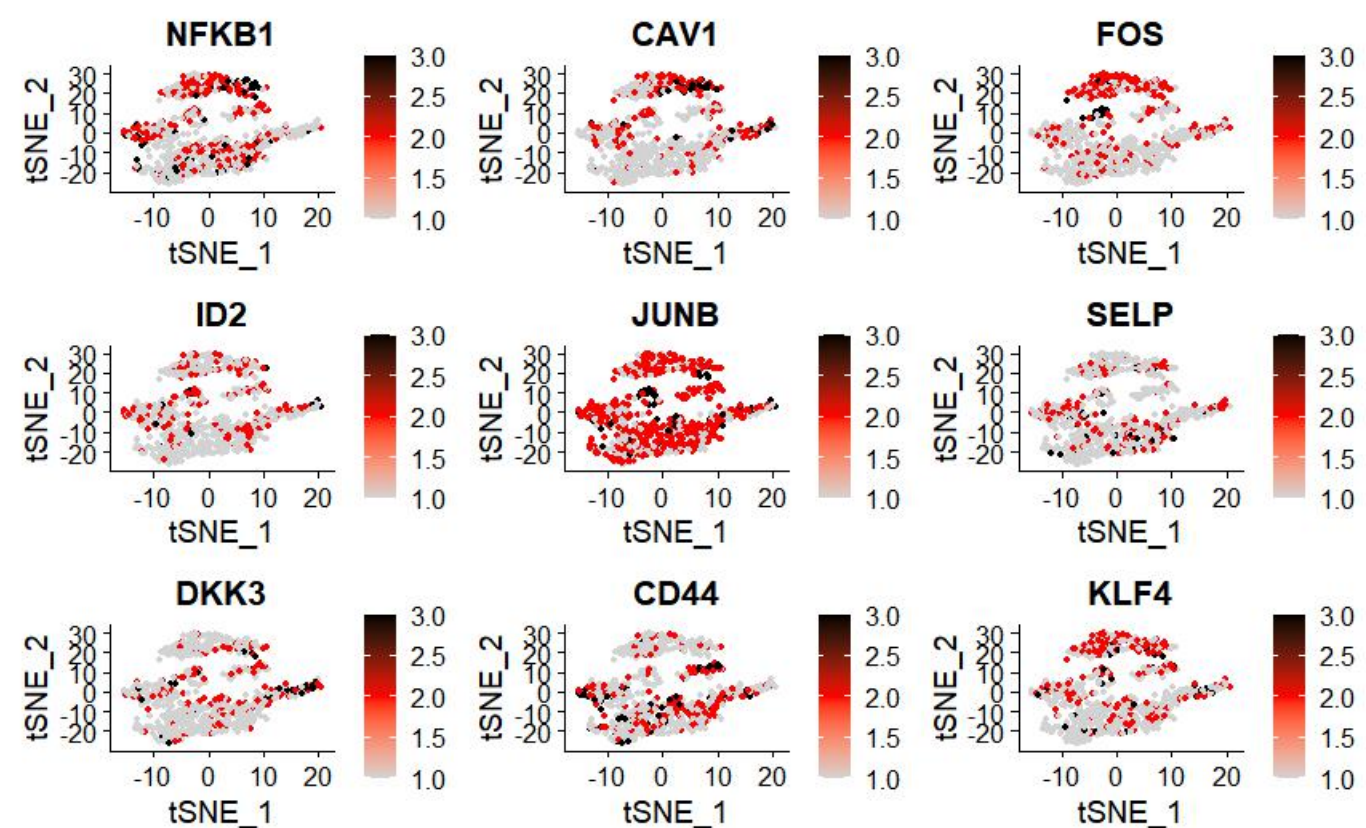
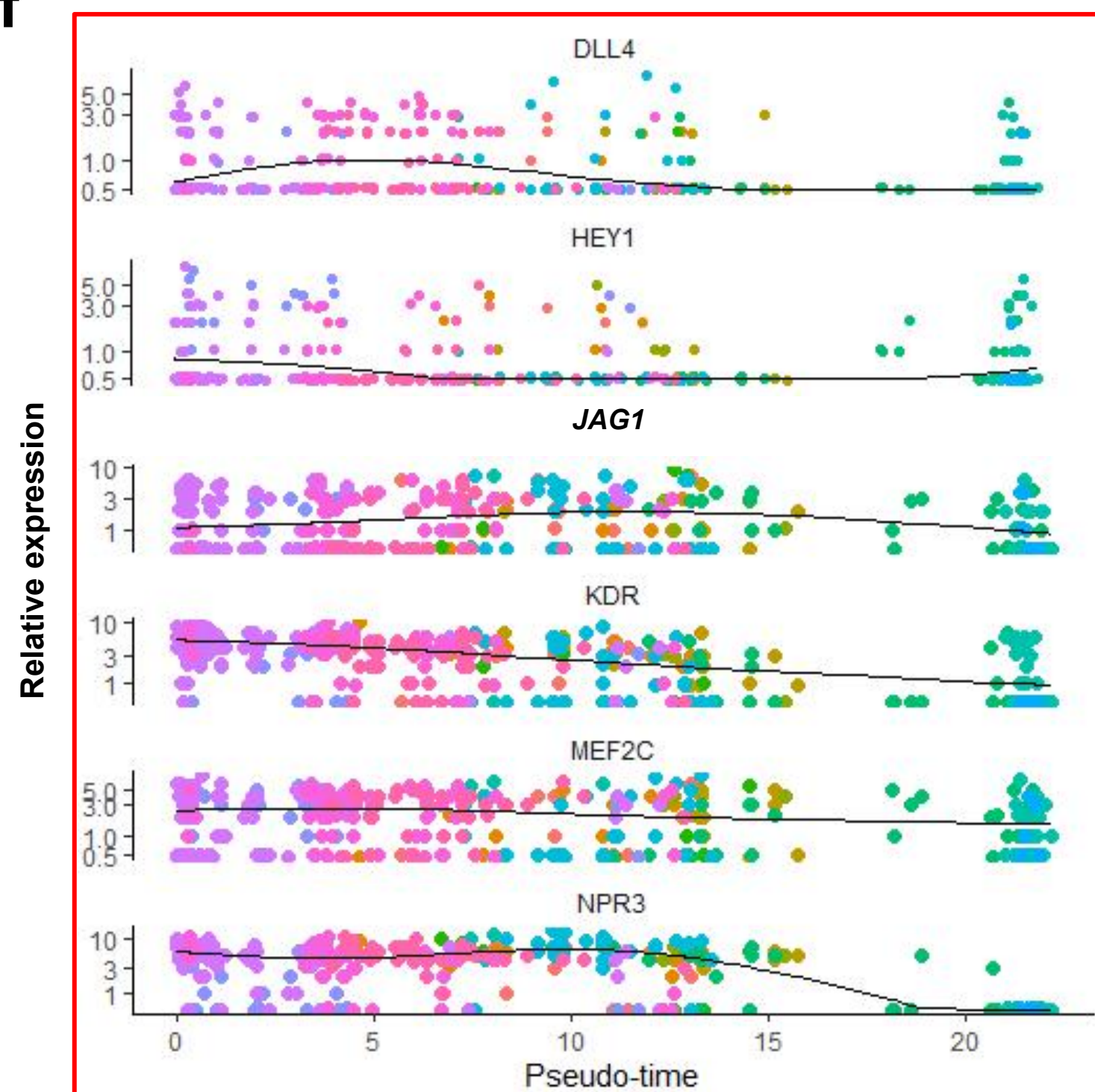
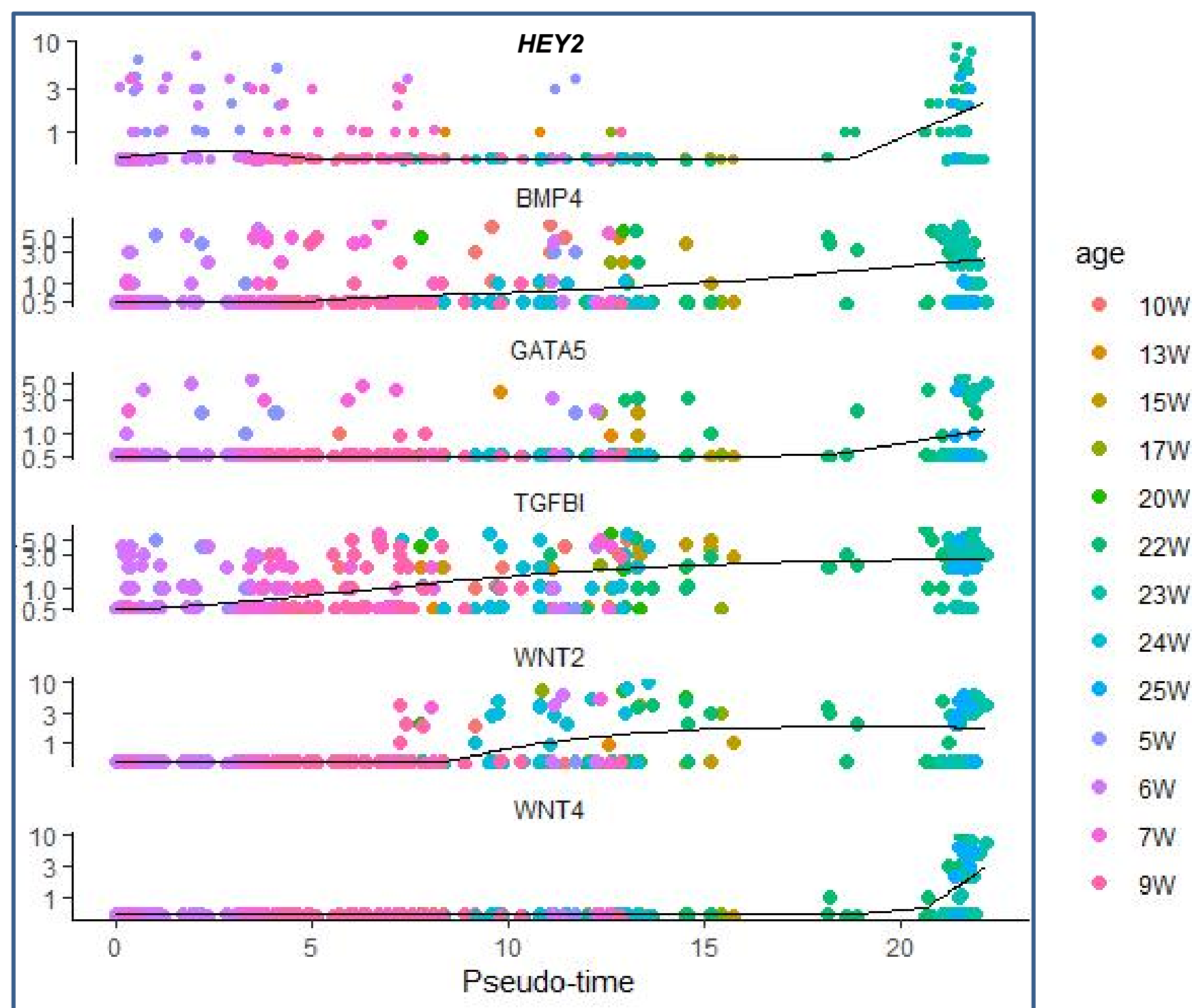
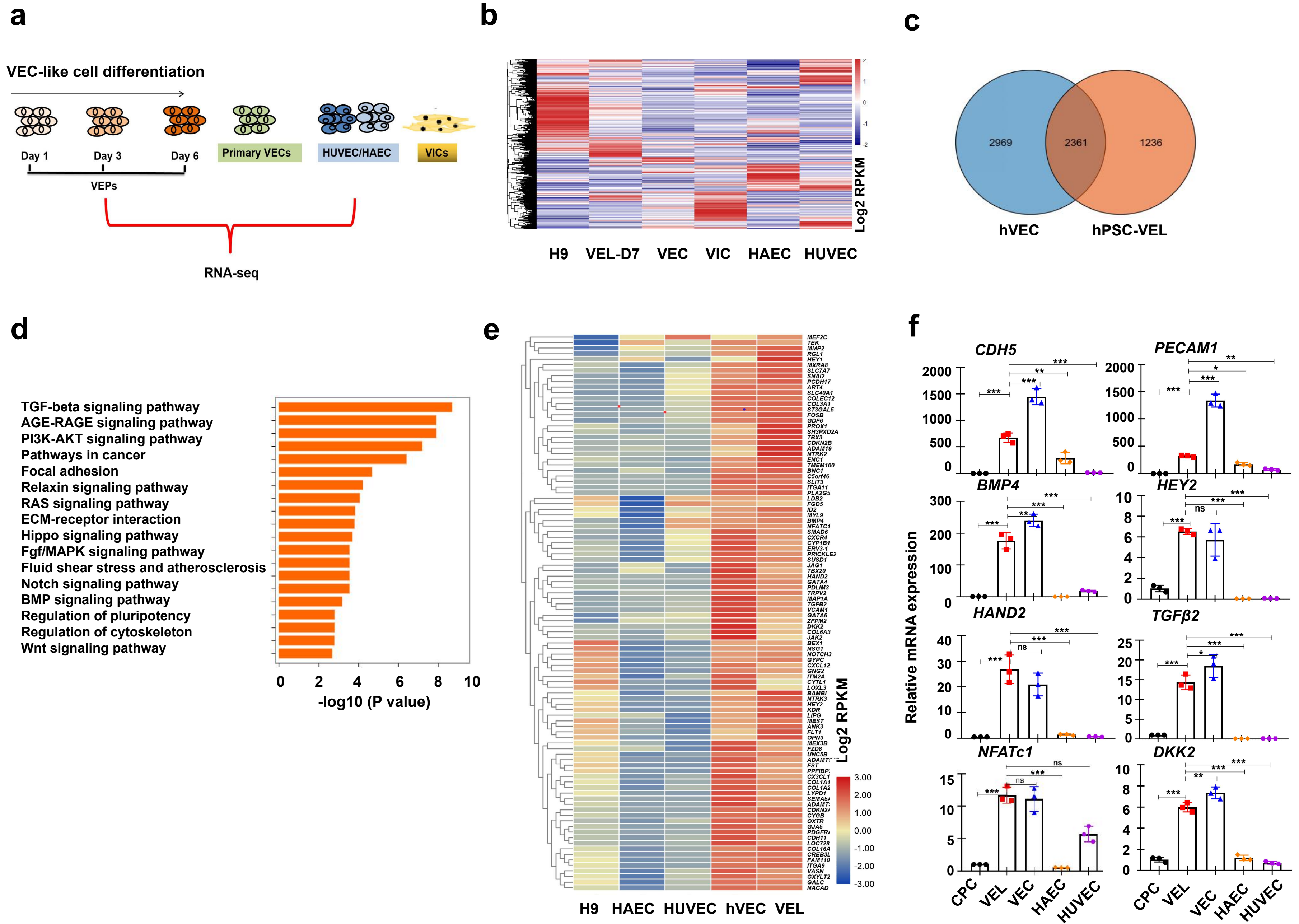
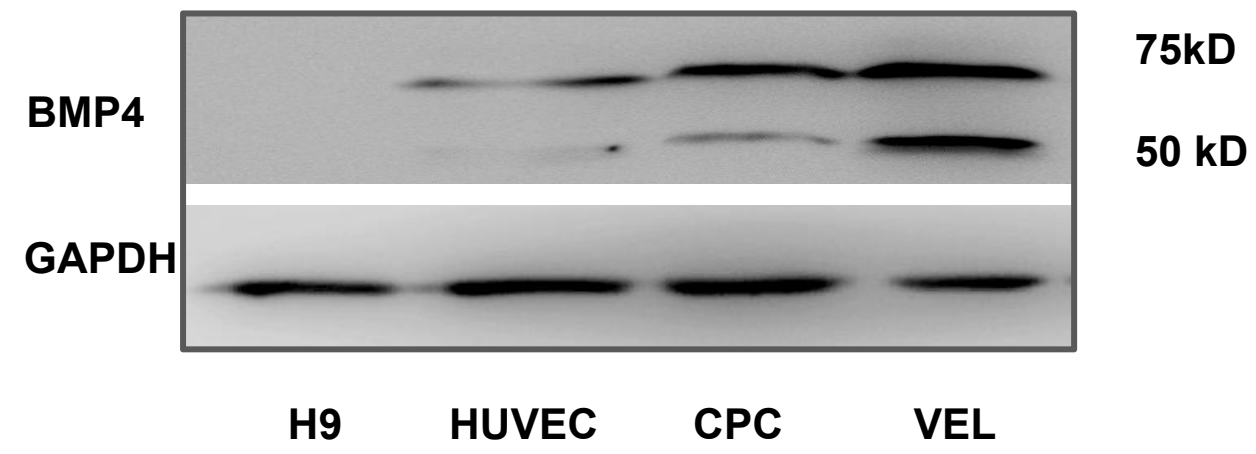
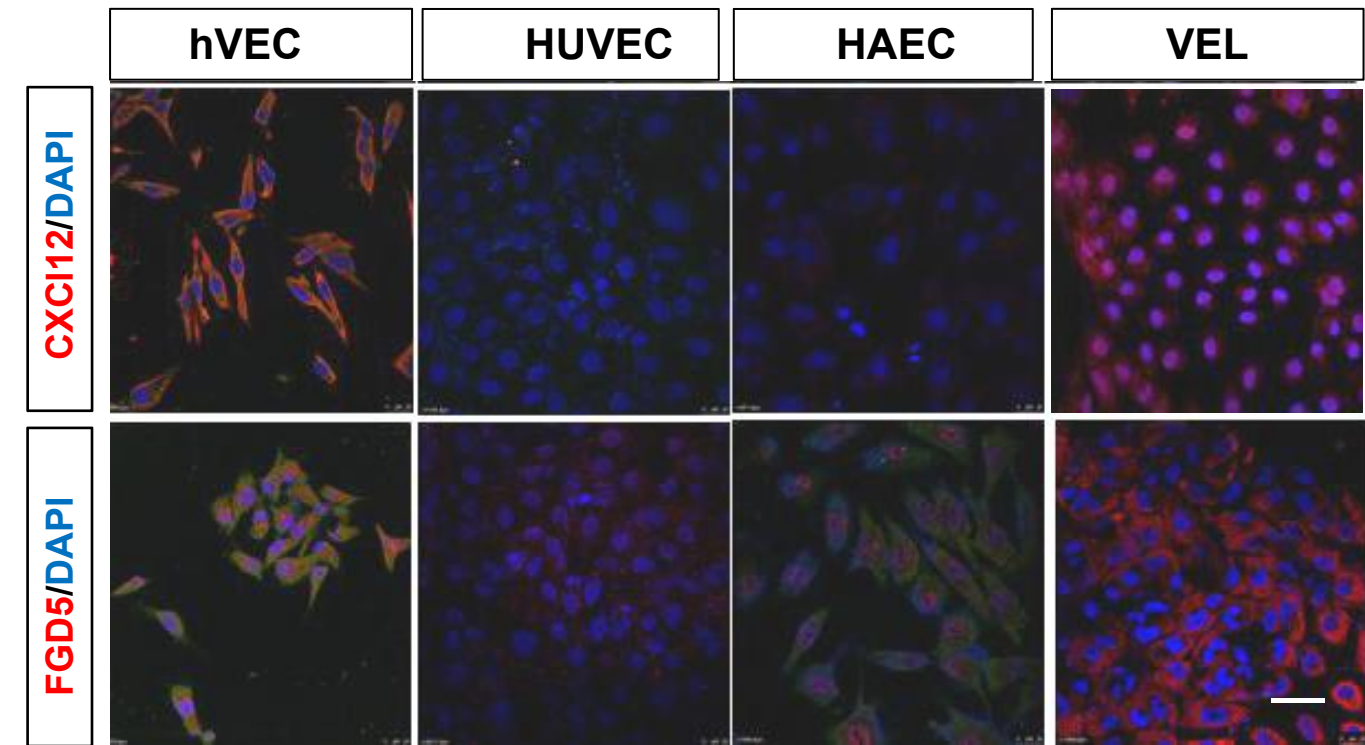
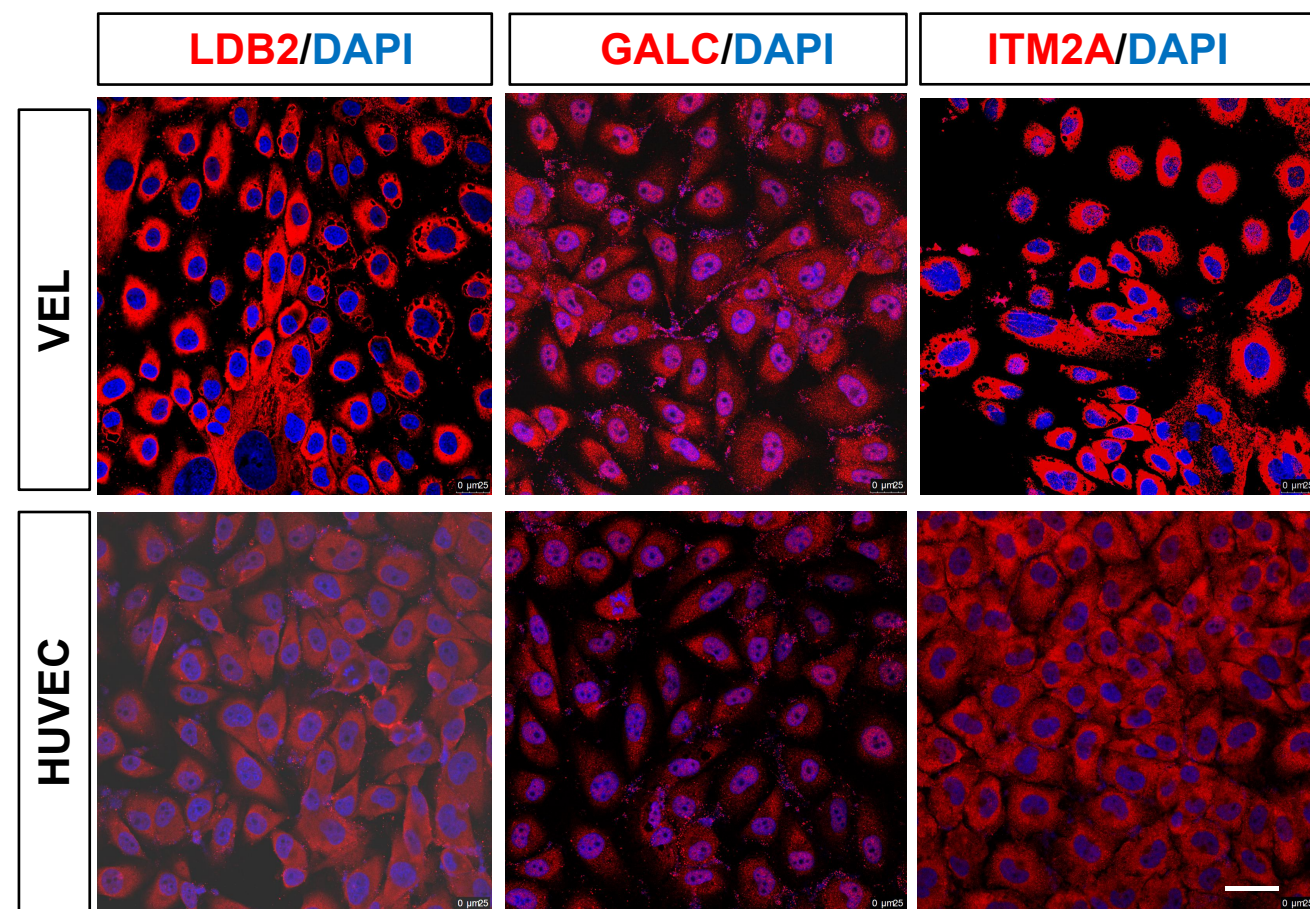
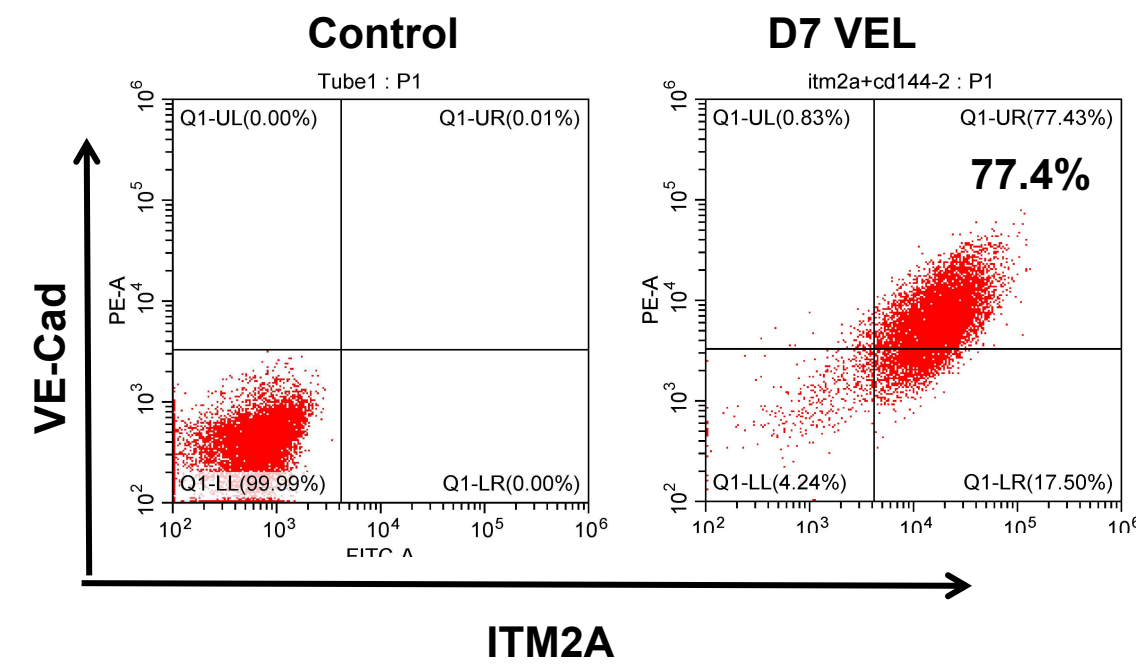
e**g****f****Representative G1 genes****Representative G2 genes**

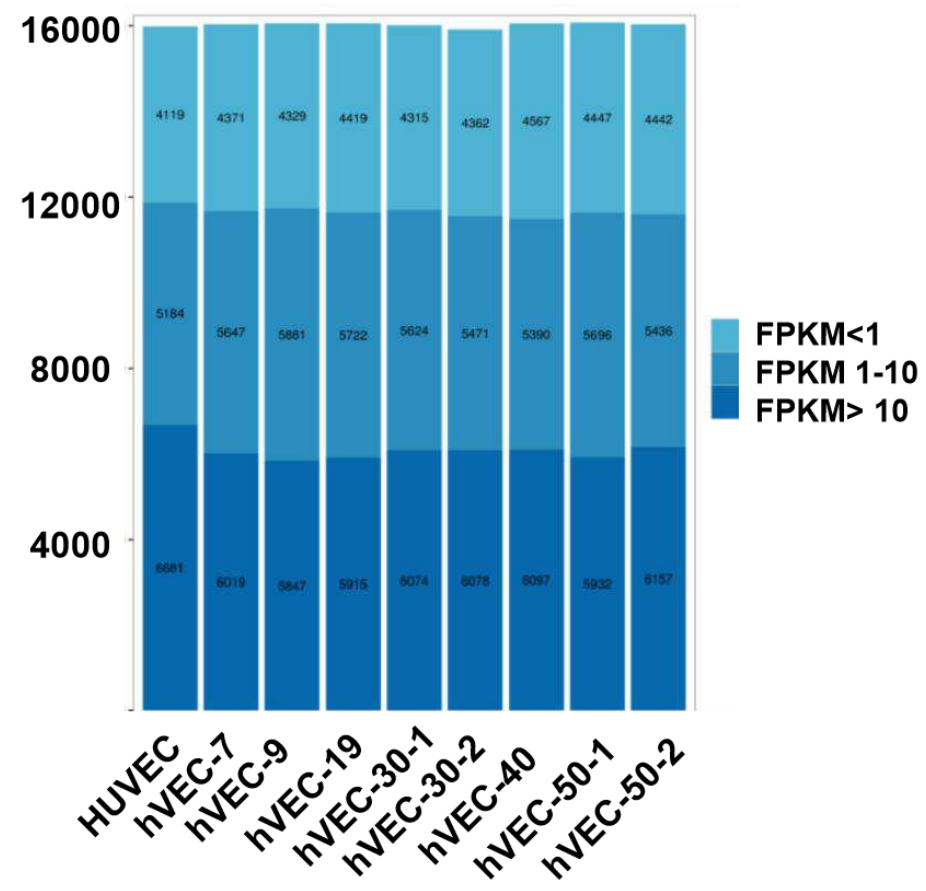
Figure 4 Global transcriptome comparison between VELs and primary VECs



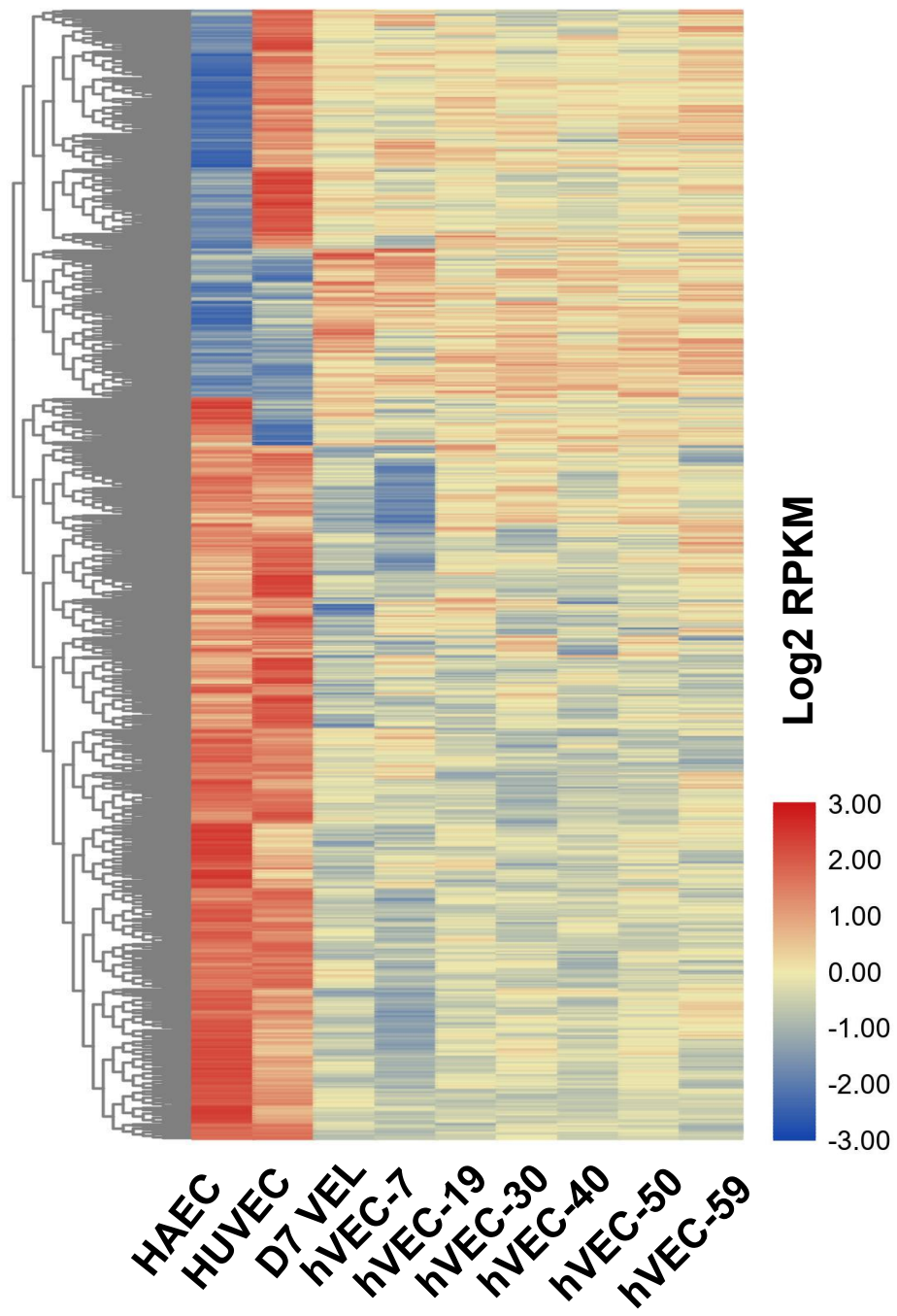
g**h****i****j**

Supplementary Figure 4

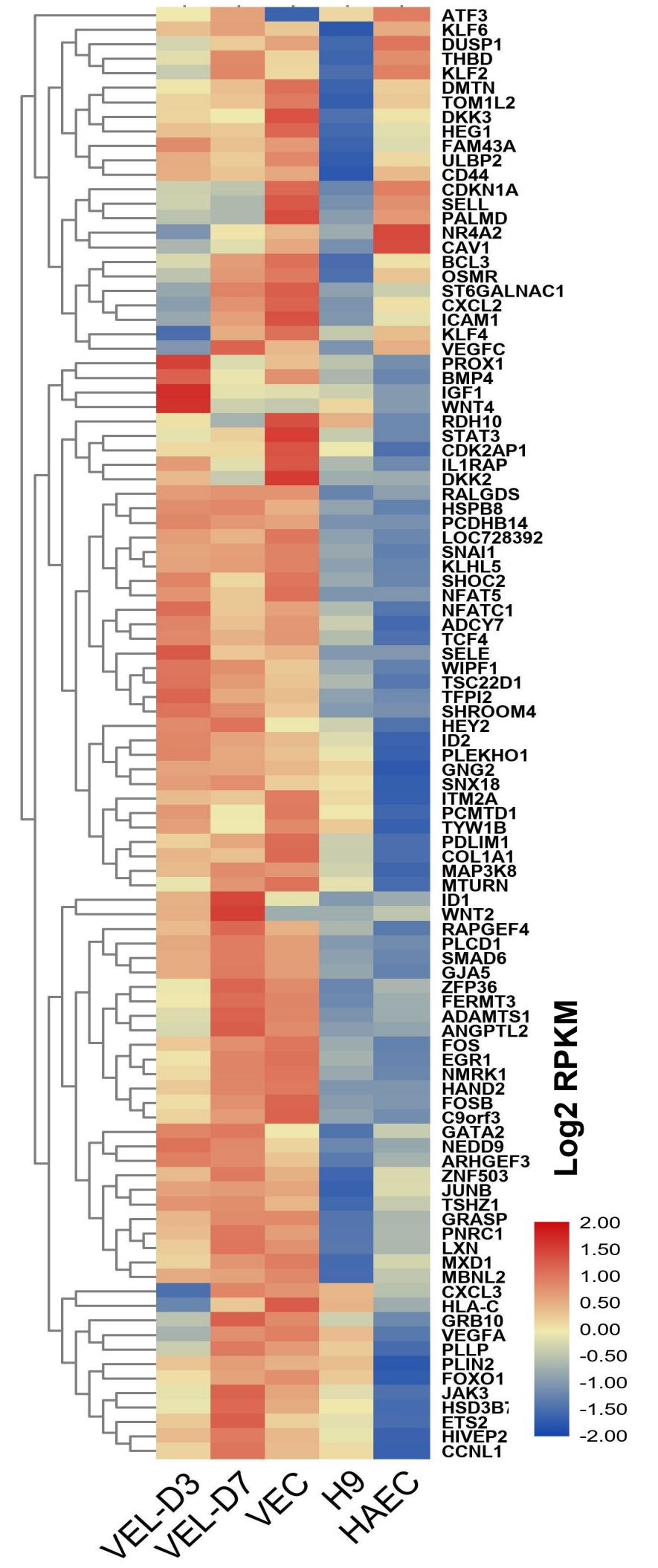
a



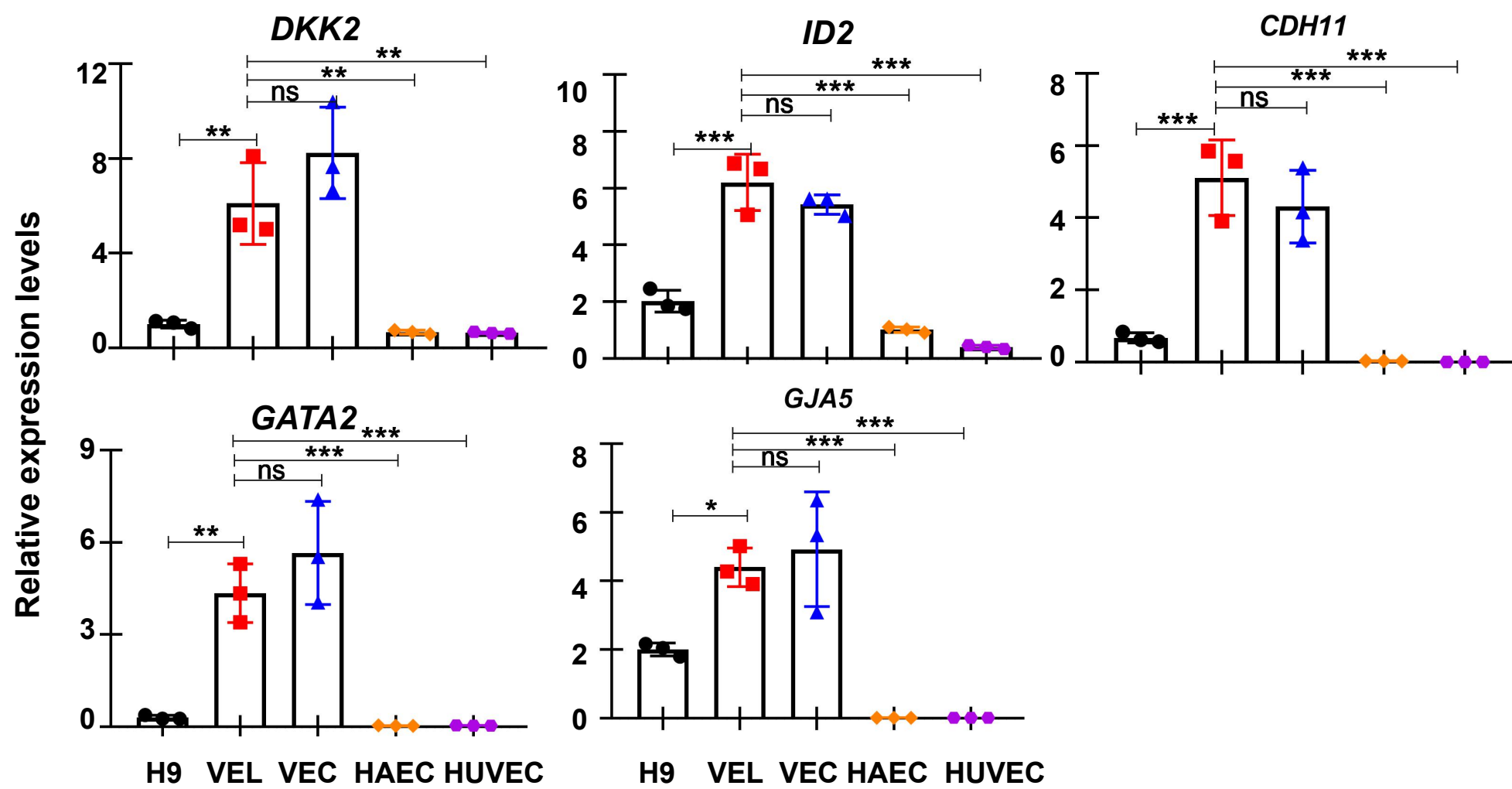
b



c



d



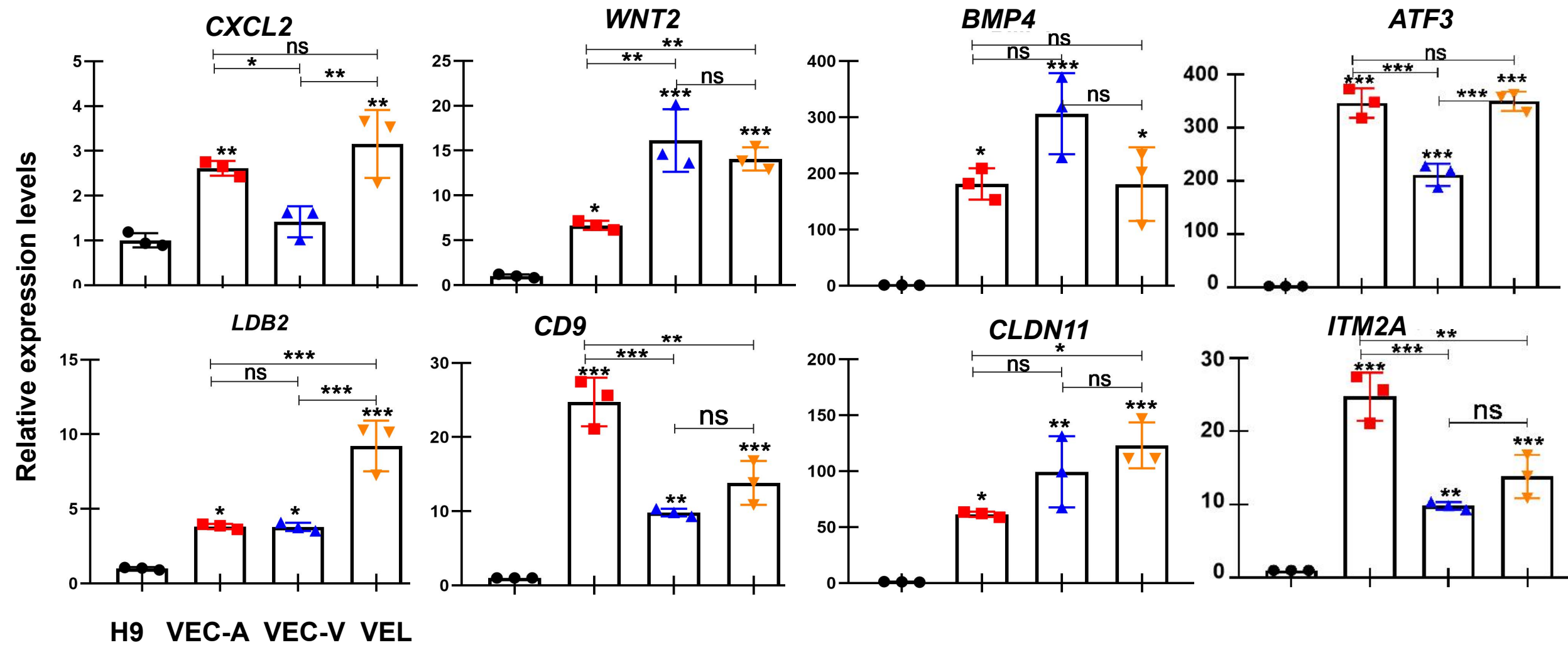
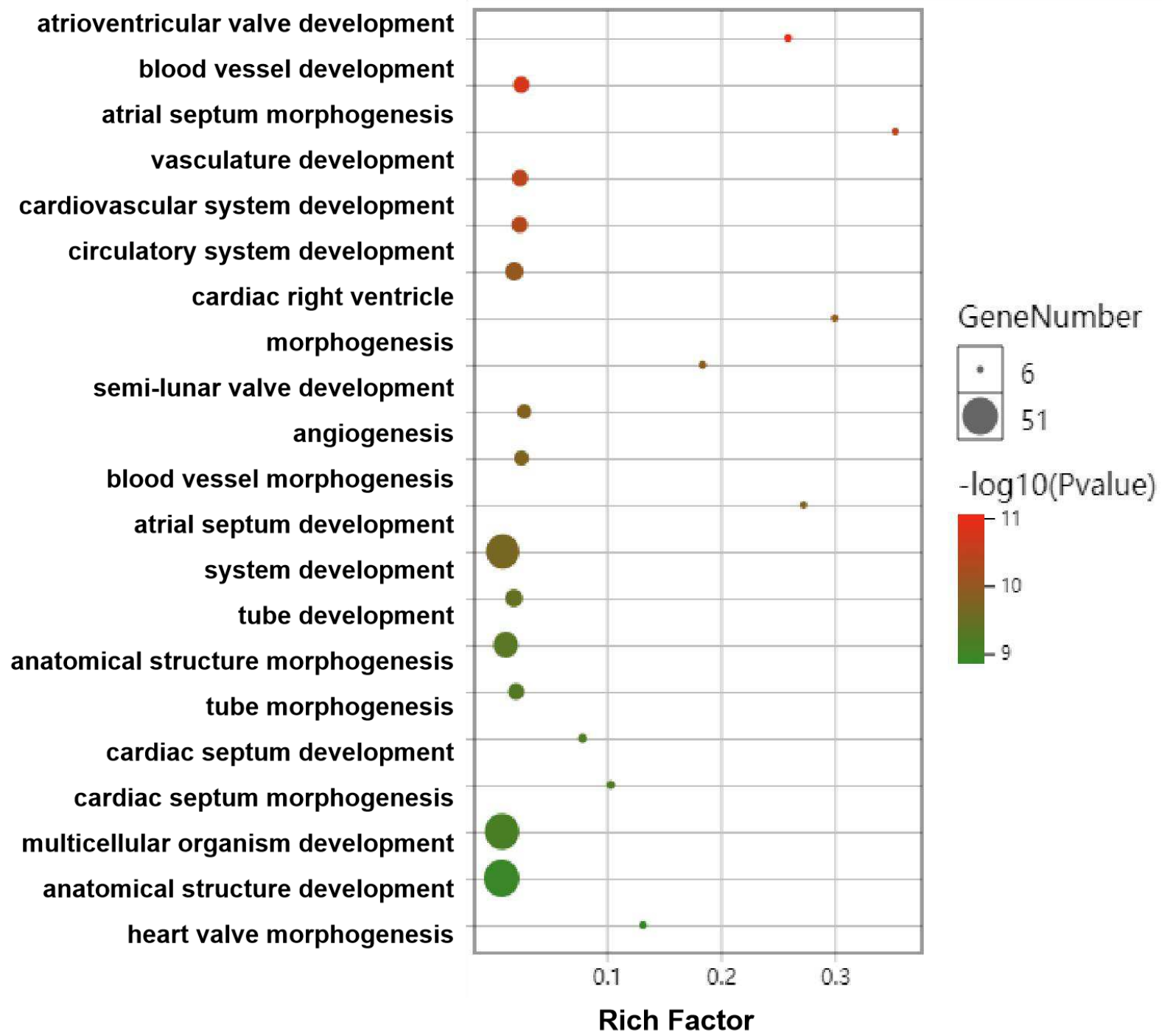
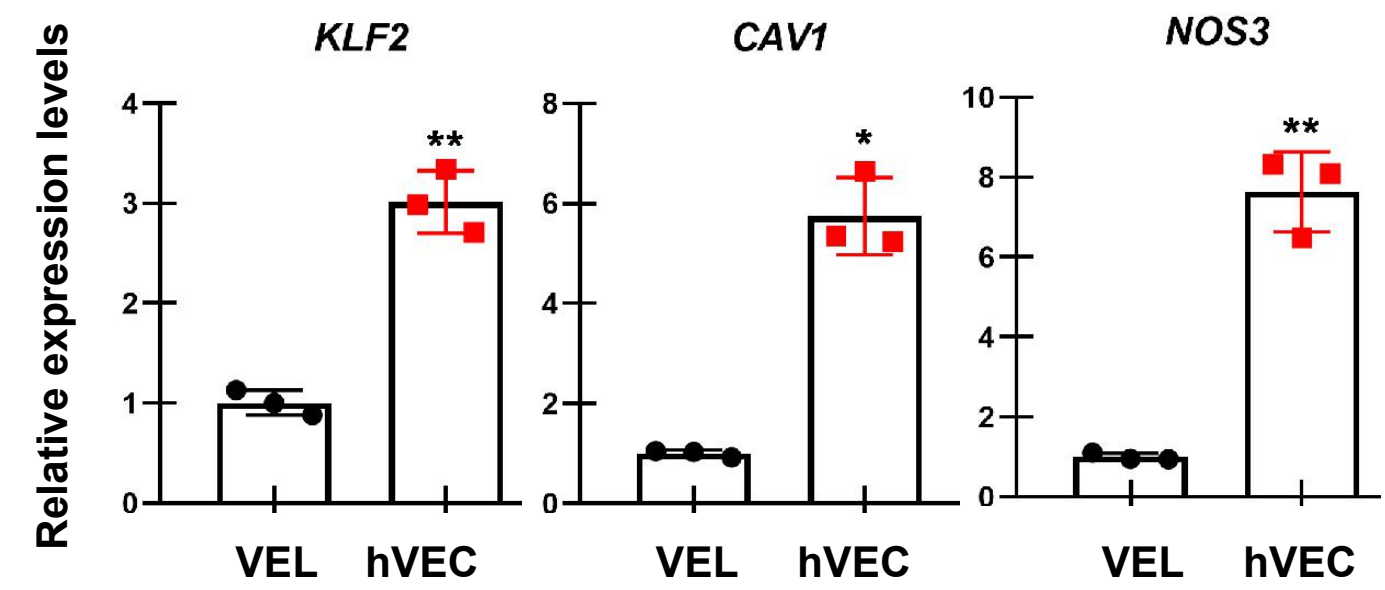
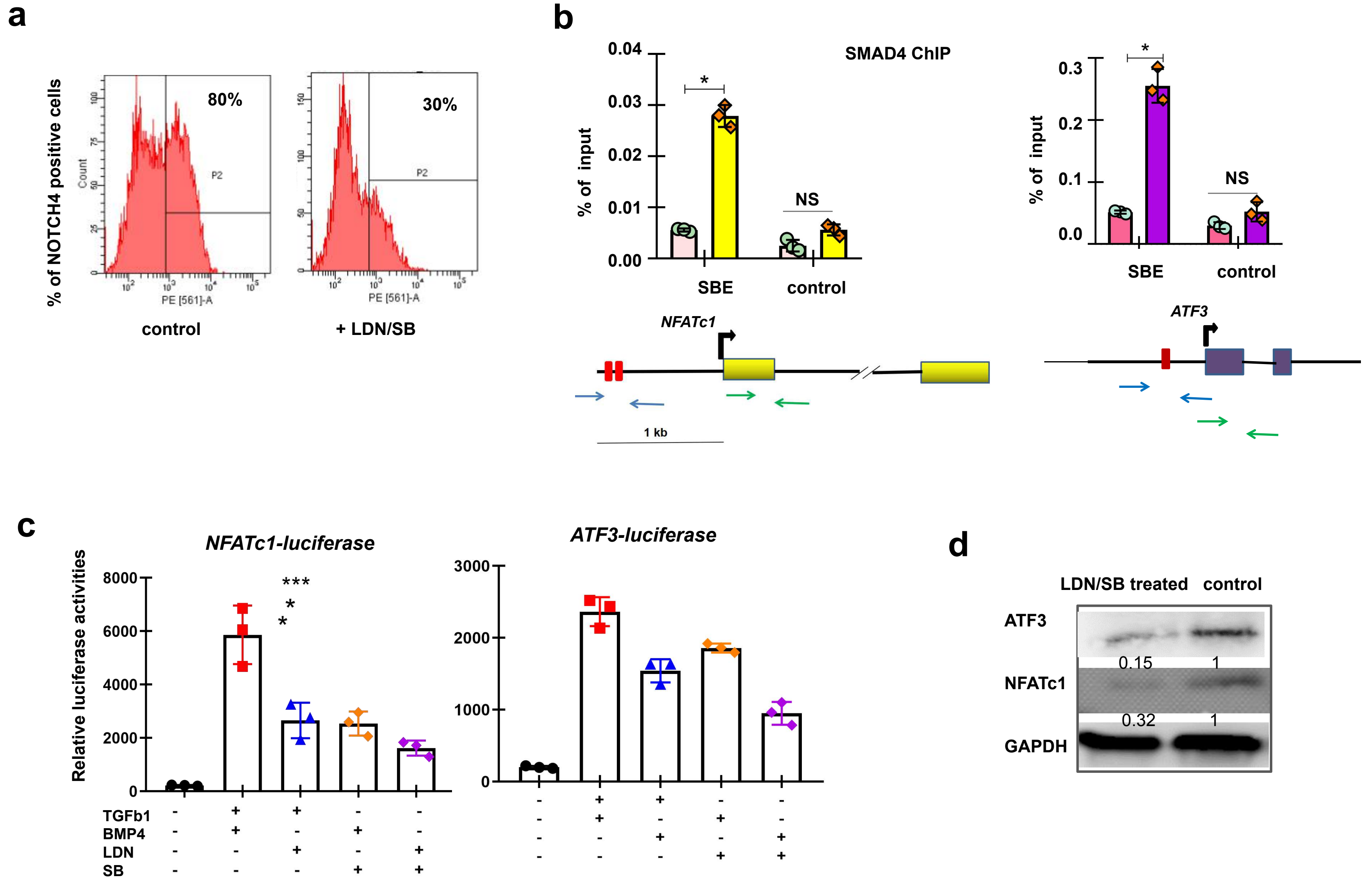
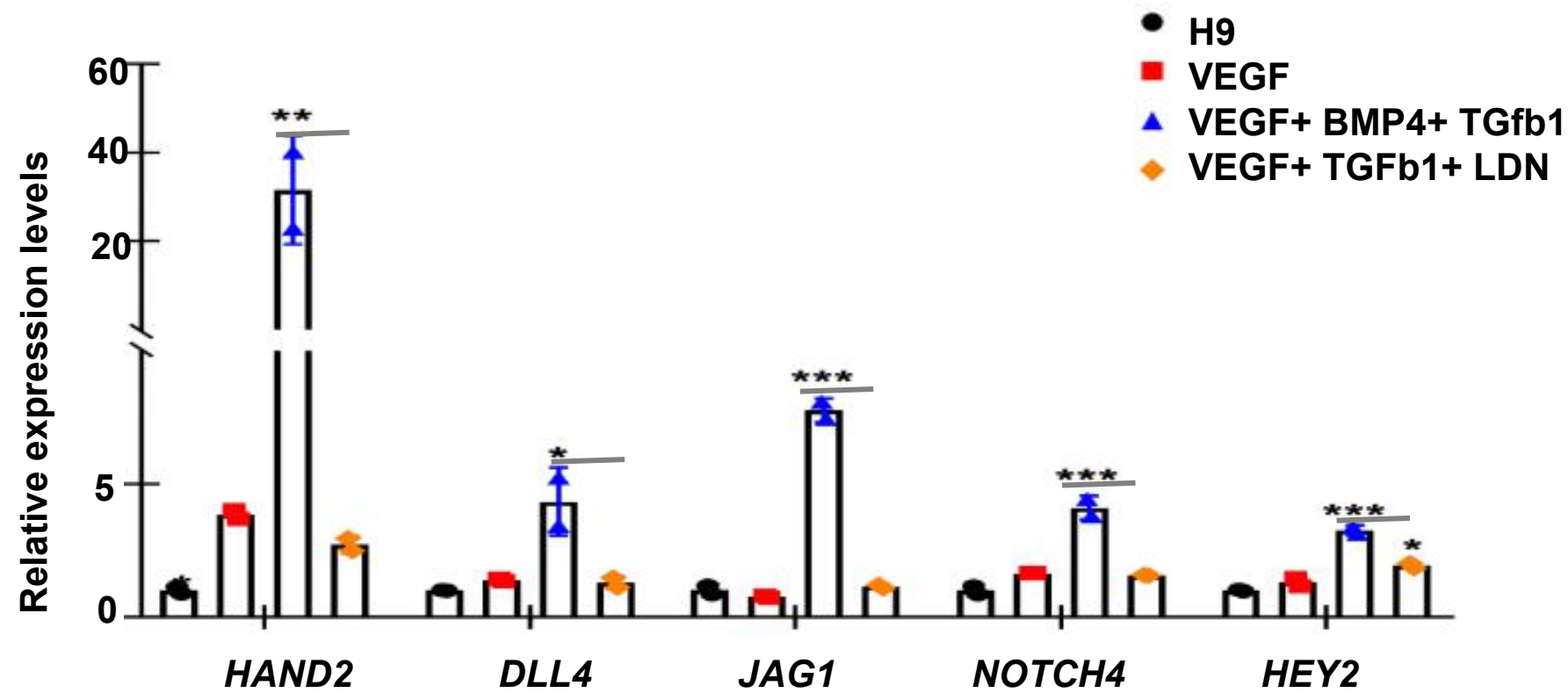
e**f****g**

Figure 5 BMP4 and TGFb1 induce VEC fate by promoting *NFATc1*

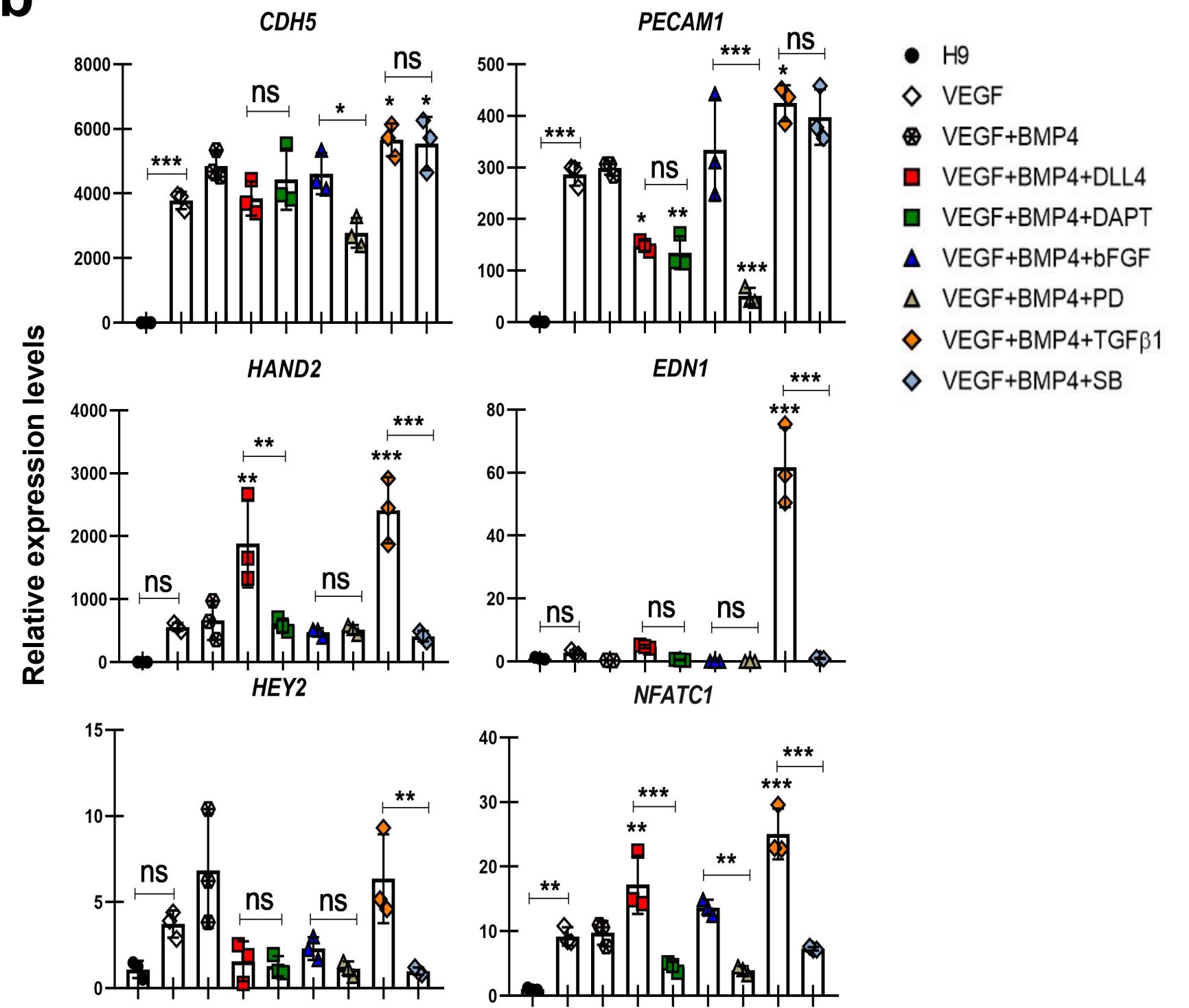


Supplementary Figure 5

a



b



c

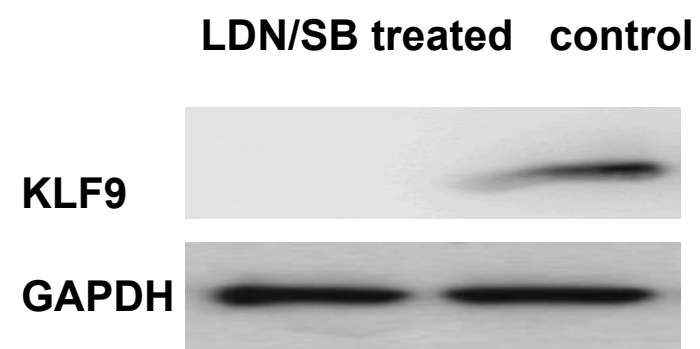
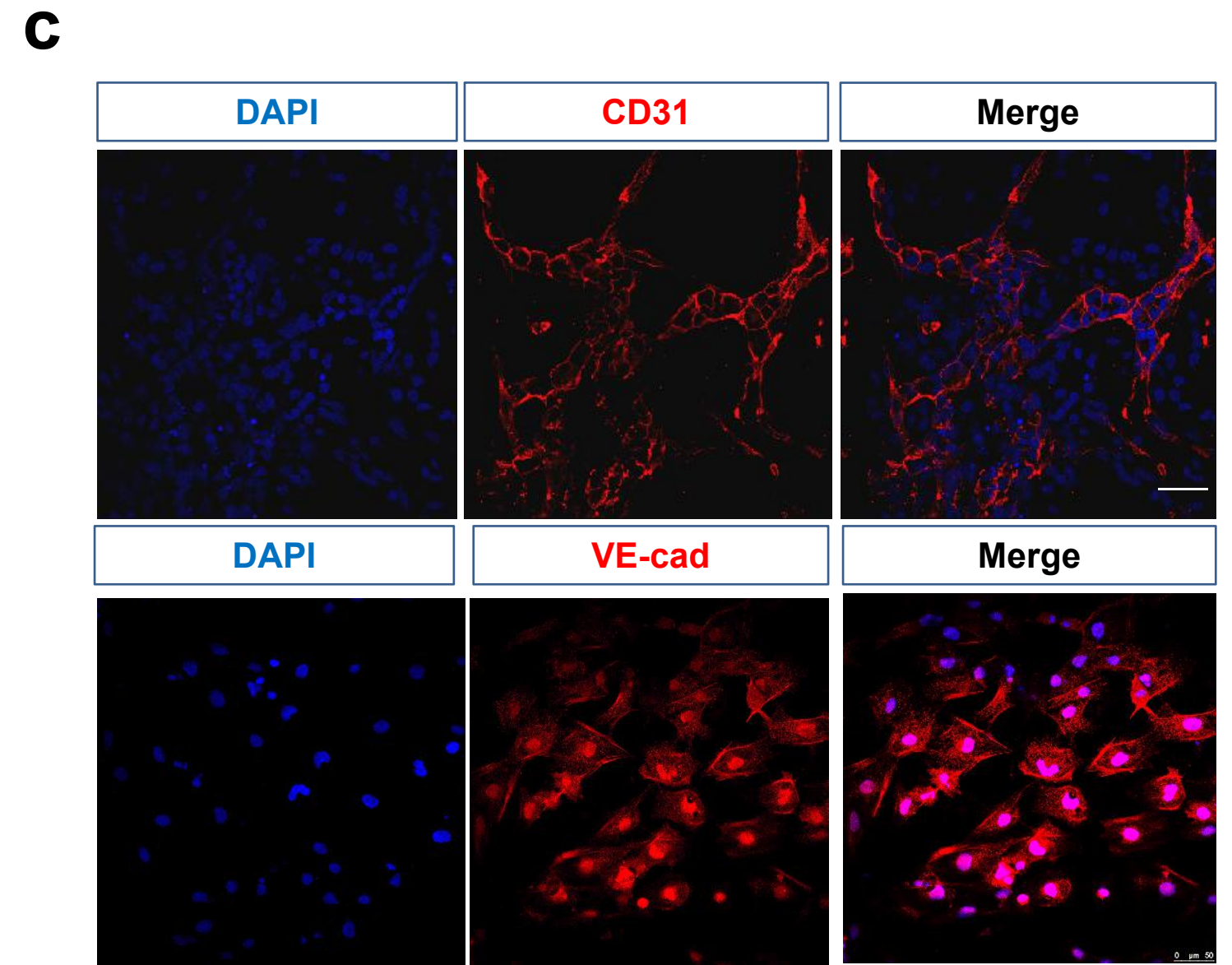
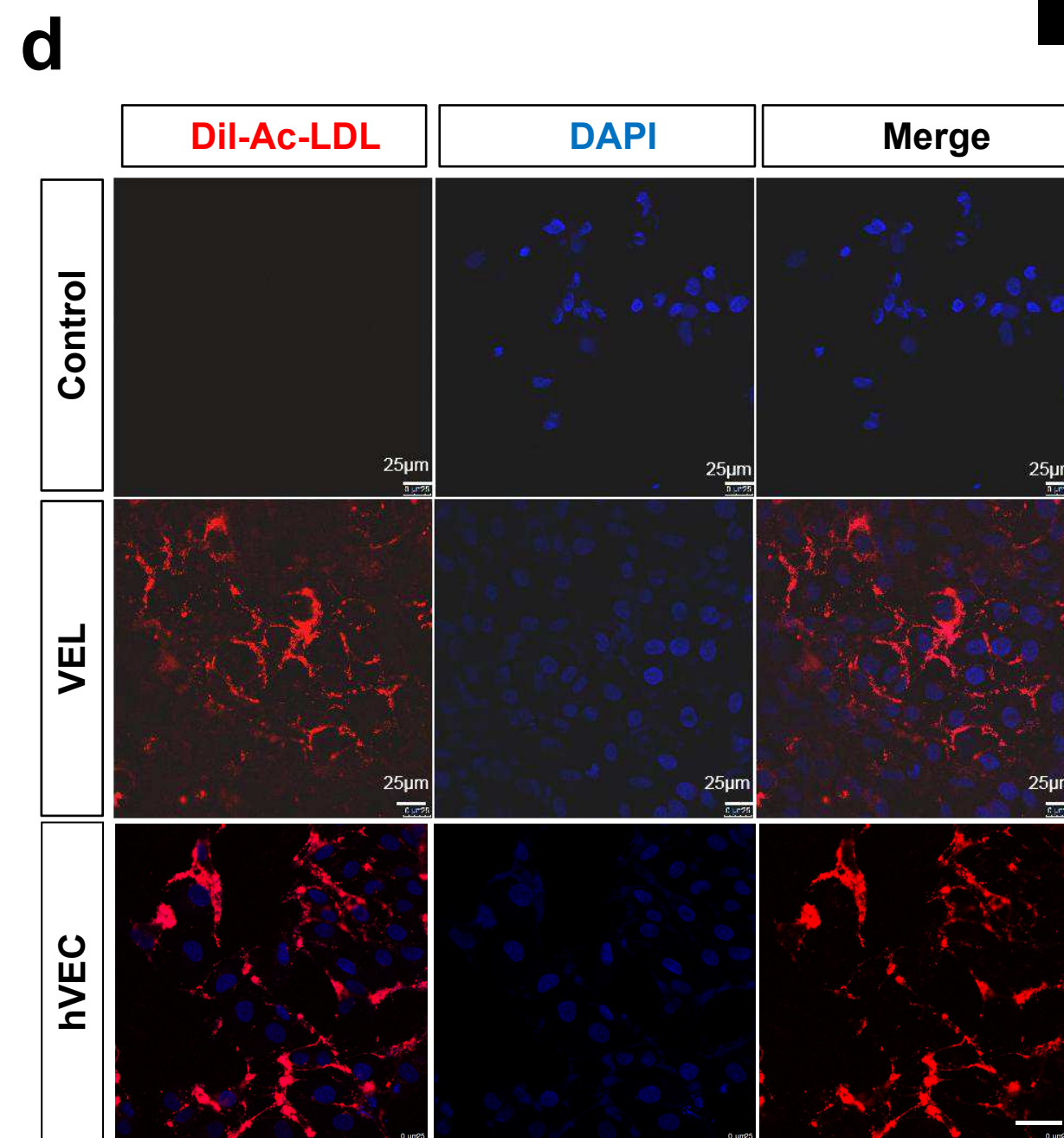
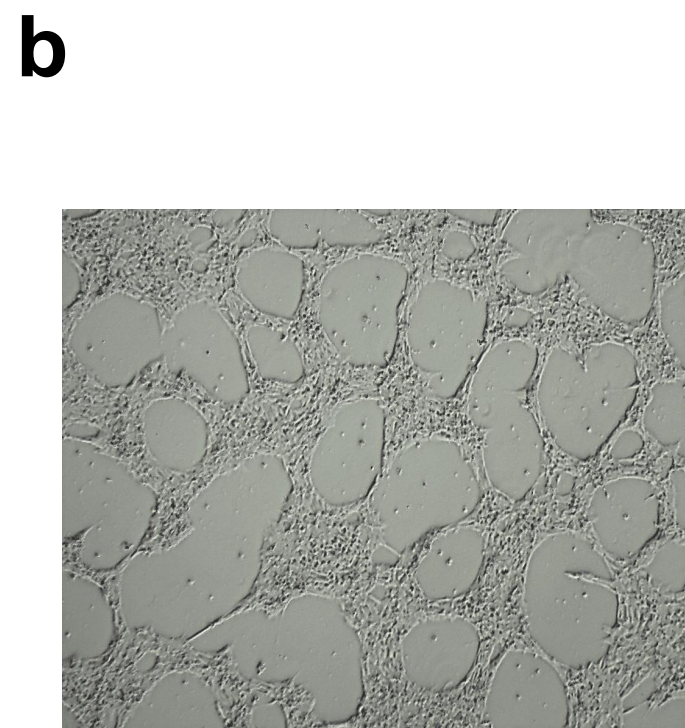
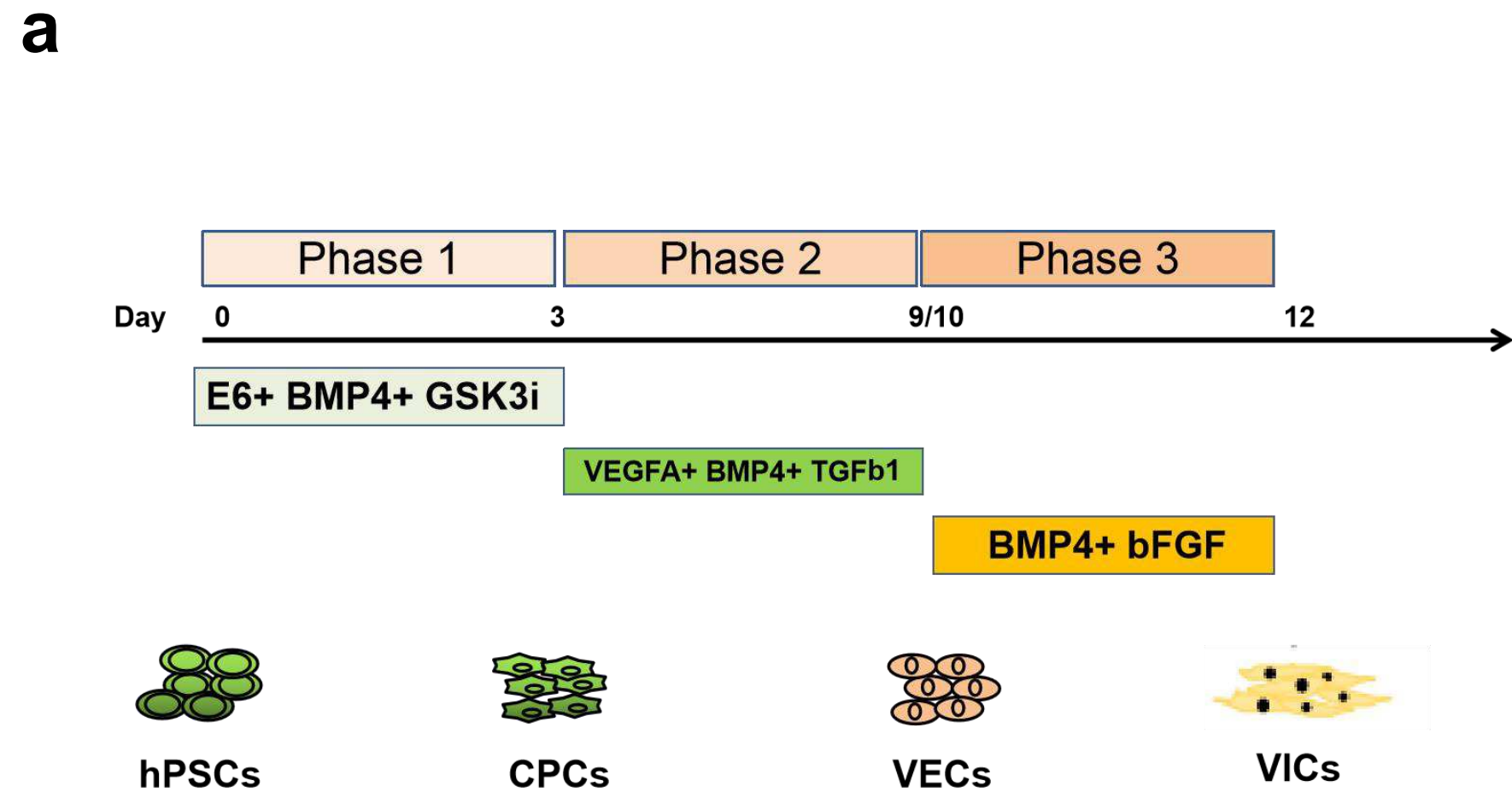
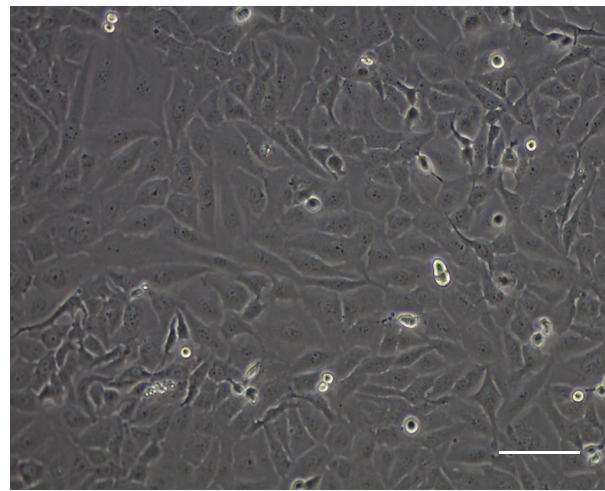


Figure 6 Functional characterization of hPSC-derived VELs



Supplementary Figure 6

a



Passage 5

b

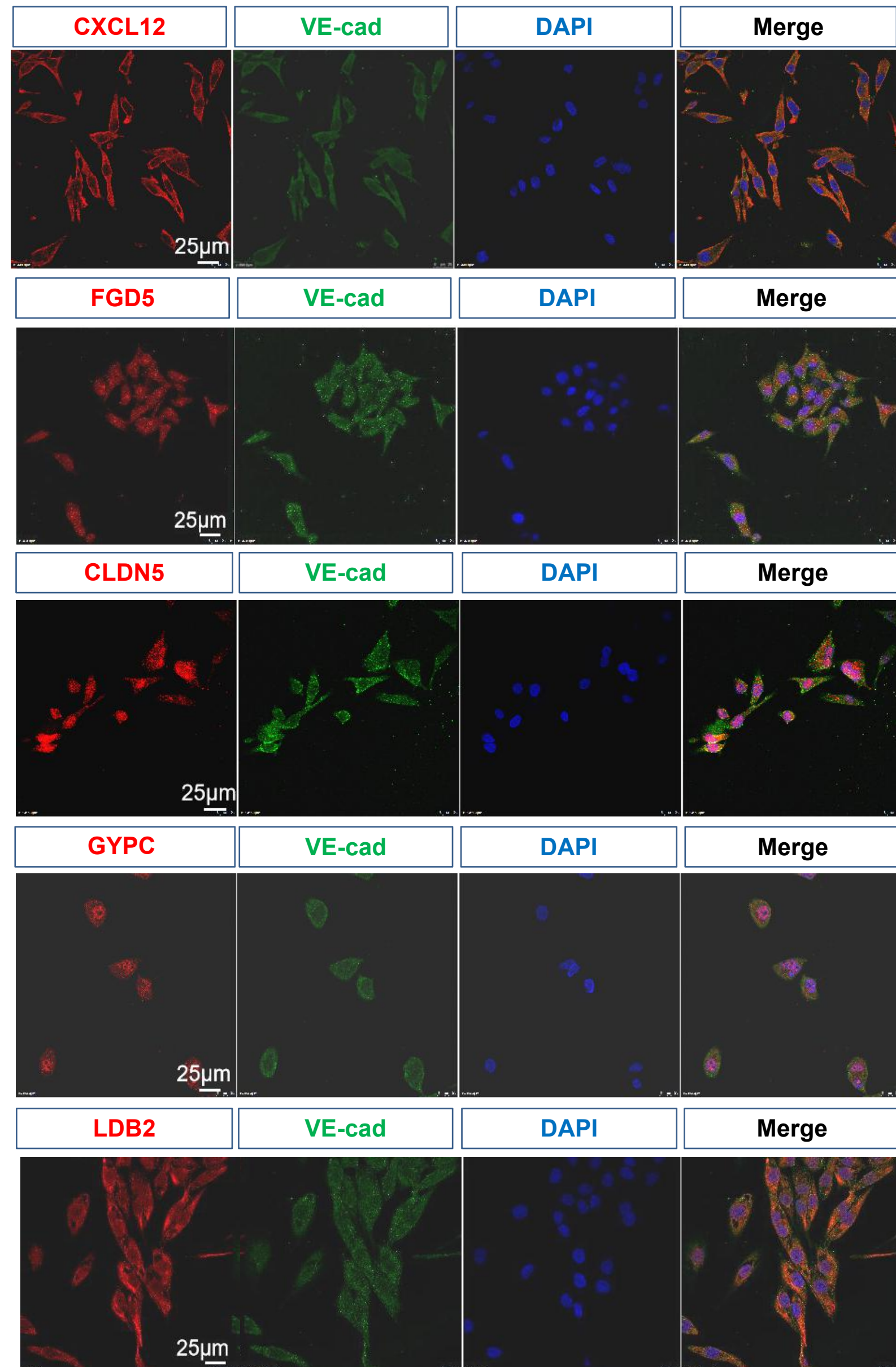
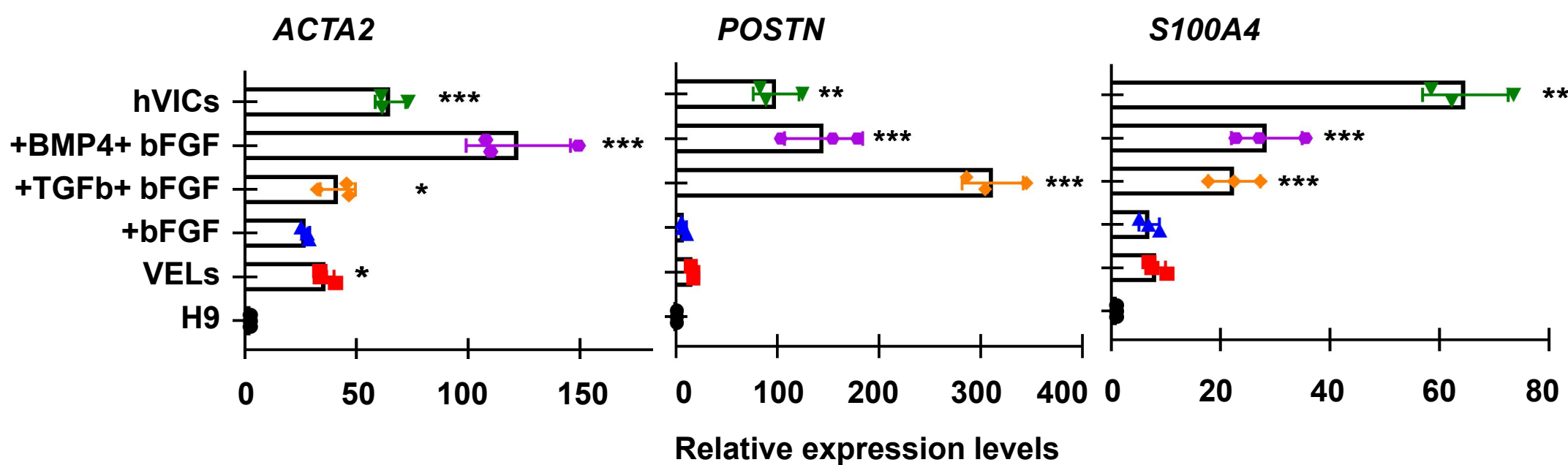
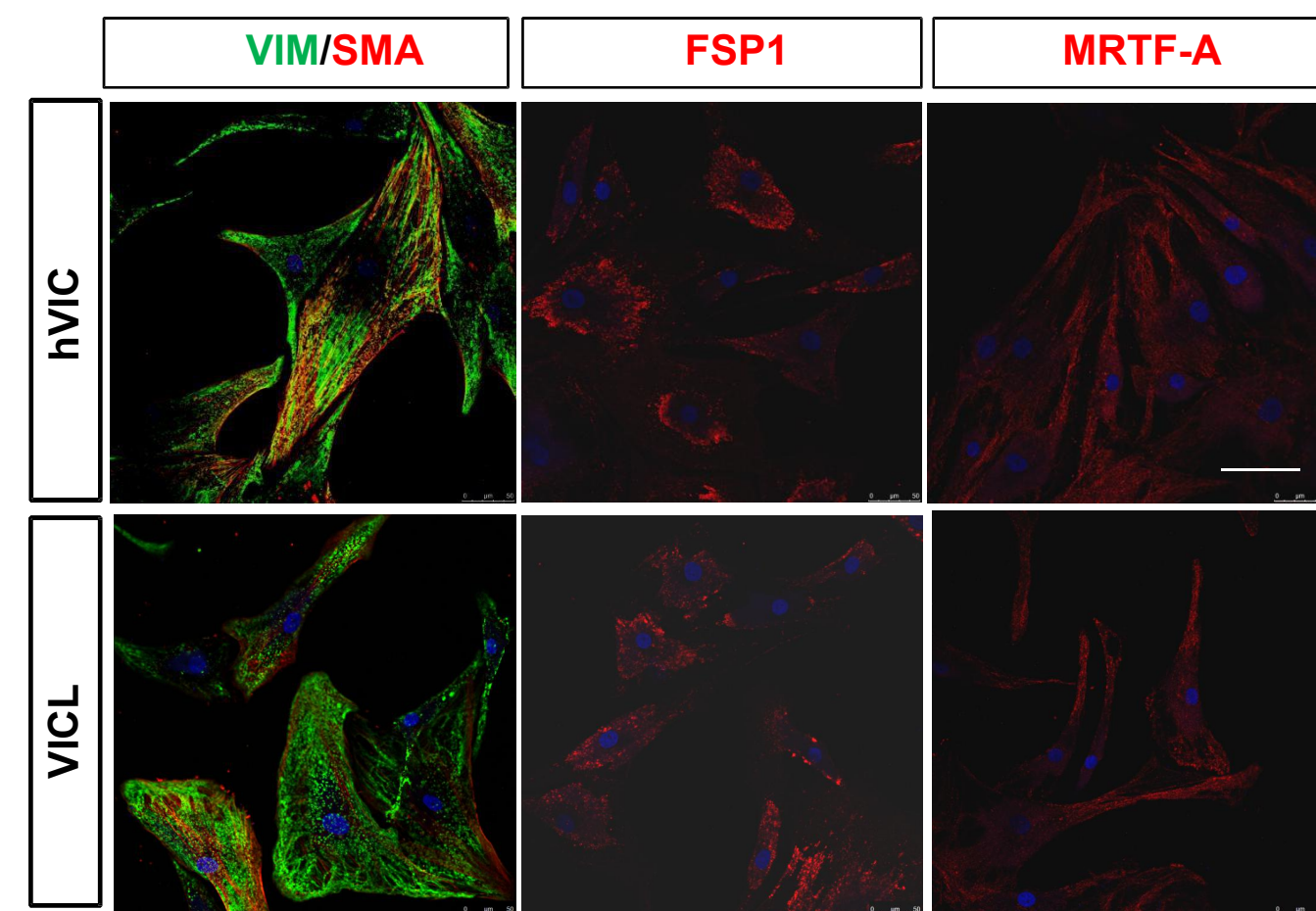


Figure 7 hPSC-derived VELs to VIC-like cells by inducing EndoMT

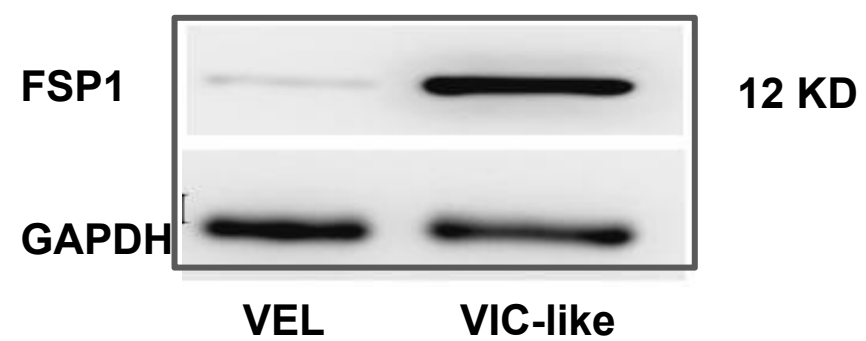
a



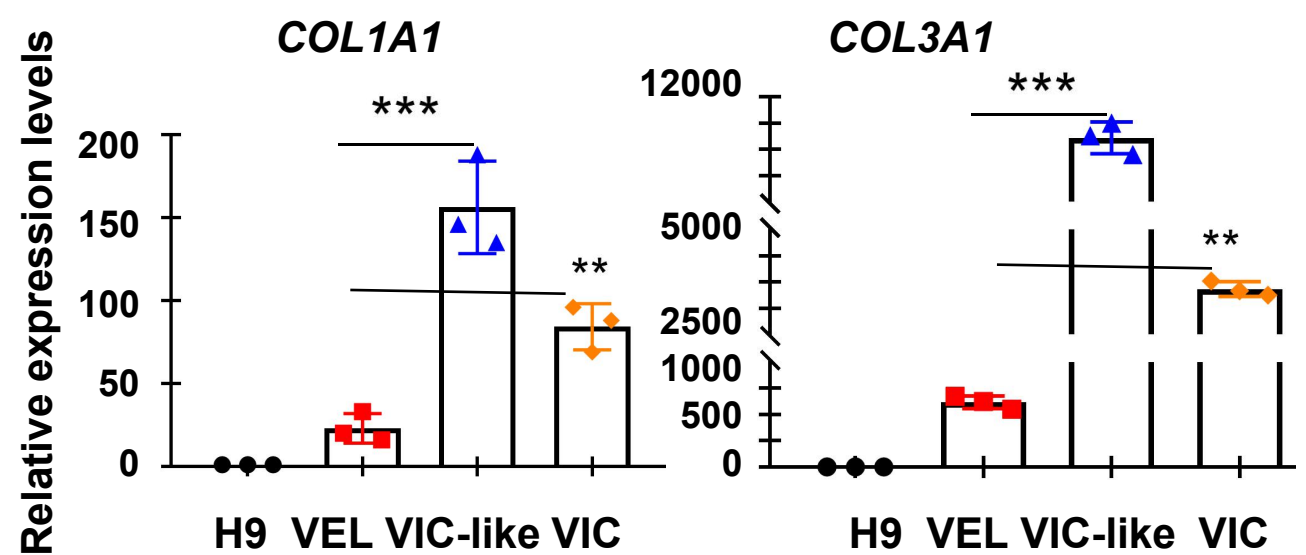
b



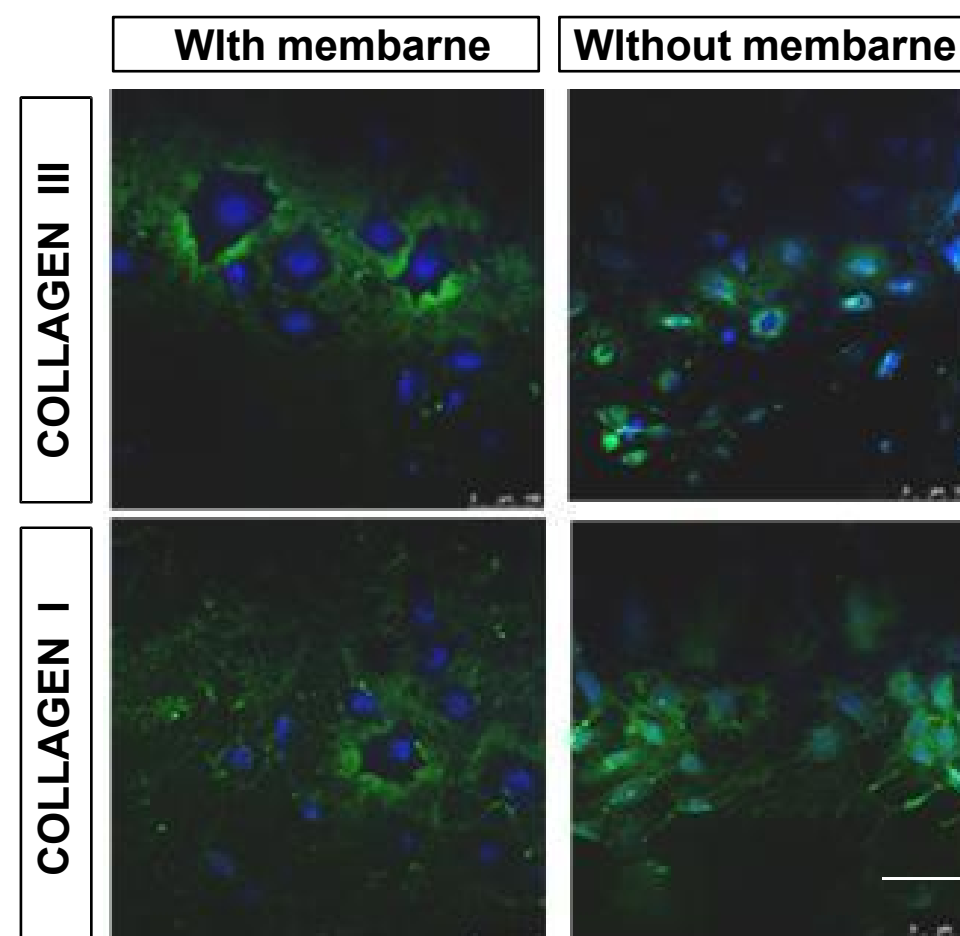
c



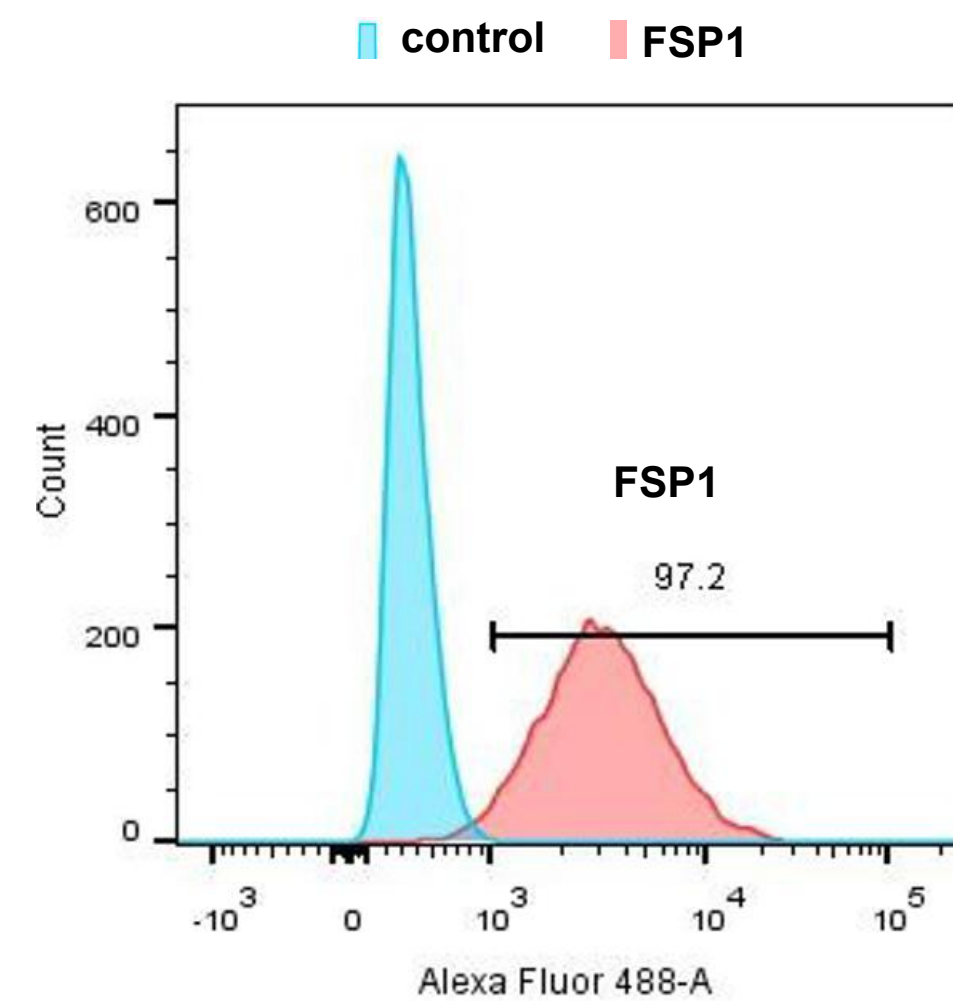
d



e



f



Supplementary Figure 7

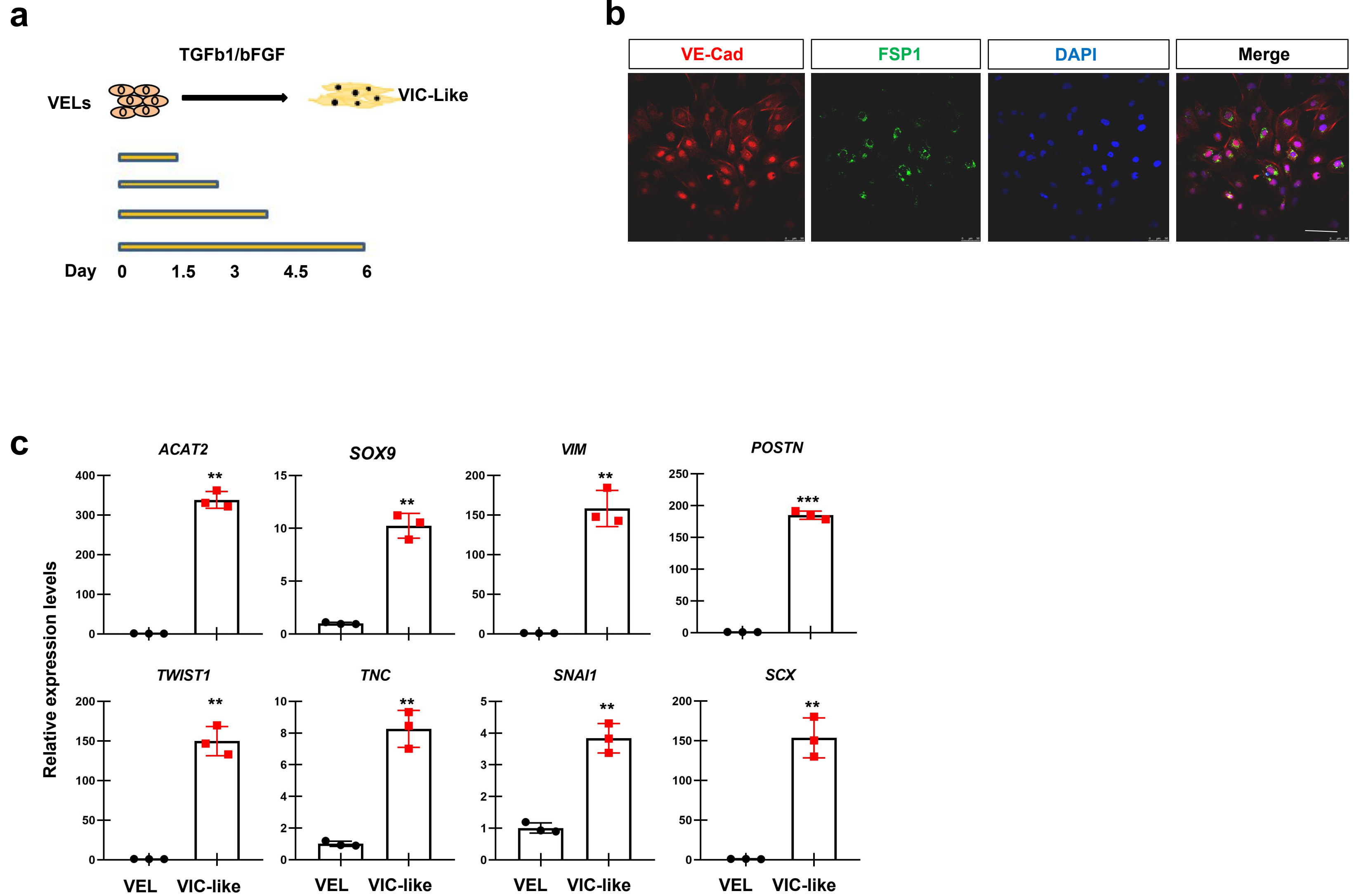
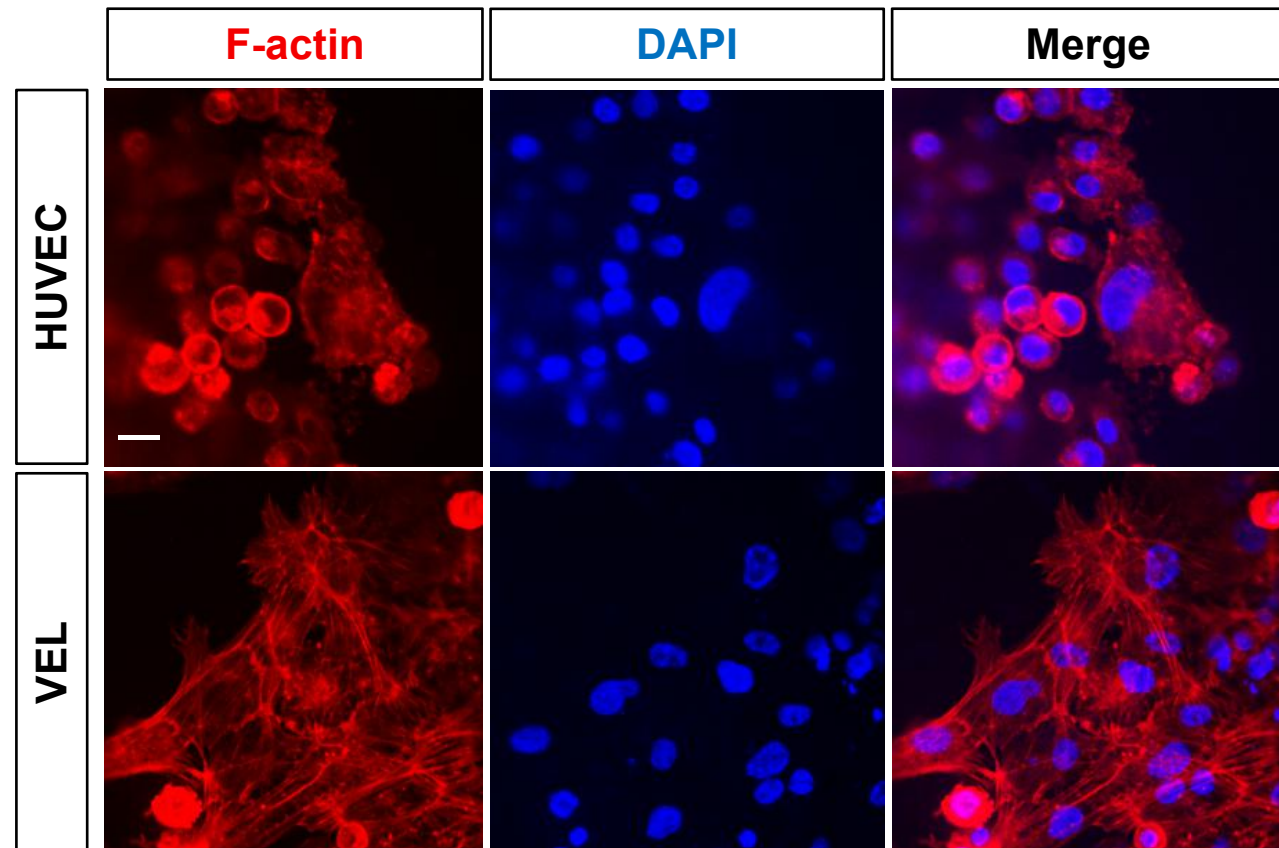
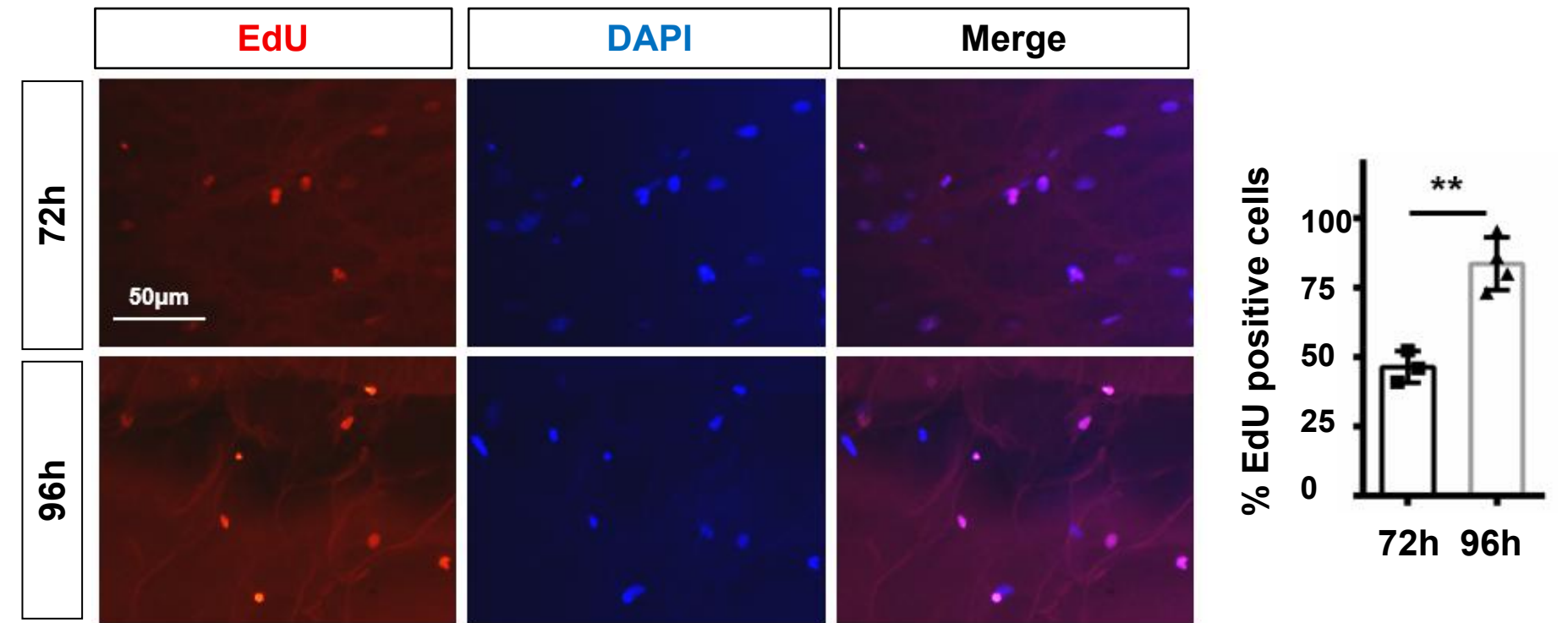


Figure 8 HPSC-derived VELs seeded on de-cellularized porcine heart valves

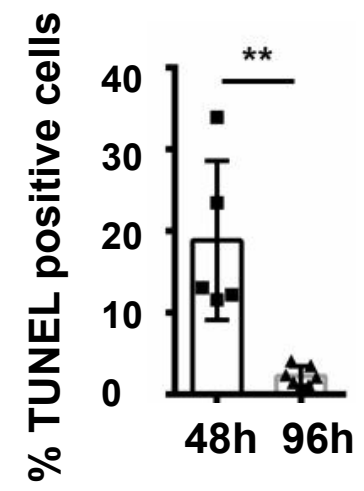
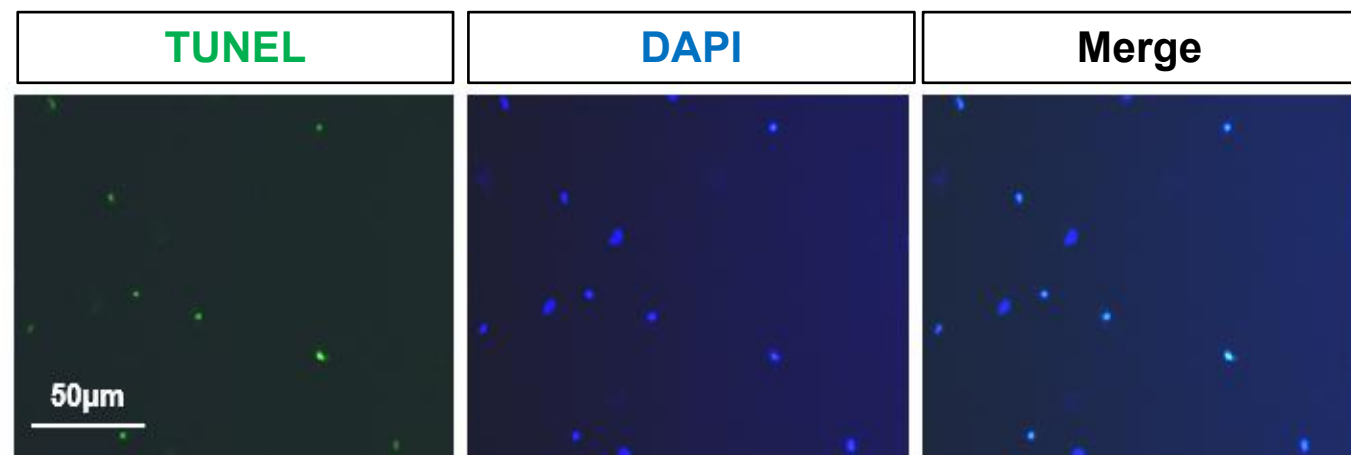
a



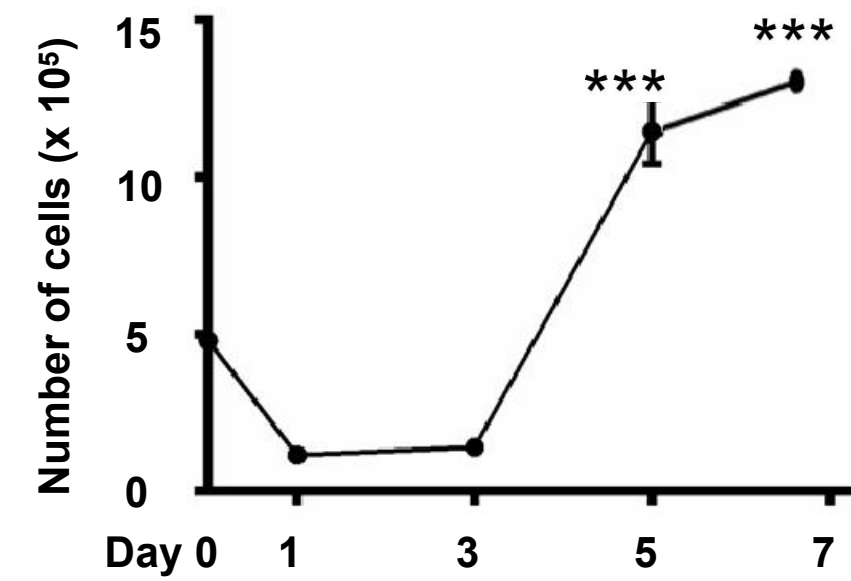
b

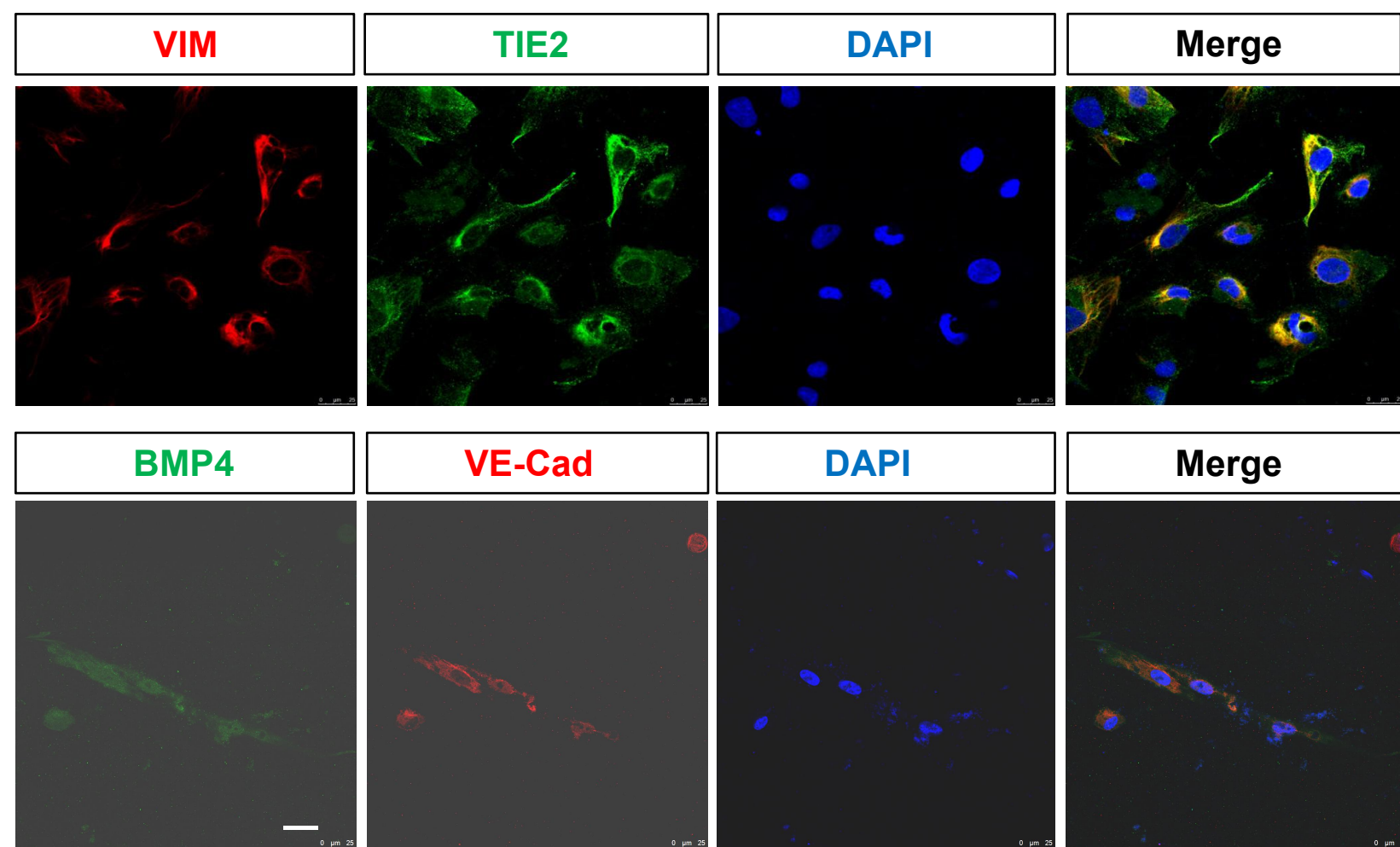
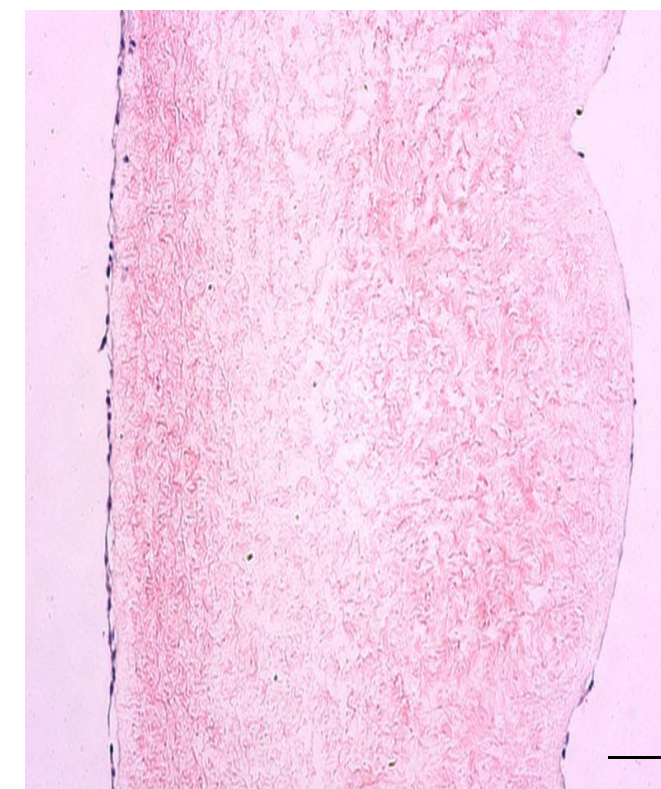
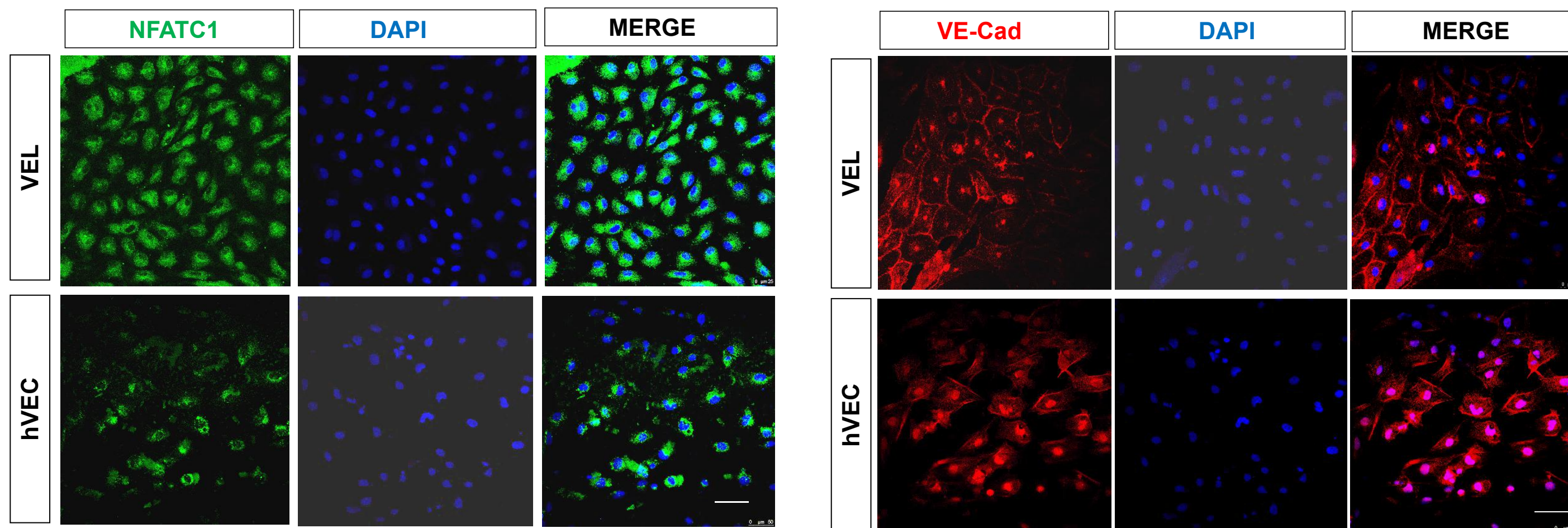


c



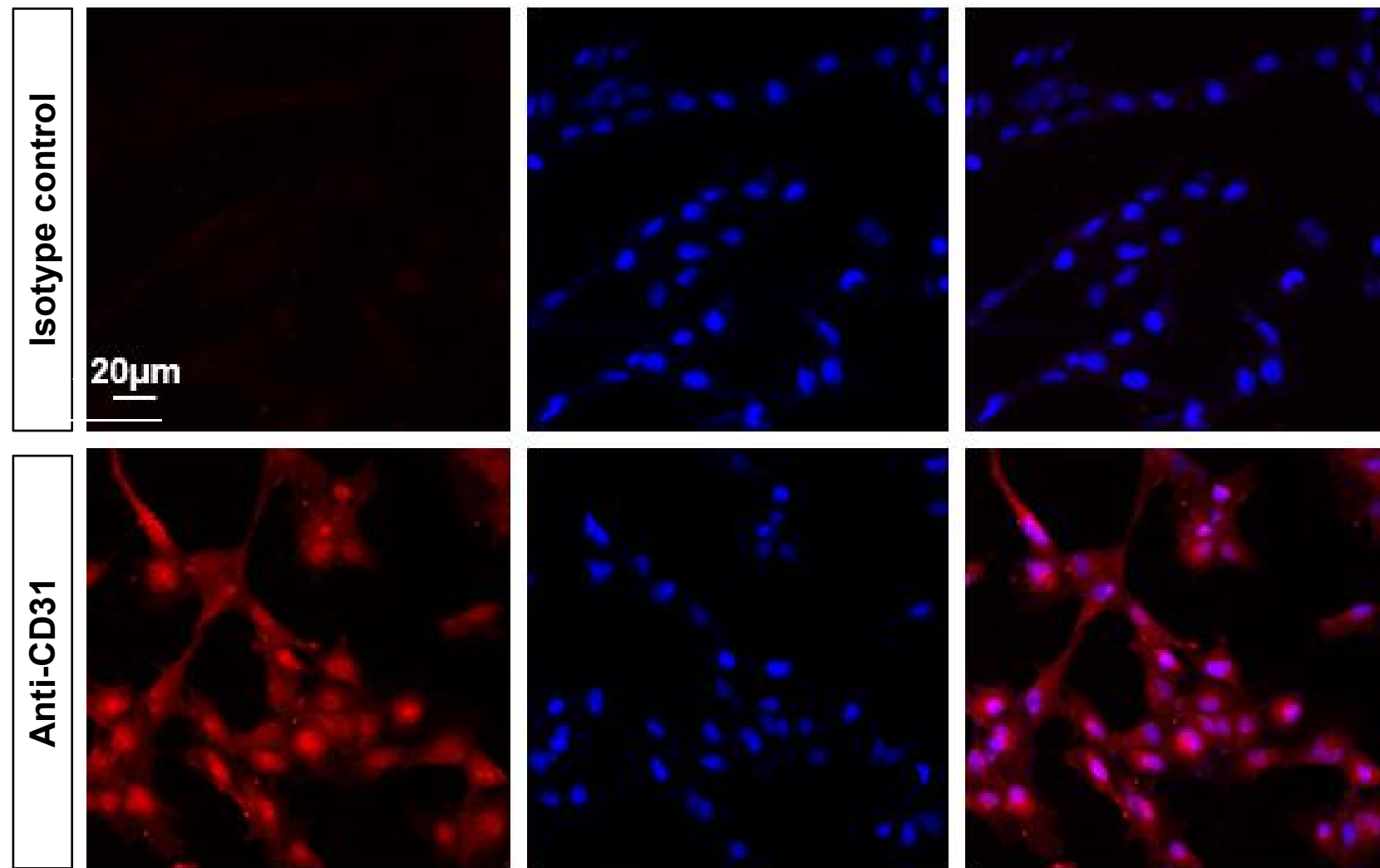
d



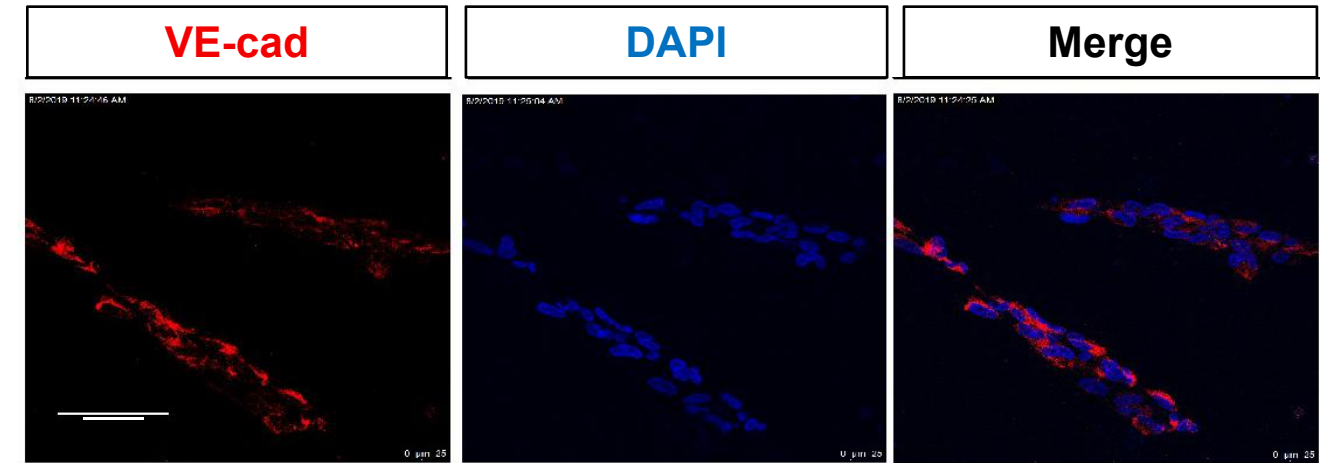
e**f****g**

Supplementary Figure 8

a



b



Figures

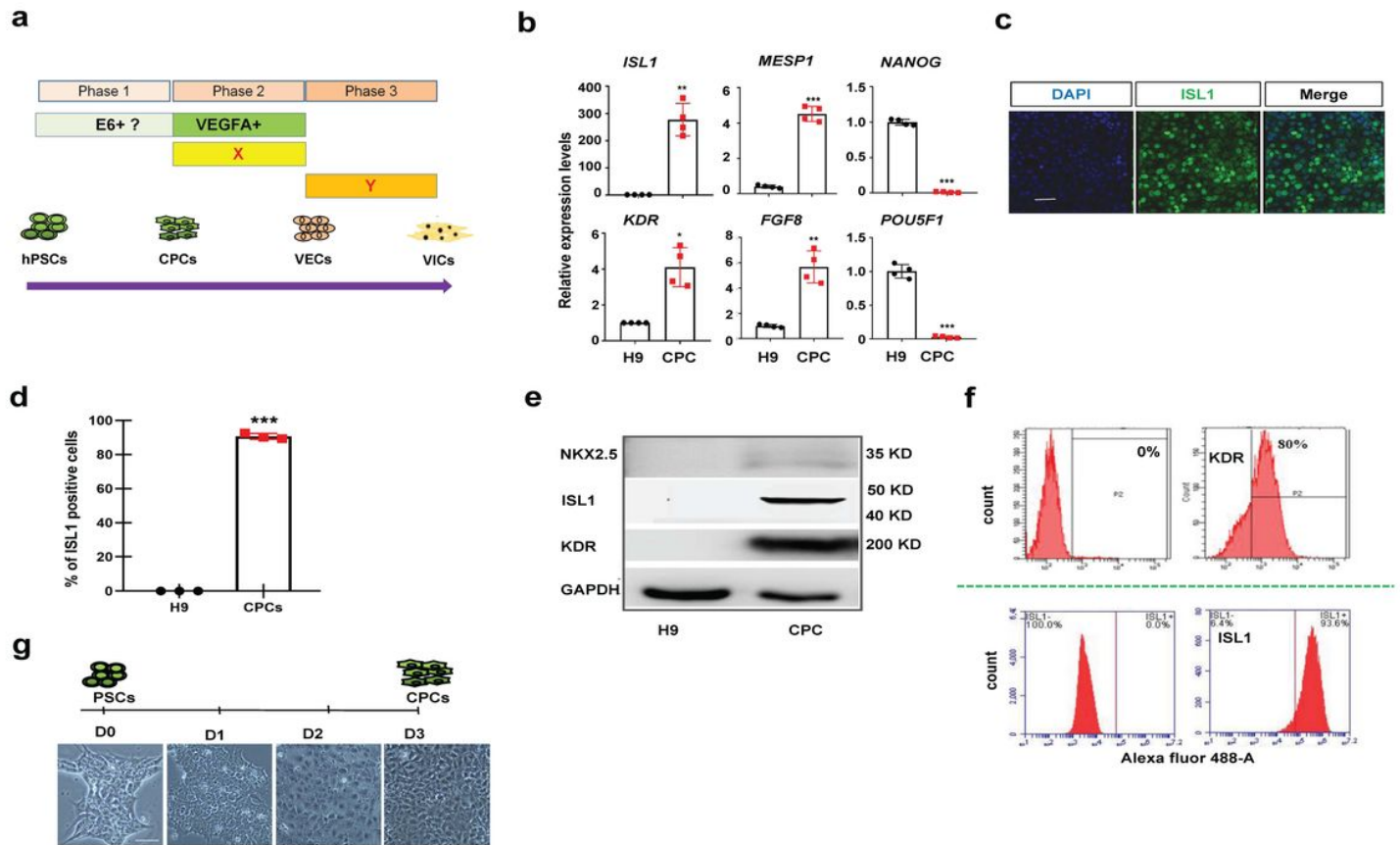


Figure 1

PSCs to cardiogenic mesoderm cells (CPCs) expressing KDR and ISL1